Summer 8-1-2017

An Ecological Examination of Johnson Bayou (Pass Christian, MS) With a Reproductive Histological Analysis of *Rangia cuneata*, and a Comparative Morphological Study of the Foot and Shell of *Rangia cuneata* and *Polymesoda caroliniana*

Brandon Drescher
University of Southern Mississippi

AN ECOLOGICAL EXAMINATION OF JOHNSON BAYOU (PASS CHRISTIAN, MS) WITH A REPRODUCTIVE HISTOLOGICAL ANALYSIS OF *RANGIA CUNEATA*, AND A COMPARATIVE MORPHOLOGICAL STUDY OF THE FOOT AND SHELL OF *RANGIA CUNEATA* AND *POLYMESODA CAROLINIANA*

by

Brandon David Drescher

A Dissertation
Submitted to the Graduate School,
the College of Science and Technology,
and the Department of Biological Sciences
at The University of Southern Mississippi
in Partial Fulfillment of the Requirements
for the Degree of Doctor of Philosophy

August 2017

AN ECOLOGICAL EXAMINATION OF JOHNSON BAYOU (PASS CHRISTIAN, MS) WITH A REPRODUCTIVE HISTOLOGICAL ANALYSIS OF *RANGIA CUNEATA*, AND A COMPARATIVE MORPHOLOGICAL STUDY OF THE FOOT AND SHELL OF *RANGIA CUNEATA* AND *POLYMESODA CAROLINIANA*

by Brandon David Drescher

August 2017

Approved by:

_____
Dr. Jennifer M. Walker, Committee Chair
Associate Professor, Biological Sciences

_____
Dr. Rebecca Fillmore, Committee Member
Assistant Professor, Biological Sciences

_____
Dr. Jake Schaefer, Committee Member
Professor, Biological Sciences

_____
Dr. Brian Kreiser, Committee Member
Professor, Biological Sciences

_____
Dr. Alan Shiller, Committee Member
Professor, Ocean Science and Technology

_____
Dr. Karen S. Coats
Dean of the Graduate School

Published by the Graduate School

ABSTRACT

AN ECOLOGICAL EXAMINATION OF JOHNSON BAYOU (PASS CHRISTIAN, MS) WITH A REPRODUCTIVE HISTOLOGICAL ANALYSIS OF *RANGIA CUNEATA*, AND A COMPARATIVE MORPHOLOGICAL STUDY OF THE FOOT AND SHELL OF *RANGIA CUNEATA* AND *POLYMESODA CAROLINIANA*

by Brandon David Drescher

August 2017

Johnson Bayou is an estuarine system located in Pass Christian, MS. Research involved a biotic and abiotic examination of Johnson Bayou, resulting in the identification of numerous species of plants and animals, including *Rangia cuneata* (Mactridae) and *Polymesoda caroliniana* (Cyrenidae), sympatric species of infaunal bivalves. Environmental factors (e.g., water temperature, salinity) were measured over three years to describe the system from an abiotic standpoint, and used in a qualitative and quantitative reproductive histological study on *R. cuneata*. Results revealed differences in timing of gamete production and spawning between three subpopulations of this species. Sediment samples taken from the study areas had statistically different levels of organic matter and sediment particle sizes. A laboratory-based experiment was undertaken to examine the effect of three sediment types on the number and length of burrowing events between both species of clams. It was found that the number of burrowing events and the length of burrowing events differed significantly, and the difference in length of burrowing events in silt between species was significant.

Infaunal bivalves are ecosystem engineers, capable of altering the morphology of sediment and water column via burrowing with their foot. However, little research has examined the foot morphology and ultrastructure of bivalves between sympatric species from different families. A comparative study using light and electron microscopy methods revealed that *R. cuneata* and *P. caroliniana* have the same general organization of foot tissue, with a thick internal musculature, subepithelial region, and ciliated, simple epithelium. However, the composition of glandular tissue comprising the subepithelium was different between species. While *P. caroliniana* produces only acidic mucopolysaccharides, *R. cuneata* produces both acidic and nonacidic mucopolysaccharides.

Bivalve shells provide shelter and substrate for numerous organisms and as a source of calcium and carbonate ions. Shell of either species has not been examined from a system in MS. Using microscopy methods, *R. cuneata* produces four shell layers, while *P. caroliniana* produces three. Presence of iron and titanium were detected from the periostracum, silicon and strontium in the nacre, but not from the adductor muscle scar, and the elemental composition of the outer and middle layers was the same.

ACKNOWLEDGMENTS

I would like to thank the following undergraduates for their dedicated time and effort in learning new techniques and assisting in observations, data acquisition, and subsequent analyses: Cassy Porter, Christopher Griffin, Samantha Allen, Elizabeth Jacavone, and Rebecca Crosby. I would like to thank Nancy Brown-Peterson at the Gulf Coast Research Laboratory for her time in training me and assisting with histological techniques and image analysis. Additional people at GCRL I thank for their time include Jeremy Johnson and Binnaz Bailey, both of which were instrumental in teaching me techniques in lab-based aquaculture. I am grateful to Dr. Shelia Brown for her assistance in identifying various species of plants in Johnson Bayou, and to Darrin Cooper, manager of the machine shop in the Department of Polymer Sciences, for his assistance is cutting shells for morphological examination. My committee and advisor have been kind, patient, and supportive with their feedback during my time as a student. I formed the ideal doctoral committee. I must thank the members of the Environmental Protection Agency with whom I collaborated on various projects; in addition, they provided important materials with which I was able to complete some projects reported in this dissertation. A special thanks to Janeal McKee, Jensa Besse, and Robin Johnson for their support and guidance throughout my time at USM. Last, a final thanks to Dr. Francis Lucas who without her help, I would have never been able to continue my research as a graduate student.

TABLE OF CONTENTS

LIST OF TABLES

LIST OF ILLUSTRATIONS

LIST OF ABBREVIATIONS

A-P	Anterior-Posterior
D-V	Dorsal-Ventral
EDS	Energy Dispersive X-ray Spectroscopy
EtOH	Ethanol
H&E	Hematoxylin and Eosin
OM	Organic Matter
P-A	Posterior-Anterior
ROI	Region-of-Interest
SAV	Submerged Aquatic Vegetation
SEM	Scanning Electron Microscope
TDS	Total Dissolved Solids
TEM	Transmission Electron Microscope
V-D	Ventral-Dorsal
V	Ventral

CHAPTER I – LITERATURE REVIEW OF *RANGIA CUNEATA* AND *POLYMESODA CAROLINIANA* WITH RESPECT TO ECOLOGY, AND FOOT AND SHELL ULTRASTRUCTURE

Background

Historical and current background on Rangia cuneata

Prior to the Eocene, the wedge clam, *Rangia cuneata* (G. B. Sowerby I, 1831), was restricted to the Gulf of Mexico. According to fossil records, by the time of the Pleistocene, *R. cuneata* had expanded into estuaries and rivers along the Atlantic coast, but for reasons unknown, the populations died out (Richards 1962a). Beginning around 1955, living specimens of *R. cuneata* were reported in estuaries stretching from Maryland to Florida. This resurgence or reinvasion of *R. cuneata* was likely due to anthropogenic actions (Hopkins and Andrews 1970). For instance, a stable population in the Hudson River is hypothesized to have arisen as a result of ballast water exchange from the Gulf of Mexico (Carlton 1992). Today, the range of *R. cuneata* extends from the Chesapeake Bay area and vicinity (Richards 1962b; Pfitzenmeyer and Drobeck 1964; Hopkins and Andrews 1970; Abbott and Morris 1995) down the Atlantic coast into the Gulf of Mexico (Woodburn 1962; Andrews 1971) and as far south as parts of Veracruz (Stark 1977) and Laguna de Pom of Laguna de Terminos, Campeche, Mexico (Alvarez-Legorreta et al. 1994). There is a report of this species found in the mangroves of the Martinique Islands in the Caribbean (Lécuyer et al. 2004). *Rangia cuneata* has since invaded the Baltic Sea (Rudinskaya and Gusev 2012) and other parts of European coastal waterways. Due to rapidly increasing population numbers in certain habitats, infrastructure has been affected including blockage of fire hoses in Delaware (Counts III 1980) and industrial water pipes

in Antwerp (Verween et al. 2006). It is proposed that blockages can occur because *R. cuneata* is able to exploit even a thin layer of soft sediment to establish a population. Once settled, sedimentation increases due to the presence of the clams, which leads to increasing numbers of clams and consequent blockage of the pipes (Verween et al. 2006). Aside from reported annoyances and invasions, various aspects of this species have been studied in some detail ranging from human consumption and life histories to environmental impacts.

Two other species have been described in the genus *Rangia*, *Rangia flexuosa* and *Rangia mendica*. Both species may be found alongside or in the same system as *R. cuneata*. *Rangia cuneata* and *R. flexuosa* are known to occur sympatrically (Conrad, 1839) (Foltz et al. 1995). *Rangia flexuosa* has been reported in the Gulf of Mexico from Louisiana (Abbott and Morris 1995) to Vera Cruz, Mexico (Stark 1977), but is not nearly as common as *R. cuneata* (Andrews 1971). Some of the morphological differences between *R. flexuosa* and *R. cuneata* include a greater elongation of the posterior end of the shell in the former. Between these two species, the pallial sinus is described as more defined in *R. cuneata* and *R. cuneata* also possesses a longer posterior lateral tooth compared to that found in *R. flexuosa* (Wakida-Kusunoki and MacKenzie 2004). The third species in this genus, *R. mendica* (Gould 1851), has been found in low salinity estuaries along the coast of Mexico (Stark 1977). Little to no information is available for *R. mendica* besides its reported existence along the Atlantic and Pacific coasts of Mexico (Huber 2010).

Life history and sympatry

Much of the life history of *R. cuneata* has been studied from gonadogenesis and gametogenesis to growth rates and proposed life spans in various ecosystems. *Rangia cuneata* is a dioecious species with an exception mentioned by Olsen (1976a) who found that 2.1% (n = 238 slides) of a population in Ochlokonee River Estuary, Florida, was hermaphroditic. In some bivalves, such as freshwater mussels and blood clams (*Anadara* spp.), male and female gonad can be differentiated based on color of the tissue (Walker et al. 2006; Afiati 2007). Gonadal coloration and appearance of a single species may differ depending on the locality within a single system; however, in most cases this is due to presence or absence of gametes. For example, Fairbanks (1963) noted that *R. cuneata* along the north shore of Lake Pontchartrain possessed pale and flaccid gonads in contrast to those along the south shore that possessed opaque and firm gonads when observed along the same time frame. Additionally, a gonadal tissue color range of white, orange, or red is not uncommon (Fairbanks 1963; Cain 1972) in any studied population of *R. cuneata*. These differences in coloration and appearance are not surprising given that temperature, salinity, and other environmental factors affect gametogenesis and spawning. Thus, depending on the environmental factors of the system in which a population of *R. cuneata* is found, reproductive stages can be inter- and intraspecifically different.

Gonadogenesis was thought to begin once a shell length of approximately 25 mm was obtained (Fairbanks 1963); however, clams as small as 14 mm have been reported to possess gonads (Cain 1972). Water temperature and salinity are the most important cues (10-15°C; 3-5 ppt) for gametogenesis and spawning to occur (Cain 1972; Jovanovich and

Marion 1989), with fully ripe gonads forming with increasing water temperature (Cain 1975). Spawning, triggered by increasing salinity, occurs from late spring to early fall, but can occur more than once in a single year (Fairbanks 1963; Chanley 1965; Jovanovich and Marion 1989). Variations in reproductive cycles and spawning periods are not unusual given the extent of *R. cuneata*'s range (Cain 1975; Lane 1986; Fritz et al. 1990). Asymmetrical reproductive cycles have been reported in populations of other bivalve species located at different latitudes (Giese 1959; Ropes 1968; Loosanoff 1969; Jovanovich and Marion 1989). Local conditions may play a role within populations (Giese 1959), but whether or not populations of *R. cuneata* differ with respect to when they become reproductively active based on their location is unclear (Giese 1959).

With regard to gametogenesis, Ropes and Stickney (1965) have established five gametogenic phases for males and females (early and late active, ripe, partially spawned, and spent), but advise that divisions between the phases may not be obvious or easy to determine under microscopy. Other references may use a different scale with added sub-phases and with more or less than the stated five phases. For example, Delgado and Camacho (2005) listed four stages in a study determining gonadal development relationship to food availability in the venerid *Ruditapes decussatus*. The stages included sexual rest (I), initiation of gametogenesis (II), advanced gametogenesis (III), and reproduction period (IV). Partial spawning may occur during stage IV (Delgado and Camacho 2005). Stages were determined based on developmental phase of gametes. Partial spawning may be indicated by a reduction in the number of ripe gametes, but a large (~50%) percentage of gametes are still present in the gonad. This may be followed in subsequent months by another increase in the number of gametes and a final spawning

event, in which nearly all gametes are released from the gonad. A study by Afiati (2007), on two species of *Anadara*, used a follicular system based on gametogenic stages such as early, developing, ripe, spawning, spent, and redeveloping. These stages were further broken into three sub-stages (e.g., "redeveloping female stage 2"; Afiati 2007). Modifications of previously published descriptions of gonadal phases or stages (Marroquin-Mora and Rice 2008) were also encountered in the literature.

At the periphery of the female gonad, oogonia are embedded in or attached to the follicle (also called alveolar) wall via a peduncle, marking the early active or first phase. These oocytes are not of a singular shape (Cain 1972; Olsen 1976a). The nuclei of oocytes can range anywhere from 5 to 20 μm in diameter. The late active or second phase of gametogenesis begins when primary oocytes begin to enlarge away from the follicle walls. The third phase is the ripe phase, recognized when interstitial fluid is virtually absent (Olsen 1976a) and oocyte nuclei are approximately 30 μm in diameter (Cain 1972). The last two gametogenic phases, partially spawned and spent, involve eggs that were not released and are eventually broken down by immune cells (Olsen 1976a) or hemocytes.

In males, spermatozoa can be found abundantly located along thickened follicle walls indicating an early active phase of gametogenesis. Spermatocytes fill the lumen in the late active phase. Primary and secondary spermatocytes are a few microns in diameter. Secondary spermatocytes, or spermatids (Cain 1975), multiply, forming dense masses or sperm balls (Cain 1975), and become spermatozoa with eosinophilic tails directed towards the center of the lumen when males are in the ripe phase. For reasons unknown, males may remain ripe long after female gonads are spent (Cain 1972).

Partially spawned and spent phases in males are similar to females where the lumens appear to be near or completely empty of gametes. Remaining sperm undergo cytolysis by immune cells (Cain 1975; Olsen 1976a).

Rangia cuneata are known broadcast spawners where the gametes of both sexes are released through the excurrent siphon into the water column and observed as a pale coloration with a granular texture (female oocytes) or a thin milky white stream (male sperm) upon release (Cain 1975). In contrast, Chanley (1965) states that gametes of both sexes appear as a thin white stream. After fertilization, zygotes obtain a diameter of nearly 70 μm. Within nearly nine hours, a ciliated blastula develops followed by a pelagic trochophore stage at 26 hours (Fairbanks 1963). However, Chanley (1965) reported that within 24 hours post-fertilization, the larvae form a shell with a straight-hinge, and a yellow color that darkens and intensifies with growth. As growth continues to a size of 60-75 μm, the larvae become rounded and the straight-hinge line becomes masked. Metamorphosis typically begins after six days (~ 160 μm in length) with the first sight of a functional foot. A statocyst is present at the base of the foot. Gills form shortly thereafter at a larval length of approximately 180 μm. At the cost of shell length, shell height increases, and rounded anterior and posterior ends become the most noticeable characteristics of larvae prior to metamorphosing into a juvenile (Chanley 1965). From here, juvenile clams retain a similar shape into adulthood (Chanley 1965).

In terms of environmental conditions, embryos are unable to develop in freshwater (Cain 1975). Cain (1975) reported optimal conditions for embryos at 18-29°C and 6-10 ppt. Larvae can survive a range of temperatures as well as salinity, but appear to better tolerate a temperature and salinity range of 8-32°C and 2-20 ppt, respectively (Cain

1972; Cain 1973). Adults appear to be able to tolerate a similar temperature and salinity range, with a preferred salinity range of 0-18 ppt (Hopkins et al. 1973) and a reported limit of 20 ppt (Cain 1972), but have been known to tolerate up to 38 ppt (Hopkins et al. 1973).

Sympatric species

Whereas *R. cuneata* accounts for a major percentage of the benthic biomass in certain areas (e.g., upper James River Estuary, Chesapeake Bay) (Cain 1972; Pfitzenmeyer 1972), other species of bivalves may be present including *Macoma balthica*, *Macoma mitchelli*, and *Ischadium recurvum* (Wells 1961; Cain 1972). In a study of the fauna associated with oyster beds in Newport River, Beaufort, NC, *R. cuneata* was present in the muddy substrate between or under the eastern oyster, *Crassostrea virginica* (Wells 1961). *Polymesoda caroliniana* (Bosc 1801; Veneridae, Cyrenidae), the marsh clam, coexists with *R. cuneata* in estuarine systems in Florida (Olsen 1976a, 1976b; Marelli 1987), Alabama (Swingle and Bland 1974), Mississippi (Duobinis-Gray and Hackney 1982), Louisiana (Fairbanks 1963; Hoese 1973), and in areas of Eastern Mexico (Wakida-Kusunoki and MacKenzie 2004).

Less information is available on *P. caroliniana* than *R. cuneata*. More research has been published on a congeneric species inhabiting parts of the Philippines (e.g., *Polymesoda erosa*), specifically its reproductive strategies and cycles (Dolorosa and Dangan-Galon 2016). While there is no known economic value for *P. caroliniana* in the United States, species of *Polymesoda* in the Southeast Asian countries are harvested for food. Over harvesting and habitat loss seem to be driving the increase in studies assessing life span and reproductive strategies for *P. erosa* (Dolorosa and Dangan-Galon 2016). No

studies assessing the phylogenetic relationships within the genus *Polymesoda* were found. Specimens of *P. caroliniana* are not described to reach reported sizes of *P. erosa*, but size may be influenced by location (i.e., more food availability and warmer temperatures in the Philippines).

Although *R. cuneata* and *P. caroliniana* can be found near each other, one reference stated that the physiology of *P. caroliniana* allows it to be intertidal while *R. cuneata* is only subtidal (Marelli 1987). It remains unclear as to whether physiological differences cause this spatial separation, but it has been proposed that larvae of *R. cuneata* fail to settle or survive in intertidal zones (Marelli 1987). Regardless, the assertion that *R. cuneata* is strictly subtidal does not hold true in the study site reported in this dissertation, as *R. cuneata* have been found in areas exposed to the air during low tide for several hours.

Environmental impacts of Rangia cuneata

Bivalves biochemically alter the composition of the water column and the sediment they inhabit through filtering particulates from the water column and bringing in material from the sediment via the foot or mantle cavity. Nearly all elemental biogeochemical cycles are affected including carbon (Doering et al. 1986; Chauvaud et al. 2003), nitrogen and phosphorus (Asmus et al. 1995), silicate (Dame et al. 1991), and sulfur (Hansen et al. 1996). For example, ammonia fluxes are noticeably higher in bivalve beds in contrast to substrate with no bivalves (Prins and Smaal 1994). In addition to alterations as a result of filtration, bivalves deposit biochemically altered and unaltered, or indigestible, material known as pseudofeces onto the sediment surfaces (Norkko et al. 2001). Pseudofeces may be mixed with unaltered or incompletely digested

algae (e.g., diatom frustules) (Olsen 1976b) and sand, and then expelled from the mantle cavity (Fairbanks 1963; Wong et al. 2010). Feces and pseudofeces are an important component of sediment, because the nutrients are cycled and may be used further by microbial or pelagic organisms (Vaughn and Hakenkamp 2001). As a result, bivalves are able to transfer energy to other trophic levels (Rosenberg 2001). Local microbial food webs, infaunal and epifaunal macrobenthic organisms, phytoplankton and pelagic predators that inhabit the same area are all affected by transfer of energy (Schaffner et al. 1987; Rosenberg 2001). Sediment characteristics such as permeability, porosity, and the microtopography of the sediment surface can be drastically altered by the deposition of feces, pseudofeces or mucus, bivalve movement through the sediments, and formations such as pits or mounds (Graf and Rosenberg 1997). In addition, sediment chemistry is also affected (Phelps et al. 1969); for example, higher oxygen levels can be detected in the top few centimeters of sediment or deeper when in proximity to burrowed or burrowing bivalves (Aller 1982). By altering the microtopography of the sediment surface and sublayer, bivalves can indirectly allow or enhance the formation of bacterial mats and films of diatoms (Graf and Rosenberg 1997). Diatom films reduce shear stress causing turbulence in the water column to develop at higher angular velocities (de Jonge and van der Bergs 1987; Delgado et al. 1991) resulting in greater stabilization of sediments. While sediment stabilization via diatom-produced mucilage has been reported from laboratory studies, it has only been suggested from field observations (Paterson 1989). In contrast, bare sediments (e.g., coarse sand with little to no microbial life) experience greater turbulence, causing scouring at the sediment surface (de Jonge and van der Bergs 1987), which may affect recruitment and settlement of bivalve larvae.

Although bivalves may allow formation of microbial mats, they will also filter and consume microbes, detritus, and possibly even larvae of bivalves and those of other organisms. Gut contents of *R. cuneata* have reportedly contained detritus (> 50%), algae (~17-20%), and sand (Darnell 1958). Plant material and diatom frustules or remnants have also been reported (Darnell 1961, Cleveland 2003). The effect of bivalves on larval recruitment of any organism that broadcast spawns has been under debate. Theoretically, any filter-feeder could filter out suspended gametes or larvae and consequently alter the future distribution of organisms. For example, Commito and Boncavage (1989) found a positive correlation between mussel beds and oligochaete abundance (i.e., greater the density of mussels, the more oligochaetes were present).

Filtering also affects water column turbidity and clarity. Few studies have been conducted on water column clearance rates by *R. cuneata* in a laboratory setting or in the field beyond those conducted in Lake Pontchartrain and the upper region of Barataria Estuary in southeastern Louisiana (Lakes Cataouatche, Salvador and Lac des Allemands) (Wong et al. 2010). Bivalve clearance rates are generally calculated based on the reduction of Chlorophyll-*a* concentration within a selected time span. For this calculation to be accurate, the volume of the ecosystem or mesocosm as well as the initial Chl-*a* concentration must be known. In Lake Salvador and Lac des Allemands, *R. cuneata* were determined to filter approximately 1.35 and 2.27 L h^{-1}, respectively; while a filtration rate of 2.06 L h^{-1} g^{-1} was determined by dry tissue weight for both systems (Wong et al. 2010). Assuming an active filtration period of 24 hours per day, with a biomass of 15.9%, 40%, and 99.9% (Lake Cataouatche, Lac des Allemands, Lake Salvador, respectively), authors estimated a filtering rate of the lakes between 1.0 and 1.5 days (Wong et al.

2010). Although there is no information on differences in clearance rates between juveniles and adults, due to morphological size differences and differing metabolic requirements, adults would presumably be able to clear a greater volume of water faster than juveniles. While epifaunal bivalves (e.g., *Geukensia demissa*) can filter the water column, but live attached to a hard substrate, infaunal bivalves such as *R. cuneata* and *P. caroliniana* live buried in the substrate. A strong foot is required for settlement and burrowing into a substrate.

Burrowing and pedal shape

While pedal shape differs between some families of bivalves, as a likely result of coevolution with habitat substrate, burrowing appears to vary little between families and species of infaunal bivalves (Stanley 1975). A sequence of burrowing behaviors has been recognized (Stanley 1975), which involves probing with the foot upon the sediment until it reaches a certain depth, presumably the maximum length of extension. Closure of the siphons in conjunction with contraction of the adductor muscles causes an increase in pressure in the mantle cavity, subsequently increasing hemolymph volume in the foot for anchorage. Retractor muscles pull the shell forward in a rocking motion. Once the animal is pulled forward to its farthest extent, the siphons open relieving pressure in the mantle cavity. Several burrowing events in any species of infaunal bivalve must take place in repetitive cycles. After one cycle, the foot probes deeper and initiates the next series of burrowing activity (Trueman 1966). The clams undergo a rocking motion, which is critical to successful burrowing, because an erect clam on top of the sediment cannot push (or pull itself) straight down (Stanley 1975). Clams have two retractor muscles, anterior and posterior. The orientation of these muscles, the weight distribution of the

clam, and the distribution of any resisting forces of the sediment adjacent to the shell are important factors in order to reduce upward slippage and maintain a downward direction when burrowing (Stanley 1975). In burrowing bivalves, a prosogyrous shape with a nearly flat lunule helps the bivalve to resist strain from burrowing into coarse sediment. Otherwise, the organism would slide forward instead of down (Stanley 1970).

Pedal Morphology and Ultrastructure of Clams

Background on bivalve pedal morphology and ultrastructure

Evolution appears to have favored foot morphology that facilitates living in a specific type of sediment (Rhoads and Young 1970). Foot morphology correlates strongly with the type of substrate and habitat, and less so with burrowing depth (Stanley 1970; Oliver and Allen 1980). *Rangia cuneata* is an infaunal siphonate deposit feeder (Kranz 1974) that possesses a wedge- or hatchet-shaped foot with an ill-defined heel curving smoothly from the visceral mass towards a well-developed, pointed toe. The foot appears to provide two major functions. The primary function of the foot is for burrowing and anchoring the body into the substrate. In addition to this, it has been shown that the foot is likely used for feeding and removal of sediment from the region of the mouth (Morton 1973). While at least one researcher has stated that *R. cuneata* lacks the structures for possible pedal feeding (Marelli 1987), evidence collected to date and reported in this dissertation contradicts that presumption.

A review by Cooper (1981) stated that there had been little interest in *R. cuneata* besides the few studies that observed its ability to osmoconform and osmoregulate. Since then, some research has been performed beyond tolerance of salinity regimes, but a study on the pedal ultrastructure in this species has not been undertaken. While pedal

ultrastructure has been reviewed in other species (e.g., *Mytilus edulis*, *Gomphina veneriformis*) there are debates on how similar the ultrastructure is between species, particularly between sympatric species. For instance, alongside *R. cuneata* exists *Polymesoda caroliniana* (Veneroida: Cyrenidae) in Johnson Bayou, MS. Very little is known about *P. caroliniana*, and pedal ultrastructure is one of the areas where knowledge is lacking. The range of *P. caroliniana* extends in estuarine systems from Virginia to parts of the Gulf Coast (Duobinis-Gray and Hackney 1982). One report stated that *P. caroliniana* has a well-developed foot, but their position in the substratum is limited or difficult for them to maintain (Andrews and Cook 1951). This statement is unclear based on lack of previous gross morphological evidence, and observations reported in this dissertation in which *P. caroliniana* has been found burrowed as deeply as *R. cuneata*. A comparative look into the pedal ultrastructure will provide new insights into these species' ability to burrow and their role in estuarine ecosystems, particularly in Johnson Bayou where multiple types of sediments are present.

A major focus of this project involved understanding the pedal musculature, as the foot is capable of movements including elongation, contraction, torsion, and bending (Kier 1988). The system for pedal motion is thought to be hydrostatic, in which cavities within the tissue become distended with hemolymph, causing an increase in pressure and consequential swelling (Kier 1988). The hydrostat system relies on antagonism between the pressure produced by incoming hemolymph and the pedal musculature; however, this has been studied in few bivalves (Kier 1988). In conjunction with a neuromuscular system, local muscle contractions occur depending on the pattern and direction of burrowing (Trueman 1966; Trueman 1967; Kier and Smith 1985). A bivalve's foot

movement is thought to be largely via hydrostatic pressure regardless of burrowing or feeding positions (Kranz 1974; Kier 1988).

Research performed by Park et al. (2012) on the foot of the venerid *Gomphina veneriformis* is one of the most recent studies on pedal ultrastructure. The foot, as described from outer to inner, has an epithelial layer of ciliated columnar cells and secretory cells, a connective tissue or subepithelial layer rich in collagen fibers, and a muscular layer (Park et al. 2012). Observations utilizing transmission electron microscopic (TEM) techniques revealed a dense microvilli layer present amongst the cilia on the epithelium of *G. veneriformis* (Park et al. 2012). Two types of secretory cells in the pedal epithelium contain acidic mucopolysaccharide-rich granules confirmed from Alcian Blue - Periodic-acid Shiff (AB-PAS) (pH 2.5) staining (Park et al. 2012).

The production of mucus (or mucins, as reported in some of the literature), particularly in invertebrates, has been shown to be essential in movement patterns, defense, and prevention of desiccation among other functions (Denny 1989). Mucins are lipids or proteins linked to sugars, that when combined make mucin (Nakamura et al. 2013). However, the term "mucin" is somewhat vague, and "mucus" is the preferred term for external secretions from an epithelium (Davies and Hawkins 1998). In addition to locomotion through and adhesion to sediment particles during burrowing, the cilia and mucus might function in capturing and transporting food particles toward the gills or labial palps for processing. This would lend credence to so-called pedal feeding (Marelli 1987).

In bivalves, mucus production occurring from the pedal aperture, an unfused portion of the mantle margin from which the bivalve foot emerges, has been observed

since the early 1900s (Norenburg and Ferraris 1990). Norenburg and Ferraris (1990) studied glands from which mucus is produced and released in *Mya arenaria*. Glands located in the mantle tissue surrounding the pedal aperture give this tissue a brownish color. These glands produce mucus from two types of secretory cells, mucus goblet and bacillary mucus cells. Mucus goblet cells are outnumbered by bacillary mucus cells in *M. arenaria* (Norenburg and Ferraris 1990). Also in *M. arenaria*, homogenous, granular material packed in small secretory vesicles (0.3-0.6 μm in diameter) is found in mucus goblet cells and heterogeneous granules are abundant in bacillary mucus cells. The secretory vesicles stain positive for sulfated and nonsulfated mucosubstances; the latter apparently predominates in bacillary mucus cells (Norenburg and Ferraris 1990). In species that do not burrow (e.g., *Mytilus edulis*), multiple glands may be found in the foot prior and during settlement and subsequent metamorphosis. Up to nine glands were found in the pediveliger foot of *M. edulis*. Of the nine glands, two secrete weak acidic mucopolysaccharides and proteinaceous vesicles, which is presumably used to enhance ciliary gliding during pedal movement and thought to function in adhesion during pedal crawling, respectively (Lane and Nott 1975). The remaining glands are involved in byssus formation (Lane and Nott 1975). Infaunal clams do not produce a byssus, but it may be possible to see how the foot and its composition compare between species (infaunal and epifaunal), shedding light on evolutionary relationships based on phenotypes and how close the morphology is of structures between species of different families and orders.

Shell Morphology and Ultrastructure of Bivalves

Shell morphology and growth in bivalves

The shell of bivalves has four major orientations or regions: dorsal, ventral, posterior, and anterior. The dorsal part of the shell, the umbo, is the oldest part, and the ventral margin is the youngest, indicating that growth occurs outward from the umbo. Depending on the species, shell formation may not be a uniform, unidirectional process. Scallops (e.g., *Pecten* spp.) are an exception because they have equivalves, and formation is consequently fairly uniform, but in all bivalves the deposition of shell material occurs the fastest across the area of greatest inflation (Rosenberg 1980).

Bivalve shells are generally comprised of three major regions: periostracum, prismatic, and nacre. With the exception of the periostracum (a thin, organic layer covering the external surface of the shell), the other layers are composed of aragonite (e.g., nacre), calcite, or both (Carter 1980). The prismatic layer of the shell in many bivalve Orders is composed of aragonite, but some (e.g., oysters and some venerids) may be composed of calcite, possibly in addition to aragonite (Carter 1980). The inner prismatic layer may be composed of compact sheets or variously oriented crystals of calcium carbonate. In many species, there are two structurally different prismatic layers, separated by a pallial myostracum. The myostracum is the site of mantle tissue attachment. The mantle tissue is responsible for controlling shell deposition. As shell growth progresses from the umbo to ventral margin, the soft tissue also grows and the prior points of attachment between mantle tissue and shell fills in with aragonite, but leaves a distinct line that can be visualized in shells that have been sectioned (Fritz and

Haven 1983; Fritz et al. 1990). The nacre is the innermost shell layer that is in direct contact with the soft body of the organism.

Why certain bivalves produce shells out of aragonite and others of calcite is unknown. Aragonite is more dense (2.93 g mL^{-1}) than calcite (2.71 g mL^{-1}), but the latter is more thermodynamically stable (Epstein et al. 1953). The outer prismatic layer is typically composed of calcite. It is hypothesized that the presence of a less dense, but more stable crystalline structure in contact with the external environment provides support for infaunal bivalves. Thus, the production of calcium carbonate in the form of calcite can decrease density to prevent sinking of the clam too deep or easily, and the clam can acquire protection from water quality extremes (e.g., increase in acidity or erosion) (Carter 1980).

Shell is laid down as rings, or microgrowth increments, that form growth bands. According to Lutz and Rhoads (1980), there are at least five temporal categories of microgrowth increments: annual, fortnightly, monthly, semidiurnal and diurnal, and semiperiodic (e.g., spawning events). These increments or bands have been used to determine growth patterns and age in bivalves since the mid- to late 1900s (Clark 1979; Fritz and Haven 1983; Fritz et al. 1990).

The shell ultrastructure of several species (e.g., *Mercenaria mercenaria*, *Geukensia demissa*, *Arctica islandica*, *Anadara granosa*, *Cerastoderma edule*) (Ansell 1968; Pannella and MacClinktock 1968; Farrow 1971; Brousseau 1984; Richardson 1987; Weidman 1995) have been extensively studied, including *Rangia cuneata*. A study by Taylor et al. (1973) on the shells of *R. cuneata* discerned three primary carbonate layers: a thin pallial myostracum composed of aragonite in between outer and inner

crossed lamellar layers. The lamellae may be composed of crystalline sheets of foliate crystals or rod-like crystals. These lamellae may cross one another's orientation during growth (Lutz and Rhoads 1980). According to Taylor et al. (1973) and Fritz et al. (1990), the outer shell layer consists of three orders (1°, 2°, and 3°) of lamellae. These orders are based on how the crystals of carbonate are arranged. First-order (1°) are concentrically arranged and parallel to the ventral margin, while second-order (2°) are laid down in an imbricated fashion. Third-order (3°) lamellae are rod-like crystals, but these are difficult to visualize, because of their small size and apparently compose some 2° lamellae (Taylor et al. 1973, Fritz et al. 1990).

Fritz et al. (1990) discovered two types of crossed lamellar microstructure comprising the outer shell layer in a Delaware estuary population of *R. cuneata*. A fast-growth microstructure layer deposited during the spring and fall, and a slow-growth microstructure layer deposited in the summer. Distinction between the crossed lamellar microstructure was determined from the width of the 1° lamellae, angle deposition of this lamellae towards the inner shell surface, and the interdigitation of 2° lamellae between adjacent 1° lamellae (Fritz et al. 1990). Typically, 1° lamellae are broad while 2° lamellae are narrower and can be sharply angled with respect to the inner shell surface. Prismatic bands, or sublayers, can be deposited and replace lamellae during winter, which has been used to determine age (Ropes et al. 1984, Fritz et al. 1990). Whether this replacement is a result of shell dissolution of previously formed lamellae is unclear. No growth occurred during winter in the Delaware population as established by replacement of crossed lamellar microstructure by the prismatic bands (Fritz et al. 1990). Albeit rare, more than one prismatic band can be found during a single winter season (Fritz et al. 1990). The

presence of multiple bands in a single winter season is likely more common in faster growing juveniles (Fritz et al. 1990). Slow-growth crossed lamellar microstructure is composed of larger, more ordered 1° lamellae in this population indicating a population of slow-growers (Fritz et al. 1990).

Caution must be taken in interpreting which bands and increments indicate "after-the-fact" results. In a study on *M. mercenaria*, broad, translucent bands were interpreted to indicate fast growth, and narrow, opaque bands indicate slow growth (Clark 1979). Yet, others state the opposite (thin, opaque bands indicate fast growth) (Fritz and Haven 1983; Fritz et al. 1990). Most agree that broad, thick growth bands indicate warm water temperatures, while narrow, tightly packed growth bands indicate cold water temperatures at the time of shell deposition (Lutz and Rhoads 1980; Fritz and Haven 1983; Fritz et al. 1990). According to Fritz et al. (1990), *R. cuneata* grew at a faster rate in the most northern limits of this species, but cautioned that the methods utilized and compared with other studies (e.g., Fairbanks 1963; Wolfe and Petteway 1968), can affect the interpretation of the results. Nearly all published literature regarding shell growth and cessation states that environmental variables play a major role in shell growth rate (Lutz and Rhoads 1980, Fritz et al. 1990).

Research on shell growth has shown that species respond differently to environmental factors (Ansell 1968; Kennish and Olsson 1975; Green 1980). Temperature appears to be the strongest environmental factor for shell growth (Kennish and Olsson 1975), and is correlated with growth patterns (Jones et al. 1990). Bivalves may cease shell growth or produce very little during winter, most likely due to colder temperatures (Fairbanks 1963; Clark 1979; Green 1980; Tanabe 1988; Dettman et al.

1999; Chauvaud et al. 2005). A study on *R. cuneata* in Lake Pontchartrain showed that the highest growth rate occurred during early summer (Fairbanks 1963). Similarly, in the marine clam, *M. mercenaria*, band widths are correlated positively with annual average water temperature (Jones et al. 1990), but in another marine clam, *Spisula solidissima*, band widths are negatively correlated with water temperature (Jones 1980). While studying two populations of *M. mercenaria*, Kennish and Olsson (1975) reported that thermal discharge from a nuclear generating station in Oyster Creek, NJ kept the surrounding water temperature at 30°C, which stunted the growth (growth is curbed around 25°C; Ansell 1968; Kennish and Olsson 1975) and consequently prevented spawning events from occurring in clams within a mile radius from the discharge canal. In contrast, clams in the nearby Barnegat Bay (< 30°C) showed normal growth patterns and undertook expected spawning events (Kennish and Olsson 1975). Thus, these reported discrepancies could be based on hypothetically optimal temperature values for maximum growth. At which point, if temperatures increase beyond this optimal value, growth may be negatively affected.

In addition to temperature and seasonality, high sedimentation and storms can cause siphon and mantle closure with subsequent cessation of shell accretion (Fairbanks 1963). During times of valve closure, the bivalve cannot feed or acquire oxygen. Bivalves can switch to anaerobiosis for a time, but build-up of succinic acid will cause metabolic harm. To counteract the effects of succinic acid build-up, shell may be broken down by actions of organic material and be used as an internal alkali buffer (Seed 1980). An indication that dissolution occurred may be indicated by a greater presence of organic material (organic matrix) (Gordon and Carriker 1978) and depressions in the shell layers.

Microgrowth increments and growth bands of fossil shells and those of living bivalves can show signs that the bivalve was stressed, because an interruption occurs in the normal deposition of shell material. However, the actual disturbance can be difficult to determine if ecological and environmental parameters were not recorded at that time (Ridgway et al. 2011).

Other environmental factors and geographical location are also known to have an effect on growth and shell deposition. For example, it has been found that an increase in salinity correlates with a decrease in the shell size of *R. cuneata* (Hoese 1973; Tarver and Dugas 1973). Food supply and available nutrients are provided by tidal periodicity and the clams' intertidal position (Kennish and Olsson 1975; Lutz and Rhoads 1980). *Mercenaria mercenaria* and *Tridacna squamosa* are two bivalves whose growth patterns show tidal periodicity (Pannella and MacClintock 1968). As a factor of substrate composition, water circulation above sand generally provides greater food availability to a bed of clams. In support of this, Kennish and Olsson (1975) discovered a correlation between substrate type and growth rate in a population of *M. mercenaria* in Barnegat Bay, New Jersey. Clams in muddy substrate grew at a much slower rate than those in sand (Kennish and Olsson 1975).

In times of stress such as extreme winter temperatures, storms, or other disturbances or physiological changes (e.g., spawning), rearrangement of structural elements will affect how the inner and outer shell layers are constructed (e.g., as studied in a *M. mercenaria* population in Connecticut and Massachusetts; Pannella and MacClintock 1968). These "growth breaks" can offer valuable insight into the relationship between bivalves and their environment, specifically with respect to seasonal

changes or abrupt events. Different growth breaks correspond to a specific type of shock, which can be observed when looking at growth increments. According to Kennish and Olsson (1975), every event or shock is an interruption in the daily deposition of shell material. Depressions in the shell layers, differences in band coloration, and crossed lamellae (e.g., crossing of rods or foliate crystals) are various indications that shocks have occurred and a severe stress imposed on the organism. The main types of "shock" are storm, spawn, tidal, and thermal-, heat-, and freeze- (or cold-) shock (Kennish and Olsson 1975). Abrasion is considered a growth break, similar to thermal-shock, but is typically less conspicuous, because the bivalve recovers more quickly (Kennish and Olsson 1975).

While shocks may affect the growth pattern or stunt growth (Hallam 1965), the species and location seem to have the largest effect on whether the animal will add material to its shell, based on variability within and between populations, even if the populations are under the same environmental influences (Green 1980; Fritz and Haven 1983). Populations at different latitudes show mixed results. A population of *M. mercenaria* off the coast of Georgia did not show any growth bands indicative of winter cessation compared to other populations along the Atlantic coast (Clark 1979; Fritz and Haven 1983). In contrast, no growth variation was reported within or across six populations of *G. demissa* between Connecticut (Brousseau 1984) and Georgia (Kuenzler 1961). The production of growth bands along a particular growth pattern influenced by the environment has been shown to be highly conserved. Transplantation studies with *M. mercenaria* that show shifts in microgrowth increments, particularly with respect to conditioning and spawning, support this observation (Rhoads and Pannella 1970; Doall et

al. 2008). Thus, populations of *R. cuneata* in the Gulf of Mexico versus the northern Atlantic coast of the United States may differ in growth rate and life span.

The growth of *R. cuneata* in Trent River, NC was studied for two years by Wolfe and Petteway (1968) using a hypothetical decaying exponential equation known as the von Bertalanffy growth curve (von Bertalanffy 1938). This growth curve has been used extensively for other bivalves (e.g., *G. demissa*; Brousseau 1984, *Macoma balthica*; Cloern and Nichols 1978). Wolfe and Petteway (1968) determined that sizes of *R. cuneata* in Trent River fell into five distinct classes. These size classes are based on length of the maximum axis of growth (of the left valve) and a calculated percentage frequency of each length for every sample of clams. Based on their observations, calculations, and that larval settling of *R. cuneata* is presumed to occur when a shell length of 0.375 mm is reached (Fairbanks 1963), a clam could reach a length of 75 mm in 10 years (Wolfe and Petteway 1968). Being entirely hypothetical, out of an average number of 524 clams measured from 12 samplings in the Trent River, only seven clams with lengths in excess of 70 mm, with a reported maximum of 73 mm, were encountered (Wolfe and Petteway 1968).

Shell size has been and may still be used as a proxy for estimating age in several species of bivalve (Fairbanks 1963, Kennish and Olsson 1975, Green 1980). While not addressed for *R. cuneata* and *P. caroliniana* in this dissertation from Johnson Bayou, it should be stressed that aging and interpretation of age continues to be a highlight of research. Growth rings are the most common method for estimating age, specifically those formed in the hinge ligament. However, in species that live > 300 years (e.g., *A. islandica*; Schöne et al. 2005), the rings may become too compressed to be reliable. The

compression of growth bands has been reported in *Modiolus modiolus*, the horse mussel. This species is native to the North Sea and surrounding areas and produces growth lines that converge and get compressed into blocks of aragonite, making the process of resolving age and growth pattern difficult (Anwar 1990). Outer growth rings are then counted as a means of estimation (Wanamaker et al. 2009; Butler et al. 2013). Even then, growth breaks and the physiological responses bivalves have under the influence of environmental factors makes age determination by counting growth rings hypothetical and sometimes unreliable.

Based on shell size, *R. cuneata* reportedly lives four to five years (Fairbanks 1963) with a maximum age range of 15-20 years (Hopkins et al. 1973; Harrel and McConnell 1995). The age range of *Polymesoda caroliniana*, the second species of interest in this dissertation, is and remains unknown. The shell of *P. caroliniana* is too thin, much like that of *Mya arenaria* (Cerrato et al. 1991), and is too easily eroded or chipped to be reliable in estimating age.

Shell ultrastructure and growth patterns are important to understand when the species is of economic interest (e.g., age of reproductive capability), used to examine population dynamics (e.g., mortality and recruitment; Hallam 1972), and used to analyze the presence of specific elements within shell and compare levels to past environmental levels.

Elemental analysis

As species deposit shell material, the levels of elements incorporated into the shell (namely oxygen, carbon, and calcium) are in equilibrium with the external environment. Since the elements are essentially trapped in shell unless dissolution occurs, one may

determine the level of elements in a body of water at the time the bivalve was alive. For those that lived hundreds of years before the present, the shells can be used as paleoproxies (Lutz and Rhoads 1980, Schöne et al. 2005).

As an example, Weidman (1995) was able to reconstruct a 109-year record of bottom water temperatures from Nantucket Shoals by analyzing the $\delta^{18}O$ measurements from shells of *A, islandica*, because oxygen in the carbonate of the shell is in isotopic equilibrium with that in seawater. Bivalves primarily living in low latitudes have been the main subjects in sclerochronological research, because of their long lifespans (e.g., *A. islandica*; Jones 1983, Schöne et al. 2005). The first step regarding composition of shells of any species is to determine what elements are present. As reported in this dissertation, energy dispersive X-ray spectroscopy (EDS) is an invaluable tool for providing evidence of what elements are incorporated in shell material, leading to inferences and future research of potentially spatially mapping the elements and making connections between control of biomineralization and elements present in the habitat.

References

Abbott RT, Morris PA. 1995. A field guide to shells: Atlantic and Gulf Coasts and the West Indies. 4th ed. New York. Houghton Mifflin Company.

Afiati N. 2007. Gonad maturation of two intertidal blood clams *Anadara granosa* (L.) and *Anadara antiquata* (L.) (Bivalvia: Arcidae) in Central Java. J Coast Dev. 10(2):105-113.

Aller RC. 1982. The effects of macrobenthos on chemical properties of marine sediment and overlying water. In: McCall PL, Tevesz MJS, editors. Animal-sediment relationships. New York (NY): Plenum Press. p. 53-102.

Alvarez-Legorreta T, Gold-Bouchot G, Zapata-Perez O. 1994. Hydrocarbon concentrations in sediments and clams (*Rangia cuneata*) in Laguna de Pom, Mexico. Bull Environ Contam Toxicol. 52:39-45.

Andrews J. 1971. Seashells of the Texas Coast. Austin. University of Texas Press.

Andrews JD, Cook C. 1951. Range and habitat of the clam *Polymesoda caroliniana* (Bosc) in Virginia (Family Cycladidae). Ecology. 32(4):758-760.

Ansell AD. 1968. The rate of growth of the hard calm *Mercenaria mercenaria* (L) throughout the geographical range. J Cons Perm Int Explor Mer. 31:364-409.

Anwar NA. 1990. Age determination, growth rate, and population structure of the horse mussel *Modiolus modiolus*. J Mar Biol Assoc UK. 70(2):441-457.

Asmus H, Asmus RH, Zubillaga GF. 1995. Do mussel beds intensify the phosphorus exchange between sediment and tidal waters? Ophelia. 41:37-55.

von Bertalanffy L. 1938. A quantitative theory of organic growth (inquiries on growth laws. II). Human Bio. 10(2):181-213.

Brousseau DJ. 1984. Age and growth rate determinations for the Atlantic ribbed mussel, *Geukensia demissa* Dillwyn (Bivalvia: Mytilidae). Estuaries. 7(3):233-241.

Butler PG, Wanamaker AD, Scourse JD, Richardson CA, Reynolds DJ. 2013. Variability of marine climate on the North Icelandic Shelf in a 1357-year proxy archive based on growth increments in the bivalve *Arctica islandica*. Palaeogeogr Palaeocl. 373:141-151.

Cain T. 1972. The reproductive cycle and larval tolerances of *Rangia cuneata* in the James River, Virginia. [Dissertation]. [Charlottesville (VA)]: University of Virginia.

Cain TD. 1973. The combined effects of temperature and salinity on embryos and larvae of the clam *Rangia cuneata*. Mar Bio. 21:1-6.

Cain TD. 1975. Reproduction and recruitment of the brackish water clam *Rangia cuneata* in the James River, Virginia. Fish Bull. 73(2):412-430.

Carlton JT. 1992. Introduced marine and estuarine mollusks of North America: an end-of-the- 20th-century perspective. J Shellfish Res. 11(2):489-205.

Carter JG. 1980. Environmental and biological controls of bivalve shell mineralogy and microstructure. In: Rhoads DC, Lutz RA, editors. Skeletal growth of aquatic organisms: Biological records of environmental change. New York (NY): Plenum Press. p. 69-113.

Cerrato RM, Wallace HVE, Lightfoot KG. 1991. Tidal and seasonal patterns in the chondrophore of the soft-shell clam *Mya arenaria*. Biol Bull. 181:307-311.

Chanley P. 1965. Larval development of the brackish water mactrid clam, *Rangia cuneata*. Chesap Sci. 6(4):209-213.

Chauvaud L, Lorrain A, Dunbar RB, Paulet Y-M, Thouzeau G, Jean F, Guarini J-M. 2005. Shell of the great scallop *Pecten maximus* as a high-frequency archive of paleoenvironmental change. Geochem Geophy Geosy. 6(1): doi:10.1029/2004GC000890.

Chauvaud L, Thompson JK, Cloern JE, Thouzeau G. 2003. Clams as CO_2 generators: The *Potamocorbula amurensis* example in San Francisco Bay. Limnol Oceanogr. 48(6):2086-2092.

Clark GR. 1979. Seasonal growth variations in the shells of Recent and prehistoric specimens of *Mercenaria mercenaria* from St. Catherines Islands, Georgia. Anthropol Pap Am Mus Nat Hist. 56:161-179.

Cleveland CM. 2003. Benthic-pelagic coupling in northern Gulf of Mexico estuaries: contribution of the suspension-feeding bivalve, *Rangia cuneata* (Bivalvia: Mactridae). [Dissertation]. [Ann Arbor (MI)]: The University of Mississippi.

Cloern JE, Nichols FH. 1978. A von Bertanlanffy growth mode with seasonally varying coefficient. J Fish Res Board Can. 35:1479-1482.

Commito JA, Boncavage EM. 1989. Suspension-feeders and coexisting infauna: an enhancement counterexample. J Exp Mar Biol Ecol. 125:33-42.

Cooper RB. 1981. Salinity tolerance of *Rangia cuneata* (Pelecypoda: Mactridae) in relation to its estuarine environment: a review. Walkerana. 1(1):1-31.

Counts III CL. 1980. *Rangia cuneata* in an industrial water system (Bivalvia: Mactridae). The Nautilus. 94(1):1-2.

Dame R, Dankers N, Prins T, Jongsma H, Smaal A. 1991. The influence of mussel beds on nutrients in the Western Wadden Sea and Eastern Scheldt estuaries. Estuaries. 14(2):130-138.

Darnell RM. 1958. Food habits of fishes and larger invertebrates of Lake Pontchartrain, Louisiana, an estuarine community. Public Institute Marine Science University of Texas. 5:353-416.

Darnell RM. 1961. Trophic spectrum of an estuarine community, based on studied of Lake Pontchartrain, Louisiana. Ecology. 42(3):553-568.

Davies MS, Hawkins SJ. 1998. Mucus from marine molluscs. Adv Mar Biol. 34:1-71.

Delgado M, Camacho AP. 2005. Histological study of the gonadal development of *Ruditapes decussatus* (L.) (Mollusca: Bivalvia) and its relationship with available food. Sci Mar. 69(1):87-97.

Delgado M, de Jonge VN, Peletier H. 1991. Experiments on resuspension of natural microphytobenthos populations. Mar Biol. 108:321-338.

Denny MW. 1989. Invertebrate mucous secretions: functional alternatives to vertebrate paradigms. Symp Soc Exp Biol. 43:337-366.

Dettman DL, Reische AK, Lohmann KC. 1999. Controls on the stable isotope composition of seasonal growth bands in aragonitic fresh-water bivalves (unionidae). Geochim Cosmochim Ac. 63(7/8):1049-1057.

Doall MH, Padilla DK, Lobue CP, Clapp C, Webb AR, Hornstein J. 2008. Evaluating northern quahog (= hard clam, *Mercenaria mercenaria* L.) restoration: Are transplanted clams spawning and reconditioning. J Shellfish Res. 27(5):1069-1080.

Doering PH, Oviatt CA, Kelly JR. 1986. The effects of the filter-feeding clam *Mercenaria mercenaria* on carbon cycling in experimental marine mesocosms. J Mar Res. 44(4):839-861.

Dolorosa RG, Dangan-Galon F. 2016. Population dynamics of the mangrove clam *Polymesoda erosa* (Bivalvia: Corbiculidae) in Iwahig, Palawan, Philippines. Int J Fauna Biol Stud. 1(6):11-15.

Duobinis-Gray EM, Hackney CT. 1982. Seasonal and spatial distribution of the Carolina marsh clam *Polymesoda caroliniana* (Bosc) in a Mississippi tidal marsh. Estuaries. 5(2):102-109.

Epstein S, Buchsbaum R, Lowenstam HA, Urey HC. 1953. Revised carbonate-water isotopic temperature scale. Bull Geol Soc Am. 64:1315-1326.

Fairbanks LD. 1963. Biodemographic studies of the clam *Rangia cuneata* Gray. Tulane Stud Zool. 10(1):3-47.

Farrow GE. 1971. Periodicity structures in the bivalve shell: Experiments to establish growth controls in *Cerastoderma edule* from the Thames estuary. Palaeontology. 14:571-588.

Foltz DW, Sarver SK, Hrincevich AW. 1995. Genetic structure of brackish water clams (*Rangia* spp.). Biochem Syst Ecol. 23(3):223-233.

Fritz LW, Haven DS. 1983. Hard clam, *Mercenaria mercenaria*: shell growth patterns in Chesapeake Bay. Fish Bull. 81(4):697-708.

Fritz LW, Ragone LM, Lutz RA. 1990. Microstructure of the outer shell layer of *Rangia cuneata* (Sowerby, 1831) from the Delaware River: applications in studies of population dynamics. J Shellfish Res. 9(1):205-213.

Giese AC. 1959. Comparative physiology: annual reproductive cycles of marine invertebrates. Annu Rev Physiol. 21:547-576.

Gordon J, Carriker MR. 1978. Growth lines in a bivalve mollusk: Subdaily patterns and dissolution of the shell. Science. 202:519-521.

Graf G, Rosenberg R. 1997. Bioresuspension and biodeposition: A review. J Mar Syst. 11:269-278.

Green RH 1980. Role of a unionid clam population in the calcium budget of a small arctic lake. Can J Fish Aquat Sci. 37:219-224.

Hallam A. 1965. Environmental causes of stunting in living and fossil marine benthonic invertebrates. Palaeontology. 8:132-155.

Hallam A. 1972. Models involving population dynamics. In: Schopf TJM, editor. Models in Paleobiology. San Francisco (CA): Freeman, Cooper. 62-80.

Hansen K, King GM, Kristensen E. 1996. Impact of the soft-shell clam *Mya arenaria* on sulfate reduction in an intertidal sediment. Aquat Microb Ecol. 10:181-194.

Harrel RC, McConnell MA. 1995. The estuarine clam *Rangia cuneata* as a biomonitor of dioxins and furans in the Neches River, Taylor Bayou, and Fence Lake, Texas. Estuaries. 18(1):264-270.

Hoese HD. 1973. Abundance of the low salinity clam, *Rangia cuneata* in southwestern Louisiana. P Natl Shellfish Assoc. 63:99-106.

Hopkins SH, Anderson JW, Horvath K. 1973. The brackish water clam *Rangia cuneata* as indicator of ecological effects of salinity changes in coastal waters. College Station (TX): Department of Biology. [accessed 2014 July 23].

Hopkins SH, Andrews JD. 1970. *Rangia cuneata* on the East Coast: thousand mile range extension, or resurgence? Science, New Series. 167(3919):868-869.

Huber M. 2010. Compendium of bivalves. A full-color guide to 3,300 of the world's marine bivalves. A status on Bivalvia after 250 years of research. Hackenheim (Germany): ConchBooks.

Jones DS. 1980. Annual cycle of shell growth increment formation in two continental shelf bivalves and its paleoecologic significance. Paleobiology. 6(3):331-340.

Jones DS. 1983. Sclerochronology: Reading the record of the molluscan shell: Annual growth increments of bivalve molluscs record marine climatic changes and reveal surprising longevity. Am Sci. 71(4):384-391.

Jones DS, Quitmyer IR, Arnold WS, Marelli DC. 1990. Annual shell banding, age, and growth rate of hard clams (*Mercenaria* spp.) from Florida. J Shellfish Res. 9(1):215-225.

de Jonge VN, van den Bergs J. 1987. Experiments on the resuspension of estuarine sediments containing benthic diatoms. Estuar Coast Shelf S. 24:725-740.

Jovanovich MC, Marion KR. 1989. Gametogenic cycle of *Rangia cuneata* (Mactridae, Mollusca) in Mobile Bay, Alabama, with comments on geographic variation. Bull Mar Sci. 45(1):130-138.

Kennish MJ, Olsson RK. 1975. Effects of thermal discharges on the microstructural growth of *Mercenaria mercenaria*. Environ Geol. 1:41-64.

Kier WM, Smith KK. 1985. Tongues, tentacles and trunks: the biomechanics of movement in muscular-hydrostats. Zool J Linn Soc. 83:307-324.

Kier WM. 1988. The arrangement and function of molluscan muscle. In: Trueman ER, Clark MR, editors. The Mollusca. London: Academic Press. p. 211-252.

Kranz PM. 1974. The anastrophic burial of bivalves and its paleoecological significance. J Geol. 82:237-265.

Kuenzler EJ. 1961. Structure and energy flow of a mussel population in a Georgia salt marsh. Limnol Oceanogr. 6:191-204.

Lane JM. 1986. Upper temperature tolerances of summer and winter acclimatized *Rangia cuneata* of different sizes from Perdido Bay, Florida. Northeast Gulf Sci. 8(2):163-166.

Lane DJW, Nott JA. 1975. A study of the morphology, fine structure and histochemistry of the foot of the pediveliger of *Mytilus edulis* L. J Mar Biol Assoc UK. 55:477-495.

Lécuyer C, Reynard B, Martineau F. 2004. Stable isotope fractionation between mollusc shells and marine waters from Martinique Island. Chem Geol. 213:293-305.

Loosanoff VL. 1969. Maturation of gonads of oysters, *Crassostrea virginica*, of different geographical areas subjected to relatively low temperatures. The Veliger. 11:153-163.

Lutz RA, Rhoads DC. 1980. Growth patterns within the molluscan shell: An overview. In: Rhoads DC, Lutz RA, editors. Skeletal growth of aquatic organisms: Biological records of environmental change. New York (NY): Plenum Press. p. 203-254.

Marelli DC. 1987. Processes controlling intertidal zonation in an estuarine soft-bottom bivalve assemblage. [Dissertation]. [Ann Arbor (MI)]: The Florida State University.

Marroquin-Mora DC, Rice MA. 2008. Gonadal cycle of northern quahogs, *Mercenaria mercenaria* (Linne, 1758), from fished and non-fished subpopulations in Narrangansett Bay. J Shellfish Res. 27(4):643-652.

Morton B. 1973. The biology and functional morphology of *Laternula truncata* (Lamarck 1818) (Bivalvia: Anomalodesmata: Pandoracea). Biol Bull. 145(3):509-531.

Nakamura Y, Konishi M, Ohishi K, Kusaka C, Tame A, Hatada Y, Fukikura K, Nakazawa M, Fujishima M, Yoshida T, Maruyama T. Mucus glycoproteins selectively secreted from bacteriocytes in gill filaments of the deep-sea clam *Calyptogena okutanii*. Open J Mar Sci. 3:167-174.

Norenburg JL, Ferraris JD. 1990. Cytomorphology of the pedal aperture glands of *Mya arenaria* L. (Mollusca, Bivalvia). Can J Zool. 68:1137-1144.

Norkko A, Hewitt JE, Thrush SF, Funnell GA. 2001. Benthic-pelagic coupling and suspension-feeding bivalves: linking site-specific sediment flux and biodeposition to benthic community structure. Limnol Oceanogr. 46(8):2067-2072.

Oliver G. Allen JA. 1980. The functional and adaptive morphology of the deep-sea species of the Arcacea (Mollusca: Bivalvia) from the Atlantic. Philos T Roy Soc B. 291(1045):45-76.

Olsen LA. 1976a. Reproductive cycles of *Polymesoda caroliniana* (Bosc) and *Rangia cuneata* Gray, with aspects of desiccation in the adults, and fertilization and early

larval stages in *P. caroliniana*. [Dissertation]. [Tallahassee (FL)]: Florida State University.

Olsen LA. 1976b. Ingested material in two species of estuarine bivalves; *Rangia cuneata* Gray and *Polymesoda caroliniana* (Bosc). P Natl Shellfish Ass. 66:103-104.

Pannella G, MacClintock C. 1968. Biological and environmental rhythms reflected in molluscan shell growth. J Paleontol. 2, supplemental to 42(5):64-80.

Park JJ, Lee JS, Lee, YG, Kim JW. 2012. Micromorphology and ultrastructure of the foot of the equilateral venus *Gomphina veneriformis* (Bivalvia: Veneridae). Cell Biol. 1:11-16.

Paterson DM. 1989. Short-term changes in the erodibility of intertidal cohesive sediments related to the migratory behavior of epipelic diatoms. Limnol Oceanogr. 34(1):223-234.

Pfitzenmeyer HT. 1972. Molluscs of the Chesapeake Bay. Chesap Sci. 13:S107-S115.

Pfitzenmeyer HT, Drobeck KG. 1964. The occurrence of the brackish water clam, *Rangia cuneata*, in the Potomac River, Maryland. Chesap Sci. 5(4):209-212.

Phelps DK, Santiago RJ, Luciano D, Irizarry N. 1969. Trace element composition of inshore and offshore benthic populations. Proc 2nd Nat Symp on Radioecology. U.S.A.E.C. Conf. 670503:509-526.

Prins TC, Smaal AC. 1994. The role of the blue mussel *Mytilis edulis* in the cycling of nutrients in the oosterschelde estuary (The Netherlands). Hydrobiologia. 282/283:413-429.

Rhoads DC, Pannella G. 1970. The use of molluscan shell growth patterns in ecology and paleoecology. Lethaia. 3:143-161.

Rhoads DC, Young DK. 1970. The influence of deposit-feeding organisms on sediment stability and community trophic structure. J Mar Res. 28:150-178.

Richards HG. 1962a. Studies on the marine Pleistocene: the marine Pleistocene of the Americas and Europe; the marine Pleistocene mollusks of Eastern North America. T Am Philos Soc. 52(3):1-141.

Richards, HG 1962b. Animals of the seashore. Boston (MA): Humphries Inc.

Ridgway ID, Richardson CA, Enos E, Ungvari Z, Austad SN, Philipp EER, Csiszar A. 2011. New species longevity record for the northern quahog (= hard clam), *Mercenaria mercenaria*. J Shellfish Res. 30(1):35-38.

Ropes JW. 1968. Reproductive cycle of the surf clam, *Spisula solidissima*, in offshore New Jersey. Biol Bull. 135(2):349-365.

Ropes JW, Jones DS, Murawski SA, Serchuk FM, Jerald Jr. A. 1984. Documentation of annual growth lines in ocean quahogs, *Arctica islandica* Linne. Fish Bull. 82(1):1-19.

Ropes JW, Stickney AP. 1965. Reproductive cycle of *Mya arenaria* in New England. Biol Bull. 128(2):315-327.

Rosenberg GD. 1980. An ontogenetic approach to the environmental significance of bivalve shell chemistry. In: Rhoads DC, Lutz RA, editors. Skeletal growth of aquatic organisms. New York (NY): Plenum Press. 133-168.

Rosenberg R. 2001. Marine benthic faunal successional stages and related sedimentary activity. Sci Mar. 65(2 Suppl):107-119.

Rudinskaya LV, Gusev AA. 2012. Invasion of the North American wedge clam *Rangia cuneata* (G. B. Sowerby I, 1831) (Bivalvia: Mactridae) in the Vistula Lagoon of the Baltic Sea. Russ J Biol Invasions. 3(3):115-128.

Schaffner LC, Diaz RJ, Olsen CR, Larsen. 1987. Faunal characteristics and sediment accumulation processes in the James River estuary, Virginia. Estuar Coast Shelf S. 25(2):211-226.

Schöne BR, Houk SD, Castro ADF, Fiebig J, Oschmann W, Kröncke I, Dreyer W, Gosselck F. 2005. Daily growth rates in shells of *Arctica islandica*: Assessing sub-seasonal environmental controls on a long-lived bivalve mollusk. PALAIOS. 20(1):78-92.

Seed R. 1980. Shell growth and form in the Bivalvia. In: Rhoads DC, Lutz RA, editors. Skeletal growth of aquatic organisms: Biological records of environmental change. New York (NY): Plenum Press. p. 23 – 67.

Stanley SM. 1970. Relation of shell form to life habits in the bivalve (Mollucsa). Geol Soc Am Bull. p. 296.

Stanley SM. 1975. Why clams have the shape they have: an experimental analysis of burrowing. Paleobiology. 1(1):48-58.

Stark BL. 1977. Prehistoric ecology at Patarata 52, Veracruz, Mexico: adaptation to the mangrove swamp. Nashville (TN): Vanderbilt University.

Swingle HA, Bland DG. 1974. Distribution of the estuarine clam *Rangia cuneata* Gray in coastal waters of Alabama. Ala Mar Resour Bull. 10:9-16.

Tanabe K. 1988. Age and growth rate determinations of an intertidal bivalve, *Phacosoma japonicum*, using internal shell increments. Lethaia. 21:231-241.

Tarver JW. 1972. Occurrence, distribution and density of *Rangia cuneata* in Lakes Pontchartrain and Maurepas, Louisiana. New Orleans (LA): Louisiana Wild Life and Fisheries Commission.

Tarver JW, Dugas JR. 1973. A study of the clam, *Rangia cuneata*, in Lake Pontchartrain and Lake Maurepas, Louisiana. New Orleans (LA): Louisiana Wild Life and Fisheries Commission.

Taylor JD, Kennedy WJ, Hall A. 1973. The shell structure and mineralogy of the Bivalvia: II. Lucinaecea – Clavagellacea. Conclusions. Bull Br Mus (Nat Hist) Zool. 22(9):253-294.

Trueman ER. 1966. Bivalve mollusks: fluid dynamics of burrowing. Science. 152(3721):523-525.

Trueman ER. 1967. The dynamics of burrowing in *Ensis* (Bivalvia). P Roy Soc Lond B Bio. 166(1005):459-476.

Vaughn CC, Hakenkamp CC. 2001. The functional role of burrowing bivalves in freshwater ecosystems. Freshwater Biol. 46:1431-1446.

Verween A, Kerckhof F, Vincx M, Degraer S. 2006. First European record of the invasive brackish water clam *Rangia cuneata* (G.B. Sowerby I, 1831) (Mollusca: Bivalvia). Aquat Invasions. 1(4):198-203.

Wakida-Kusunoki AT, MacKenzie Jr. CL. 2004. Rangia and marsh clams, *Rangia cuneata*, *R. flexuosa* and *Polymesoda caroliniana*, in Eastern Mexico: distribution, biology and ecology, and historical fisheries. Mar Fish Rev. 66(3):13-20.

Walker JM, Bogan AE, Garo K, Saliman GN, Hoeh WR. 2006. Hermaphroditism in the Irinidae (Bivalvia: Etherioidea). J Mollus Stud. 72(2):216-217.

Wanamaker AD, Kreutz KJ, Schöne BR, Maasch KA, Pershing AJ, Borns HW, Introne DS, Feindel S. 2009. A late Holocene paleo-productivity record in the western Gulf of Maine, USA, inferred from growth histories of the long-lived ocean quahog (*Arctica islandica*). Int J Earth Sci. 98:19-29.

Weidman CR. 1995. Development and application of the mollusc *Arctica islandica* as a paleooceanographic tool for the North Atlantic Ocean. [Dissertation]. [Cambridge and Woods Hole (MA)]: Massachusetts Institute of Technology and Woods Hole Oceanographic Institute.

Wells HW. 1961. The fauna of oyster beds, with special reference to the salinity factor. Ecol Monogr. 31(3):239-266.

Wolfe DA, Petteway EN. 1968. Growth of *Rangia cuneata* Gray. Chesap Sci. 9(2):99-102.

Wong WH, Rabalais NN, Turner RE. 2010. Abundance and ecological significance of the clam *Rangia cuneata* (Sowerby, 1831) in the upper Barataria Estuary (Louisiana, USA). Hydrobiologia. 651:305-315.

Woodburn KD. 1962. Clams and oysters in Charlotte County and vicinity. St. Petersburg (FL): Board of Conservation Marine Laboratory.

CHAPTER II – A STUDY ON THE ECOLOGY OF JOHNSON BAYOU, REPRODUCTIVE HISTOLOGICAL ANALYSIS OF *RANGIA CUNEATA*, AND OBSERVATIONS ON BURROWING BEHAVIOR OF *RANGIA CUNEATA* AND *POLYMESODA CAROLINIANA* ACROSS THREE SEDIMENT TYPES

Introduction

Habitat description of Johnson Bayou

The chosen site for ecological research was Johnson Bayou, located in Pass Christian, MS. This system drains into Bayou Portage; the latter linking Johnson Bayou to St. Louis Bay, an estuary between Pass Christian and Bay St. Louis, MS. Johnson Bayou is a brackish marsh with little to no salinity for several months of the year. As a consequence, the composition of flora within the bayou is highly variable. Moving inside the bayou from the Bay, rushes and cordgrasses give way to vines, shrubs, and trees. Submerged aquatic vegetation (SAV) is abundant for most of the year particularly in the middle areas of the Bayou. The width of the channel in the lower reaches is much greater than the upper areas of the system. The banks are gently sloped and broad, but transition towards a steeper slope in the middle to the upper parts of the system. While the bottom contours of Johnson Bayou were not studied in detail, in cross-section, the channel is broad and rounded in the lower reaches, but is more V-shaped in the upper reaches of the Bayou. Scouring is greater in the upper areas of the Bayou; thus, when looking down into the Bayou, the sediment appears predominantly sand with some areas of thick clay.

An examination of this system through the measurement of biotic and abiotic parameters was undertaken as no prior record of research or work by any institution or agency has been found to date. Residents have mentioned that canals leading north-

northwest from the main channel were created for land development in the 1950s (Figures 1, 2), but records were not available to confirm this statement or time frame. The locations of these canals and properties were used in some part to measure abiotic factors and compare the results to those acquired from the channel, or natural areas of the bayou. Aside from many species of animals and plants identified during the research, two species of clams were found in Johnson Bayou, *Rangia cuneata* (Macridae) and *Polymesoda caroliniana* (Cyrenidae).

Sympatric clams

Both species are infaunal organisms that use a well-developed foot to burrow into sediment. Thus, these clams are benthic ecosystem engineers found in various estuaries along the Atlantic and Gulf coasts (Richards 1962; Woodburn 1962; Pfitzenmeyer and Drobeck 1964; Hopkins and Andrews 1970; Andrews 1971; Hoese 1973; Swingle and Bland 1974; Olsen 1976a, 1976b; Duobinis-Gray and Hackney 1982; Marelli 1987; Abbott and Morris 1995; Wakida-Kusunoki and MacKenzie 2004). As organisms that live buried in the sediments and filter the water column for food, bivalves inherently connect processes occurring in the water column and substrate; however, little information is available on their burrowing behavior, particularly across different sediment types.

Reproductive studies such as rate of gametogenesis and spawning cycles are commonly studied in species of economic or environmental interest. While the reproductive cycle of *R. cuneata* has been studied (Cain 1972, Jovanovich and Marion 1986), a histological examination of the timing of gametogenesis and spawning, correlated to salinity gradients throughout the system, has not been studied in this species

in any ecosystem along the MS coast. While noted previously that *P. caroliniana* was also found in sympatry with *R. cuneata*, the number of *P. caroliniana* encountered were low and due to concern for negative impact on this population, *P. caroliniana* individuals were not included in this reproductive cycle study. Because salinity has been hypothesized to influence gonadogenesis and spawning cycles (Fairbanks 1963; Chanley 1965; Jovanovich and Marion 1989), clams utilized in the reproductive histology experiment were removed from specific sites within Johnson Bayou that experienced different salinity regimes. The salinity gradients were established based on seasonal salinity measurements taken at various times in 2015 to determine the three study sites, indicated as lower, middle, and upper. Each site was approximately 0.1 km in length and located 1 km in distance between one another while following the channel.

To adequately assess reproductive phases of *R. cuneata* collected from the three sites in Johnson Bayou, the determination of the number of phases for reproductively active or capable bivalves followed work conducted by Ropes and Stickney (1965) and Ropes (1968), referred to in some sources as the "Ropes' method" (Schneider et al. 1997). The term "phase" was used to indicate where clams were in their reproductive cycle, while "stage" indicated the development of the gametes. The terms "follicle" and "lobule" were used to describe the regions of the female and male gonad, respectively, in which gametogenesis and gonad maturation occurred. The term "follicle" has been used in the literature as early as a study by Loosanoff in 1942 on gonadal changes in a species of oyster. While follicle is the term used herein, some differences in terminology exist in the literature with "alveoli" (Ropes and Stickney 1965; Ropes 1968) and "acinar" (Bower and Blackbourn 2003) being used to describe gonadal regions for one or both sexes. The

term “lobule” is commonly seen in studies of fish, but because it defines the male gonad and functions in the same manner, there was no reason not to use it here for *R. cuneata*.

Research aims

The research conducted in Johnson Bayou was varied, and yet connected through a primary focus on the bivalve, *R. cuneata*. In order to answer questions centered on this focal species, Johnson Bayou was observed and described through recording and identifying flora and fauna as well as measuring abiotic factors from 2014 to 2016. As a result of information gained through this type of data collection, a study involving a reproductive histological analysis of *R. cuneata* in Mississippi waters was performed in 2016. Published literature addressing reproductive cycles and spawning in *R. cuneata* populations from Louisiana (Fairbanks 1963) and Alabama (Jovanovich and Marion 1989) hypothesized that the reproductive cycle of *R. cuneata* correlated with temperature and salinity changes. Based on this assumption, the reproductive histological study conducted with *R. cuneata* from Johnson Bayou was constructed to involve inclusion of individuals from different areas of the bayou as dictated by the salinity difference measured for the chosen sites.

Due to the connection previously mentioned that burrowing bivalves have with both the water column and the sediment, organic matter (OM) and sediment particle size were examined using samples taken from the same three sites where specimens of *R. cuneata* were collected for the reproductive analysis. This study was prompted through the observations that *R. cuneata* distribution was not even throughout Johnson Bayou. Based on this uneven distribution, it was hypothesized that OM and sediment particle sizes differed between and within locations where clams were present versus where they

were absent. Last, a short-term behavioral study was undertaken to determine if *R. cuneata* and *P. caroliniana* differed in burrowing behavior across three sediment types (sand, silt, and clay) found in Johnson Bayou. Based on preliminary investigations, silt was hypothesized to be the easiest sediment type in which clams could burrow, and that sand and clay would force clams to spend a greater amount of time burrowing. All research performed provide some understanding of how *R. cuneata* and *P. caroliniana* exist and behave in this brackish marsh.

Methodology

Observations of Johnson Bayou

Images of flora and fauna were acquired in the field for identification using a Pentax GPS-4 camera (Ricoh Imaging Americas Corporation, Denver, CO). A catch and release method (i.e., fishing) was used for capturing fish and crustaceans. Plants were identified using images taken in the field or from samples taken for identification in the lab with the aid of a field guide by Tiner and Rorer (1993). *Rangia cuneata* and *P. caroliniana* were the only two species investigated with regard to population density. A 1 m^2 quadrat of PVC pipe was randomly placed upon the substrate in areas along the banks of the bayou in close proximity to the emergent grasses throughout Johnson Bayou across a 3 km total distance following the channel. An estimation of population size for *R. cuneata* and *P. caroliniana* in Johnson Bayou was not determined.

Abiotic factors – daily and seasonal measurements from Johnson Bayou from 2014-2016

From 2014 to 2016, weather permitting, environmental parameters including pH, air and water temperature, salinity (HI 98130, Hanna Instruments, Incorporated, Woonsocket, RI or Hydrolab Quanta multi-probe meter, OTT Hydromet, Loveland,

USA), and surface and bottom dissolved oxygen (DO200 YSI Incorporated, Yellow Springs, OH) were recorded at a single point (30°20.265'N 89°13.959'W) approximately in the middle section of Johnson Bayou. Calibration of all instruments were performed at least once a week using buffer solution (pH 4 and 7; ForestrySuppliers, Incorporated, Jackson, MS), and DO electrode solution available from the manufacturer for the DO200 YSI. Depth was measured either by lowering a secchi disk until it touched the bottom and then measuring the length of rope covered by water once the secchi disk was pulled up or via the use of a Hydrolab Quanta multi-probe meter lowered to the bottom, which provided the depth in a digital readout. Tidal direction and surface velocity was measured using a one foot ruler and a timer, starting and stopping when a particle floating on top of the water column crossed the entire length of the ruler. Velocity was converted to cm s^{-1}. Weather parameters included precipitation received since last recording from an 8" depth rain gauge, and atmospheric conditions were visually estimated (e.g., percent cloud cover). Because differences in abiotic factors are expected to influence organism behaviors, 34 sites were selected within the channel and canals across a 4.4 mi area of Johnson Bayou between 30°20.233'N 89°14.202'W and 30°20.274'N 89°13.419'W (Figure 1) in October of 2014, February, June, and October of 2015, and February, May, and August of 2016. Measurements of surface and bottom pH, DO, water temperature, and salinity were taken during the highest predicted tides to capture the largest difference between surface and bottom water variables.

Reproductive histological analysis of Rangia cuneata

While *R. cuneata* and *P. caroliniana* were both present in the Johnson Bayou system, *R. cuneata* was the focus species of this study due to the low numbers of *P.*

caroliniana encountered. At the end of each month in 2016, three specimens of *R. cuneata* were collected (N = 108) by hand from three sites (lower, middle, upper) along the main channel of Johnson Bayou. The sites were approximately 1 km in distance from one another with the lower referring to the area of Johnson Bayou shortly before it meets Bayou Portage (30°20.452'N 89°14.666'W) to the middle of the Bayou near the site where daily abiotic measurements were taken (30°20.265'N 89°13.959'W) and the upper site referring to the innermost area where clams were found (30°20.247'N 89°13.094'W) (Figure 2). Salinity was measured at each site when clams were taken for analysis; however, water temperature was measured only at the middle site while taking normal daily abiotic factor measurements. Clams removed from each site were taken to the lab where measurements including length, height, and inflation (Figure 3) were taken to the nearest 0.01 mm using digital calipers (CenTech, Incorporated, Pittsburgh, PA) and whole body mass (= shell + soft tissue) was measured in grams using a NewClassic SG balance (Mettler Toledo, Switzerland). After measurements were taken, macroscopic images of the clams were captured with a Pentax GPS-4 camera (Ricoh Imaging Americas Corporation, Denver, CO) prior to fixation of soft tissue. The posterior or anterior adductor muscle was severed using a razor blade placed between the two shell valves and then clams were immediately placed in 100% EtOH. Following fixation for a minimum of 48 hours in 100% EtOH, gonadal tissue was dissected (~1 mm^3) and fixed in Davidson's Modified fixative (Electron Microscopy Sciences, Hatfield, PA) for 72 hours. Tissues were washed overnight in running tap water followed by 60%, and 2 x 70% changes in EtOH for 2 hours each. Tissue was processed in a Shandon Excelsior ES tissue processor (Thermo Fisher Scientific, Waltham, MA). Following processing, tissue

was embedded using an embedding tray (Triangle Biomedical Sciences, Durham, NC) and sectioned with an AO 820 rotary microtome (American Optical, Buffalo, NY) at 4-6 µm before staining in Gill's I hematoxylin (Mercedes Medical, Sarasota, FL) and eosin Y (Thermo Fisher Scientific, Waltham, MA). Light microscopy images were captured with a Digital Eclipse DXM 1200 Nikon camera and using ACT-1 software (Nikon Instruments, Incorporated, Melville, NY).

The reproductive phase of each clam, regardless of sex, was classified using the five phases outlined by Ropes and Stickney (1965). These phases are early and late active, ripe, partially spawned, and spent (Table 1). Using three separate images taken per specimen, an average percentage of tissue type present, gonadal versus somatic, and percentage of each gametogenic stage present within the gonadal tissues per sex was calculated. Due to the difference in gamete size between males and females, female gonadal tissue was imaged at a total magnification of 100X while male gonadal tissue was imaged at a total magnification of 400X. Visual examination of gonadal tissue and determination of reproductive phases, followed methods adapted from Tomkiewicz et al. (2011) which involves the use of ImageJ version 1.48 to superimpose of a grid of 80 crosses over each image (Figure 4). Gonadal tissue and gamete stages were counted if they intersected a cross.

Organic matter analysis

At the same time that clams were acquired for the reproductive histological study, cores of sediment were obtained using a 50 mL centrifuge tube, with the conical end removed. In addition to samples taken in areas where clams were collected, random duplicate samples were taken in areas where clams were not found. Sediment samples

were taken within the same area of each site (>1 m^2) for each sampling date. Core samples were immediately processed or frozen at -20°C. Processing began by photo documentation of the core using a Pentax GPS-4 camera (Ricoh Imaging Americas Corporation, Denver, CO) after the core was removed from the sampling tube. Frozen samples were allowed to thaw before removal from the sampling tubes and imaging occurred. The mass of each sample was determined in a pre-weighed crucible using an AdventurerPro AV212C balance (Ohaus Corporation, Pine Brook, NJ). Samples were dried at 103-105°C (Steinman and Lamberti c1996) in a Precision compact drying oven (Thermo Fisher Scientific, Marietta, OH) for 72 hours or until mass was <4% of the previous mass. After determining water mass, samples were burned at 550°C for 6-8 hours in a muffle furnace (Lindberg/Blue M, Thermo Fisher Scientific, Asheville, NC), then weighed, and the ash-free dry mass was calculated by subtracting the mass of the sample before and after burning.

Sediment particle size analysis

Burned sediment samples were analyzed for particle size distribution through a stainless steel soil sampling sieve set (Fieldmaster 78-700, Science First, Yulee, FL). Due to compaction in the crucible for OM determination, when necessary, samples were gently broken up with a mortar and pestle upon removal from the oven. Care was taken to minimize the effect this process would have on the particle sizes of the original sample. Starting and ending mass of each particle size collected was determined using a SI-234 analytical balance (Denver Instrument, Bohemia, NY). Particle sizes were defined based on work by Wentworth (1922) on clastic sediments and mass of each particle size was used to determine any differences between sites.

Burrowing behaviors per sediment type

A total of 13 clams, 8 *Rangia cuneata* and 5 *Polymesoda caroliniana*, were randomly chosen for a study to elucidate burrowing behavior in three prominent sediment types, sand, silt, and clay, found in Johnson Bayou. This study began with each sediment type being placed in separate ten gallon tanks. Upon removal from Johnson Bayou, clams were placed into one of the three tanks and after a period of acclimation (~24 hours), clams were removed from the sediment, placed on top of the sediment in a previously undisturbed area within the tank in one of five positions designated by shell orientation in relation to the sediment (Figure 5). Subsequent behavior was video recorded using either a Pentax GPS-4 camera (Ricoh Imaging Americas Corporation, Denver, CO) or a Polaroid XS100 action camera (Polaroid Corporation, Minnetonka, MN). Care was taken not to disturb the clams after placement into a select position. Recordings ceased when the clam did not burrow further or an estimated 90% of the clam had burrowed. Behavioral observations and measurements were determined by viewing the videos following completion of a burrowing cycle and included time (in seconds) between placement in a specific orientation and beginning of burrowing activity, events, and times between events. A single event was defined as the moment the foot began to swell, followed by closure of the siphons, contraction followed by relaxation of the adductor and retractor muscles, opening of the siphons, and final relaxation of the foot. If the foot was buried or could not be observed, swelling of the foot was indicated by the leaning of the animal to the posterior and dorsal ends (i.e., the foot emerges from the anterior end). Across all sediment types, cnce a successful recording in one orientation was obtained, and a period of rest was given (~24-48 hours), the clam was placed in a new orientation

and in a previously undisturbed area on the same sediment surface for observation and recording.

Data analysis

All qualitative data (e.g., images and figures) were edited and formatted in CorelDraw X8 (Corel Corporation, Ottawa, Ontario, Canada). Descriptive statistics including range, mean, and standard deviation were calculated using Sigmaplot 13.0 (Systat Software, Incorporated, San Jose, CA). All quantitative data were recorded and analyzed, and resulting graphs were created in Sigmaplot 13.0. A Spearman correlation analysis was used to determine the presence of any correlation between salinity and pH, and water temperature and surface and bottom dissolved oxygen. A Spearman correlation analysis was also used to determine the presence of any correlation between water temperature, salinity, and gametogenesis (percent gonadal tissue) in *R. cuneata*.

A one-way ANOVA ($p = 0.05$) was performed to determine if collection location had a significant effect on the shell parameters of clams collected in 2016. After log transforming the data to correct for normality, a Pearson correlation was used to determine correlation between individual shell parameters and between whole body mass. After pooling the data from organic matter (OM) content per site, normality tests failed, regardless of transformation used. Thus, a Kruskal-Wallis one-way ANOVA on ranks was performed ($p = 0.05$) to test if OM content was statistically different across the collection sites in 2016. After separating the OM data based on sampling locations (presence versus absence of clams), the data passed normality after rank transformation. Thus, a two-way ANOVA ($p = 0.05$) was performed to determine if location and the presence of clams had a significant effect on OM. A Dunn's test ($p = 0.05$) was run to test

significance in OM content between locations where clams were present and where they were absent within and between sites. A chi-square test was performed to determine relationship between sediment particle size and site (lower, middle, and upper).

With respect to the burrowing study, after log transforming the data to correct for normality, a one-way repeated measures ANOVA ($p = 0.05$) was performed to determine if sediment type significantly influenced the number and length of burrowing events. A Holm-Sidak test ($p = 0.05$) was performed as a pairwise comparison between sediment types. Statistical analyses were performed in SigmaPlot 13.0 (Systat Software, Incorporated, San Jose, CA) and IBM SPSS Statistics (SPSS, Incorporated, Armonk, NY).

Results

Observations of Johnson Bayou

Over the course of this study, a total of 40 plants were identified to the genus or species level (Table 2). These include emergent, submerged aquatic vegetation (SAV), free-floating plants, and trees or shrubs with direct contact to the channel. Some common species include but are not limited to *Ruppia maritima* (SAV), *Alternantha philoxeroides*, and *Azolla caroliniana* (free-floating). *Alternantha philoxeroides* (alligatorweed) is an exotic invasive species; however, in 2015 and 2016, *Agasicles hygrophila* (alligatorweed flea beetle) was observed throughout much of the system damaging a great proportion of alligatorweed (Figure 6). Alligatorweed could be seen throughout the system if salinity was not above 5 ppt, but was most concentrated in the innermost parts of the system. Alligatorweed was particularly abundant in ditches and small canals throughout Pass Christian and Long Beach, MS in 2016, as observed while driving through the area

between the university campus and field site. *Myriophyllum aquaticum*, Brazilian milfoil (Figure 6), is another exotic invasive species found associated with mats of alligatorweed.

A total of 69 species of vertebrates and invertebrates were visually identified including 1 species of mammal (*Myocaster coypus*), 25 species of invertebrates (Table 3), 16 species of fish (Table 4), 16 species of bird (Table 5), and 11 species of reptile and amphibian (Table 6). Prevalent invertebrates include the economically important and often observed blue crab (*Callinectes sapidus*) and encrusting barnacles (*Balanus* sp.). Other invertebrates included an unidentified nudibranch and the Atlantic sea nettle (*Chrysaora quinquecirrha*). Additional species for which the scientific names remain to be determined include mud crabs, isopods, and an oligochaete. Commonly encountered fish included *Sciaenops ocellatus* (red drum), *Leponis macrochinus* (bluegill), and *Cynoscion nebulosus* (spotted seatrout). Common resident species of bird include the red-winged blackbird, *Agelauius phoeniceus*, and great blue heron, *Ardea herodias*. Other species included *Pandion haliaetus* (osprey), *Pelecanus occidentalis* (brown pelican), and migratory scaups such as *Aythya affinis*. Commonly observed reptiles and amphibians included *Alligator mississippiensis* (American alligator), *Ophisaurus ventralis* (eastern glass lizard), and *Chelydra serpentina* (snapping turtle).

An unusual observation in the summer of 2015 was a high abundance of *Chrysaora quinquecirrha*. Up to 100 individuals were counted in one area at the launch point for taking field measurements. The sea nettles were generally smaller (dome diameter approximately 5-10 cm) than those observed in open waters. Salinity in Johnson Bayou at this time was below 5 ppt. No record was made of unusually strong tidal flow or weather patterns that could have pushed the sea nettles into the bayou.

Rangia cuneata and Polymesoda caroliniana

The wedge and marsh clams, *R. cuneata* and *P. caroliniana* (Figure 7) were the primary species of interest during this study. Both species were observed in unequal abundance (0 – 37 m^{-2}) throughout Johnson Bayou. Tidal flats were found to be areas containing the highest abundance of this species, with many flats exposed at low tide for several hours. To date, approximately 420 individuals of *R. cuneata* and < 100 individuals of *P. caroliniana* were observed in Johnson Bayou from 2014-2016.

External and internal features of *R. cuneata* and *P. caroliniana* were examined. The shell of both species has a large prosogyrous umbo (i.e., dorsal end), where the two valves are attached via the cardinal tooth. Prosogyrosity means that the umbo curves toward the anterior end, the region from which the foot emerges from the shell. *Rangia cuneata* has a well-developed lunule on either side of the umbo, while *P. caroliniana* does not. The anterior end of both species is well rounded, but the posterior end is elongated on *R. cuneata* and not so on *P. caroliniana*. The periostracum of *R. cuneata* lacks ornamentation or sculpture, is brown in coloration in the presence of oxygenated water or sediment, and has a strong luster under sunlight (Figure 7a). The periostracum of *P. caroliniana* is dark brown to black and is ruffled (Figure 7b). The nacre of *R. cuneata* is white with scars indicating anterior and posterior adductor and retractor muscles, a pallial sinus scar formed by the siphons leading to mantle tissue, and a pallial line indicating attachment of the mantle tissue (Figure 7c). The nacre of *P. caroliniana* is a mix of white, pink, and purple coloration with little to no discernible scars (Figure 7d).

In both species, the foot emerges from the anterior end, whereas the siphons emerge from the posterior end (Figure 8). The incurrent siphon of both species is ventral

to the excurrent siphon, both of which are ringed by tentacles, but the incurrent siphon is nearly twice as large in diameter as the excurrent siphon. The siphons are fused in *R. cuneata*, but separate a few millimeters down in *P. caroliniana* (Figure 9). The siphons were observed to extend as much as 1.5 cm in both species.

In order to support or correlate the presence, absence, and location of species, including the clams in Johnson Bayou, abiotic factors were measured (from 2014-2016). The results provide a basic understanding of Johnson Bayou with regard to biotic and abiotic factors.

Abiotic factors – daily and seasonal results from Johnson Bayou from 2014-2016

Abiotic data from Johnson Bayou for the years of 2014 (280 d), 2015 (244 d), and 2016 (255 d) were recorded from the single point approximately in the middle section of Johnson Bayou. pH ranged from 4.21 to 8.37 (average = 6.60) (Figure 10). Dissolved oxygen ranged from 21.1% to 162.3% saturation (1.7 to 16.8 mg L^{-1}) (averages of 67.6% saturation; 6.0 mg L^{-1}) at the surface and 11.5% to 131.8% saturation (0.9 to 14.3 mg L^{-1}) (averages of 56.3% saturation; 5.1 mg L^{-1}) at the bottom (Figure 11). Across all years, air and water temperature ranged from 3.1°C to 38.3°C and 4.3°C to 34.9°C, respectively (averages of 22.1°C and 22.3°C, respectively). Monthly means of air and water temperature from 2014 to 2016 followed expected seasonal trends with peak temperatures in July (Figure 12). Salinity ranged from 0 to 23 ppt (average of 3.9 ppt) with the highest salinity levels in the fall and winter months (Figure 13). An analysis of values measured for salinity and pH returned a negative correlation ($r = -0.42$) between these factors, and a negative correlation was also found when water temperature was analyzed in comparison with surface ($r = -0.40$) and bottom dissolved oxygen ($r = -0.65$).

Average tidal velocity in the channel was approximately 5.8 cm s^{-1} (520 d). Velocity of water along tidal flats where clams were commonly encountered was observably slower than that in the channel. In addition to measuring abiotic factors from a single point within the bayou, the same factors were measured from 34 selected sites during selected months between 2014 and 2016 (Table 9), and demonstrate how these factors differed throughout the system and across seasons. The lowest and highest levels of pH recorded were 5.88 (bottom water; February 2016) and 7.55 (bottom water; October 2015). With regard to dissolved oxygen, the lowest and highest levels recorded were 8.9% saturation (bottom water; June 2015) and 126.7% saturation (surface water; February 2015). Overall, bottom water temperature was up to six degrees colder than surface temperatures. The lowest and highest water temperature recorded across all samples was 12.6°C (bottom water; February 2015) and 32.4°C (surface water; June 2015), respectively. Peak salinity level was recorded at 22 ppt (October 2015) near the lower reaches of the bayou and at the bottom of the water column. In August 2016, water temperature was approximately four degrees warmer on the bottom than the top of the water column. This was not entirely unexpected, as the total rainfall for the month of August 2016 was 23.5 cm, roughly 10 cm higher than average for that area at that time, and it had rained for several days prior to the sample date.

Reproductive Histological Analysis of Rangia cuneata

The gonad is part of the visceral mass, situated dorsally to the foot and flanked by the gill demibranchs (Figure 14). The color of the gonad is pale to cream colored and does not differ between sexes. When a clam is ripe, the gonad increases in size, developing around and abutting digestive glandular tissue and intestines, pushing visceral

muscle tissue outwards against the gill demibranchs (Figure 14a, b). When a clam is spent, the gonad shrinks in size resulting in a much thinner visceral mass above the foot (Figure 14c). Under light microscopy, H&E stained sections show gonadal tissue abutting digestive gland (Figure 15a). The digestive gland is a series of large anastomosing tubes or clusters of smaller tubes in cross-section. Simple cuboidal cells line these tubes. Gonadal and digestive tissue is surrounded by visceral muscle tissue with gill demibranchs to the exterior of visceral muscle tissue (Figure 15b).

While a specific salinity level is thought to trigger the release of gametes (i.e., spawning) from the clams into the water column, temperature is thought to have an effect on gametogenesis. During 2016 when collections of *R. cuneata* from the lower, middle, and upper sites occurred for the reproductive histological analysis, average temperatures peaked at 30.0°C in July and cooled to 19.9°C by the end of November. However, temperature did not differ more than 2°C between sites across measurements taken in 2016. In contrast, salinity at the lower, middle, and upper sites ranged from 0.5 – 16 ppt, 0 – 10 ppt, and 0 – 8 ppt, respectively across collection times. Salinity at the lower reaches of Johnson Bayou remained at 0 ppt until May (0.5 ppt) and peaked at 16 ppt in November. Salinity levels at the middle and upper sites remained at 0 ppt until July (0.5 ppt) and September (0.5 ppt), respectively. Salinity levels peaked at the middle and upper sites in October with 10 and 8 ppt, respectively. Precipitation throughout December brought those areas down to 0 ppt again by January. A positive correlation was found between water temperature and the average percent gonadal tissue produced by clams from the lower, middle, and upper sites throughout 2016 ($r = 0.55$, 0.76, and 0.86, respectively). However, there was a negative correlation between salinity and percent

gonadal tissue produced by clams in the lower site (r = -0.01), and a positive correlation between salinity and percent gonadal tissue produced by clams in the middle (r = 0.355) and upper sites (r = 0.141).

In 2016, 53 females and 47 male clams were collected. The sex of the remaining 8 clams was not determined. There were 8 instances where only clams of the same sex were collected (i.e., all female or all male). Due to the fact that it took approximately two weeks to collect, fix, process, section, and stain gonadal tissue before sex could be determined, it was not possible to resample without potentially overlapping with the next sampling time frame. All five gonadal developmental phases were observed from this study (Figure 16). During the winter months, gonadal tissue was found to be collapsed or with nearly empty follicles containing degenerating oocytes or lobules with degenerating sperm cells (Figure 16a, b). As water temperature increased in the spring and early summer months, early and late active phases (Figure 16c, d) were characterized by the presence of enlarged oogonia (<20 µm in diameter) and spermatogonia (>5-8 µm in diameter) embedded in the follicular and lobule walls. All stages of gametes were typically present at this time, including early and late vitellogenic oocytes (20-50 µm in length including stalk; 20-30 µm in diameter) indicated by increasing amounts of yolk and vitellogenin, but attached to the follicular walls, mature oocytes with a thin stalk attached to the wall (as much as 90 µm in length including stalk; up to 40 µm in diameter), and a few ripe ova (~35-60 µm in diameter) free in the lumen (Figure 16c). In males, this included spermatocytes (4-5 µm in diameter) in clusters along the outer lumen, spermatids farther in the lumen, but smaller in size (~0.5-2 µm in diameter), and finally spermatozoa (~0.2-1 µm in diameter) in the central lumen with characteristically

eosinophilic tails oriented toward the center (Figure 16d). The ripe phase in both sexes was indicated by swollen follicles and lobules, and reduced somatic tissue (Figure 16e, f). All stages of gametes may be observed, but at the peak before spawning, the lumens were abundant with ripe ova with large nuclei (~30 µm in diameter) and darker stained nucleoli (10 µm in diameter), and spermatozoa (Figure 16e, f). Last, partially spawned clams showed a highly reduced number of ripe ova and spermatozoa (Figure 16g, h), some of which do not get released. If no further spawning events occur, oocytes and sperm cells degenerate and the clam enters the spent phase.

In January across all sites, female clams had nearly collapsed follicles containing degenerating oocytes and infiltrating hemocytes indicating the spent phase (Figure 17a-c). Somatic tissue dominates in tissue sections from female clams taken in January with digestive and muscle tissue present in several sections. In February, female clams were only collected from the middle site, and these females were in the spent phase with degenerating oocytes. Some follicles had oogonia and early vitellogenic oocytes embedded or attached to the follicular walls (Figure 17d). In March, female clams collected from the lower site were in the early active phase, producing early and late vitellogenic oocytes, and a few mature and ripe ova (Figure 17e). Some female clams from the middle and upper sites contained residual gametes, but also possessed early vitellogenic oocytes (Figure 17f, g). In April, female clams from the lower and middle sites were ripe (Figure 17h) and in the late active phases (Figure 17i), respectively. Many female clams from the upper site still appeared spent or were producing few early vitellogenic oocytes (Figure 17j). In May, female clams from the lower site appeared to be spawning with the majority of cells being mature or ripe ova inside enlarged follicles.

Digestive tissue was observed just outside of these follicles (Figure 17k). Female clams from the middle site were producing ripe ova (Figure 17l), but remained in the early to late active phase, while female clams in the upper site were in the early active phase, producing early and some late vitellogenic oocytes (Figure 17m). By June, clams from the lower site were partially spawned or spent with unspawned and degenerating oocytes remaining in the follicles (Figure 17n). However, female clams from the middle and upper sites were between the late active and ripe phases (Figure 17o, p). In July, female clams were only collected from the lower and upper sites. Female clams from the lower site were in the early active phase, producing early and late vitellogenic oocytes with some mature and ripe ova (Figure 18a). Female clams from the upper site were progressing from the early to late active phase (Figure 18b). From August to September, female clams across all sites had progressed through the late active phase (Figure 18c-h). In October, female clams were only collected from the lower and upper sites, and were ripe, indicated by swollen follicles and an abundance of ripe ova (Figure 18i, j). By November, all female clams were spent (Figure k-m) with a few remaining unspawned ripe ova. In December, female clams were only collected from the lower and upper sites, and had some unspawned ripe ova and degenerating oocytes (Figure 18n, o).

Male clams were not always strictly maturing at the same rate as female clams. In January, all male clams were spent with near collapsed lobules (Figure 19a-c). As with females, muscle tissue and somatic tissue were commonly observed in histological sections during this phase. In February, male clams from the lower site were in the early active phase, producing gametes of all stages, but primarily spermatocytes (Figure 19d). Male clams at the middle and upper sites were spent with degenerating sperm cells in the

lumens (Figure 19e, f). Male clams from all three collection sites remained in the same phases in March as they were in February (Figure 19g-i). In April, male clams at the lower site progressed into the late active phase with increasing numbers of spermatids and spermatozoa (Figure 19j). Male clams from the middle site were in the early to late active phase (Figure 19k), while male clams from the upper site were in the early active phase (Figure 19i). In May, male clams were only collected from the middle and upper sites. Male clams from the middle site were in the ripe phase (Figure 19m). Male clams from the upper site were into the late active phase (Figure 19n). In June, male clams were only collected from the lower and middle sites. Male clams from the lower site had partially spawned or were spent as indicated by few spermatocytes and degenerating sperm cells (Figure 19o). Male clams from the middle site appeared partially spawned, but still produced gametes of all stages (Figure 19p). In July, male clams from the lower site were in the late active and ripe phases, with enlarged lobules filled primarily with spermatozoa (Figure 20a). Male clams from the middle site had partially spawned, indicated by smaller lobules and sparse amounts of spermatozoa, but numerous spermatocytes and spermatids (Figure 20b). Male clams from the upper site were in the late active phase (Figure 20c). In August, male clams from the lower site were ripe (Figure 20d), while male clams from the middle and upper sites were in the late active to ripe phases (Figure 20e, f). In September, male clams were only collected from the middle site, and these males were ripe (Figure 20g). In October, male clams from the lower site were partially spawned (Figure 20h), indicated by an increasing amount of space in the lumens of the lobules and less spermatozoa than in ripe clams. Male clams from the middle and upper sites were ripe with very little somatic tissue present (Figure

20i, j). In November, male clams were only collected from the middle and lower sites. Male clams from the middle site were spent with degenerating sperm cells present in the lumens (Figure 20k). Male clams from the upper site were partially spawned, indicated by increasing amounts of somatic tissue and fewer spermatozoa in the lumens (Figure 20l). In December, male clams from the lower site were spent with unspawned spermatozoa and degenerating sperm cells (Figure 20n). No male clams were collected in December from the upper site.

After using the methods outlined by Tomkieqicz et al. (2011) for a quantitative measurement of gonadal versus somatic tissue, and stages of gametes, the data were pooled and averaged from clams collected from each site per month (Figure 21). Data show that clams from the lower site spawned twice, once in June and again in November. This observation is based on the decrease in gonadal tissue in June and in November. Clams from the lower site had approximately 50% gonadal tissue by July, but only peaked to about 78% in October. In contrast, clams from the middle site reached about 75% gonadal tissue as early as April, but did not spawn until October, with potential exception of males undergoing partial spawning in June. Clams from the upper site reflect a similar pattern, with slightly greater than 50% gonadal tissue by April, an unexplained decrease in gonadal tissue between May and June, and peaking between August and October, but never reaching 75% gonadal tissue (Figure 21).

The data from gametic stages were pooled and averaged from clams collected from each site per month (Figure 22). Germ cells (oogonia and spermatogonia) accounted for 50% of gametic stages in two separate months (January and June) in clams from the lower site and once in clams from the middle (November). Germ cells generally

accounted for 10-30% in clams from across all sites throughout the year. Vitellogenic oocytes, which include early and late vitellogenic oocytes, and spermatocytes accounted for nearly 20% or less in clams from the lower site, with 5% or less in June and December. The percentage of vitellogenic oocytes and spermatocytes in clams from the middle and upper sites peaked between May and October, but varied from 0-20% (0% in spent clams in January) across all months. The percentage of mature oocytes and spermatids varied in clams from all sites across all months, anywhere from 0% to nearly 25% (lower site in February). Clams from the lower and middle sites may have spawned twice around June and November based on the observed increase followed by a decrease in the levels of ripe ova and spermatozoa. Clams from the upper site presented around 75% ripe ova or spermatozoa in July. From July to December, residual gametes accounted for 0% to greater than 50% in clams from the lower site. Residual gametes accounted for over 60% in clams from the middle site in January and February and over 50% in December, with 0% to ~5% between March and November. No residual gametes were counted in April or between June and September in these clams. In clams from the upper site, residual gametes decreased from over 50% in January to 0% by June, but increased from October to December to approximately 50% (Figure 22).

Shell parameters of Rangia cuneata

Using measurements taken from the 108 individuals of *R. cuneata* collected for the histological analysis, the range (Table 7), average, and potential effect of location on shell parameters and whole body mass were analyzed ($F_{3.08}$, df = 105, p = 0.05, n = 36) (lower, middle, and upper sites). The average shell length from each site (lower, middle, upper) was 58.5 ± 6.2 mm, 56.1 ± 5.4 mm, and 47.9 ± 5.2 mm, respectively (F = 35.3, p

= < 0.001) (Figure 23), while average shell height from each site was 50.1 ± 5.6 mm, 45.3 ± 4.8 mm, and 38.9 ± 3.6 mm, respectively (F = 50.6, p = < 0.001) (Figure 24). Average shell inflation from each site was 40.8 ± 4.4 mm, 37.4 ± 4.7 mm, and 31.4 ± 3.3 mm, respectively (F = 46.3, p = < 0.001) (Figure 25), and average whole body mass from each site was 97.5 ± 30.7 g, 72.9 ± 24.1 g, and 42.1 ± 13.5 g, respectively (F = 56.3, p = < 0.001) (Figure 26). There was a significant difference between shell parameters of clams between sites, with the exception of shell length in clams from the lower and middle sites (i.e., clams taken from the lower and the middle sites had statistically equal shell lengths) (Table 8). There was a positive correlation between shell parameters correlated against one another, and between each parameter and whole body mass with a correlation value (r) greater than 0.9 (Figures 27, 28).

Organic matter analysis

At the end of each month in 2016, a total of four sediment samples were taken within each collection site where clams were obtained, and samples were processed in the lab to determine percent OM. The range of OM per site was 0.9 – 21.6%, 2.3 – 17.8%, and 0.4 – 18.4% (lower, middle, and upper, respectively). The average percentage of OM per site was 8.3 ± 5.2%, 6.6 ± 4.1%, and 3.2 ± 3.1%, respectively. Analysis of these values to determine if there was a statistical difference between the OM content at these sites included Kruskal-Wallis and Dunn's test (q_{crit} = 3.53) for pairwise comparison of OM between sites, and a two-way ANOVA (F_{crit} = 3.07) followed by Dunn's test for determining if location and the presence of clams had a significant effect on OM. A critical value for Kruskal-Wallis test could not be determined due to low numbers of group sizes (= 2), but the median value was calculated at 48 (P =< 0.001), indicating a

significant difference in OM. It was determined that while there was no significant difference in percent OM between the lower and middle sites (q = 1.56), there was a significant difference in percent OM between the lower and inner (q = 6.63), and middle and inner sites (q = 5.07).

A near two-fold difference in percent OM was determined when results were separated based on where clams were present versus absent within each site. The average percent of OM where clams were present per site was 5.7 ± 3.2%, 5.3 ± 3.4%, and 2.6 ± 1.3%, respectively. While, average percent of OM where clams were absent per site was 10.9 ± 5.5%, 8.0 ± 4.4%, and 3.9 ± 4.1%, respectively. Location and presence of clams had a significant effect on OM (F = 40.7 and 19.4, p = < 0.001, Df = 138, n = 24); however, the interaction between location and presence or absence of clams showed no significant effect on OM (F = 1.8, p = 0.158). Only six pairwise comparisons out of fifteen conducted were significant (Table A1).

Sediment particle size analysis

Across all sites, based on measured mass, the dominant particle sizes fell between 0.25 and 0.063 mm. Overall, very little sediment (< 1%) was 4 mm or larger. Comparisons of particle sizes between sites revealed that the lower site had no dominant particle size. However, medium to very fine sand (0.125 mm) was the dominant particle size in samples acquired from the middle and inner sites (57% and 68%, respectively). In contrast, only 29% of sediment from the lower site was between 0.125 and 0.25 mm. Another 29% of sediment from the lower site was between 0.063 and 0.125 mm. The remaining 42% of sediment from the lower site was greater than 0.25 mm and less than 0.063 mm. Sediment particle size and site from which samples were taken were

significantly related (χ^2 probability = 102, χ^2 = 126, p = < 0.001, df = 78) as determined using a Chi-square analysis. Particles greater than 2 – 4 mm included small rocks and shell fragments (e.g., from *Geukensia demissa*). Small rocks or pebbles were more commonly collected from the inner site, while shell fragments were abundant in samples taken from the lower site.

Burrowing Behavior per sediment type

The burrowing behavior of 8 specimens of *R. cuneata* and 5 *P. caroliniana* were recorded across three sediment types (sand, silt, and clay). Per sediment type, 13 clams were recorded burrowing in the dorsal-ventral (D-V), posterior-anterior (P-A), and anterior-posterior (A-P) orientations, 12 of the 13 clams were recorded in the ventral (V) orientation (one died before a successful recording was made), and 7 of the 13 clams were recorded burrowing in ventral-dorsal (V-D) orientation.

After placement into a specific orientation, clams would remain in place anywhere from ten minutes to several days before burrowing. Burrowing behavior began with the emergence of the foot from the anterior and ventral end of the shell. Clams initiated a burrowing event by probing the sediment with their foot. While burrowing, siphonal activity was typically constant until the clam alternated contraction of the anterior and posterior adductor and retractor muscles acting to pull and rock the clam back and forth into the sediment in a wedge-like fashion. Just before contraction of the muscles, the siphons closed increasing the pressure in the mantle cavity and within foot as indicated by the clam rising slightly from the sediment. Both siphons of *R. cuneata* closed just prior to adduction of the shells. However, it was observed that the excurrent siphon would always close before the incurrent siphon in *P. caroliniana*. Any vibrations

caused by moving the camera or bumping the tank caused retraction of the siphons and foot into the shell resulting in a failed, partial burrow recording, the results of which were not included in the analysis. In these cases, siphonal activity would resume within minutes; however, burrowing might not have resumed for several more hours.

A burrowing cycle was defined from the time at which the foot emerged from the shell and began probing the sediment to cessation of burrowing activity or approximately 90% of the clam was buried and the recording was stopped. Overall, regardless of species, the total time for burrowing cycles ranged from 300 to 6675 seconds. When the length of time for only the burrowing events were summed per specimen (i.e., time between burrowing events was excluded), the range of length of burrowing events was 34 seconds to 490 seconds. If separated by sediment type, the total length of burrowing events ranged from 41 seconds to 435 seconds in sand, 34 seconds to 219 seconds in silt, and 55 seconds to 490 seconds in clay.

Using a one-way repeated measures ANOVA, it was determined that the type of sediment had a significant effect on the number of burrowing events ($F = 101.5$, $F_{crit} = 3.07$, $p = <0.001$, $df = 115$) and length of burrowing events ($F = 5.81$; $F_{crit} = 3.07$, $p = 0.004$, $df = 115$), when data from both species and all orientations were pooled. Generally, it took clams less events to burrow in silt (average = 13) than in sand (average = 28) and clay (average = 25). The results from a pairwise comparison using Hold-Sidak method ($t_{crit} = 2.42$) indicated a significant difference in the number of burrowing events between sand and silt ($t = 13.3$) and silt and clay ($t = 11.1$), but not between sand and clay ($t = 2.11$). A significant difference in length of burrowing events was measured between

sand and silt (t = 3.34), but not between silt and clay (t = 2.07) or sand and clay (t = 1.28).

Regardless of the species, a minimum of 11 events were required to burrow in sand, 10 in clay, and only 5 in silt. The greatest number of events required for burrowing for all sediment types included 69 events in sand, 57 in clay, and 23 in silt (Figure 24). When species were separately analyzed, the range of events required for burrowing in sand for *R. cuneata* versus *P. caroliniana* was 11 to 69, and 18 to 55, respectively. In silt, the number of events ranged from 5 to 23, and 6 to 22, respectively. In clay, the number of events ranged from 10 to 57, and 12 to 47, respectively. The length of events per sand, silt, and clay ranged from 1 to 16 seconds and 1 to 20 seconds, 2 to 26 seconds and 2 to 22 seconds, and 2 to 23 seconds, respectively (Figure 25). Initially, burrowing events were only 2 to 4 seconds, because the foot was penetrating the substrate. It was not possible to test for differences between species due to an unbalanced design and lack of repeated measurements. However, overall, it appears that across sediment types, *P. caroliniana* spent less time per event than *R. cuneata* (Figure 25).

When combining data from both species, but separating it out per orientation per sediment type, it appears that the number and length of burrowing events was similar across all orientations (Figure 26). In sand, the average number of events per orientation was 27 (D-V), 24 (P-A), 30 (A-P), 32 (V), and 28 (V-D). It took one clam a total of 69 (V) events to burrow. In silt, the average number of events per orientation was 13 (D-V), 10 (P-A), 14 (A-P), 13 (V), and 16 (V-D). In clay, the average number of events per orientation was 21 (D-V), 22 (P-A), 24 (A-P), 33 (V), and 29 (V-D). It took one clam a total of 57 (V) events to burrow.

Discussion

Observations of Johnson Bayou

This is the first report on some of the biological and physical characteristics that make up Johnson Bayou. While biotic and abiotic factors and observations were made throughout the bayou, during the course of 2016, three sites were chosen for primary focus. The lower reaches of Johnson Bayou opens up into Bayou Portage before reaching St. Louis Bay. In contrast, middle and upper sites, the lower reaches is much wider, surrounded by emergent grasses dominated by *Juncus roemarianus*, *Spartina cynosuroides*, and *Spartina alterniflora*, with gently sloping tidal flats that are exposed under very low tides. Water current is primarily under tidal influence, but wind may also play a large role in surface currents, because the emergent grasses are not tall enough to block the winds.

The middle portion of the bayou contains a larger variety of plant species (e.g., *Baccharis* spp.) along the banks and sediments consist of contrasting areas of silt and clay, with small areas of sand. The banks immediately adjacent to the emergent grasses may be flat and wide, or drop abruptly towards the bottom of the channel. The latter being typical of the bends where water scours and erodes the sediment. Large chunks of emergent grasses and root systems can be dislodged during storms or after heavy boat traffic. There are a few areas where accretion rates of sediment appear to be high, the presence of new plant growth is common, and as a result, clams were more commonly found. In these areas, it is not uncommon to observe surface currents flow along the banks in the opposite direction to that of the channel. These areas are ideal for infaunal and benthic organisms, because the velocity was observed to be much lower than that of

the channel, so there should be a better chance of larvae settling as well as replenishment of oxygen and food. Organic and inorganic particles may become trapped in these areas which means organisms have a greater chance of encountering particles in these areas.

Fauna and flora of Johnson Bayou

It is important to identify and record locations of native and invasive species of both plants and animals for conservation and potential management efforts. In addition, future research focused on how native and invasive species interact, consequently affecting the ecosystem in which they inhabit or invade, is of growing concern and scientific interest. During site visits, a total number of 40 species or genera of plants were identified, including the free-floating exotic invasive alligatorweed (*Alternantha philoxeroides*). A concern is the spread of alligatorweed from South America. A successful biological control for the weed is its native herbivore, the alligatorweed flea beetle. This beetle does not have a winter diapause; thus, it has to be released yearly and is apparently done so by the U.S. Corps of Engineers in an effort to control alligatorweed populations throughout the southern states (Center et al. 2009). Another exotic invasive species, Brazilian milfoil, was observed in the summers of 2014 and 2016 attached to mats of alligatorweed; however, there is no indication that this species is spreading in the bayou at the same rate as the alligatorweed and was only observed in areas with a salinity of 0 ppt. The vegetative parts of the plants die back in higher salinities and winter; however, these plants root in the soil and thus survive over periods of higher salinity and winter, making total removal of the alligatorweed and milfoil unlikely in the near future. The fact that these species exist in an easily accessible estuarine system could be valuable for future research focused on management and conservation.

Regardless of how many species of plants and animals were identified over the course of three years from Johnson Bayou, hundreds more likely remain unrecorded or unidentified. A more extensive study focused on species identification would be invaluable for further describing Johnson Bayou, a system that affects and is affected by St. Louis Bay and the MS Sound.

Abiotic factors – daily and seasonal results from Johnson Bayou from 2014-2016

Abiotic data for three consecutive years, providing a baseline of the current health of Johnson Bayou through the measurement of factors such as pH and dissolved oxygen. For estuarine systems, a pH value between 7 and 9 is desirable, while dissolved oxygen levels are typically between 80 and 110% saturation (ANZECC 2000). There were recordings of more extreme levels in pH (e.g., 4.21 and 8.37 in January and October 2014) and in dissolved oxygen (e.g., 4.7% saturation in 2015 and 162.3% saturation in 2014); however, these are single recordings from a single location in Johnson Bayou, and not enough information is available to determine why these levels of pH and dissolved oxygen drastically changed. There was a lower pH on average in the fall months, likely attributable to increased breakdown of OM, which would increase the acidity of the water. Hypoxic levels of oxygen below 15% saturation were recorded four times. All but one of these times were recorded from areas located in canals near culverts that direct water from the ditches and roads. These areas are mostly stagnant all year-round and covered in thick mats of algae and free-floating aquatic plants (e.g., *Lemna minor*). In general, above average levels of dissolved oxygen were recorded shortly after rainfall events that resulted in greater mixing of the water column. As a consequence, the bottom dissolved oxygen was higher than or equal to that of the surface.

During one of seven field measurements taken in August 2016, water temperature was approximately four degrees warmer on the bottom of the water column. This was not entirely unexpected, as it rained for several days prior to taking measurements and this water would have had less time to absorb heat. Total rainfall for the month of August 2016 was about 23.5 cm, roughly 10 cm higher than average for the area at that time. Difficulties with the research performed here involved time management and selecting the best times in which high tides are at peak levels in order to assess the greatest difference in abiotic factors between the surface and bottom of the water column. While more measurements may provide a clearer image of how these factors change throughout the seasons, this study does provide at least a baseline of what to expect in a given year and can be valuable information for determining which parts of Johnson Bayou are in need of management.

Rangia cuneata and Polymesoda caroliniana

Rangia cuneata was always found to be more abundant than *P. caroliniana* regardless of location in Johnson Bayou. This was also an observation made by Fairbanks (1963), noting that *R. cuneata* outnumbered *P. caroliniana* along the north and southern shores of Lake Pontchartrain.

Based on preliminary observations in Johnson Bayou, it was originally hypothesized that both species of clams living in the lower reaches of Johnson Bayou exhibited an increased shell inflation and whole body mass compared to those living in the middle and upper sites. However, clams living in the middle site exhibited the greatest shell length, greatest shell height, and greatest shell inflation. The clams from the lower site did exhibit the greatest whole body mass, with a maximum record of 173.8 g.

In general, clams living in the lower reaches and middle of the bayou are likely to have approximately double the whole body mass compared to those living in the innermost locations (averages of 97.5 and 42.1 g, respectively). Statistically, location had a significant effect on shell dimensions and whole body mass. When shell dimensions and whole body mass were compared between locations, the only insignificant difference was shell length of clams from the lower and middle sites. All other comparisons were significant.

Given the differences in the sizes of clams across sites, it is possible that the clams in the lower reaches of Johnson Bayou could be encountering more food and nutrients coming in from the bay compared to those living in the innermost regions of the system. In other studies, salinity has been correlated with size of *R. cuneata*; for example, larger clams have been reported to be found in areas of the Potomac River where salinity is far lower than levels reported in Johnson Bayou (Pfitzenmeyer and Drobeck 1964). Pfitzenmeyer and Drobeck (1964) measured the highest salinity level at 11.8 ppt in their study within the Potomac River. Clams living at this salinity were half the size of those in salinities at around 5.7 ppt (Pfitzenmeyer and Drobeck 1964). Further research analyzing the type and abundance of food in these areas of Johnson Bayou is necessary to determine if food is indeed a causative factor for differences in size and if salinity plays a role as well. Due to differences in biotic and abiotic parameters throughout Johnson Bayou, it is clear that based on where clams are located, they do not respond in the same manner in terms of physiological aspects. More specifically, *R. cuneata* present differences in reproductive cycles based on their location and as a result of seasonal abiotic factors.

Reproductive histological analysis of Rangia cuneata

To my knowledge, this is the first study on the reproductive cycle of *R. cuneata* in a bayou, rather than a bay or large river (e.g., Mobile Bay, James River; Cain 1975, Jovanovich and Marion 1989). The results support previously published literature on gametogenesis progressing under the influence of warming temperatures and releasing gametes under increasing salinity (Cain 1972; Jovanovich and Marion 1989). Based on visual analysis of stained tissue, clams from the lower site produced gametes earlier in the year than those from the middle and upper sites, and spawned twice between June and November (Figures 21, 22). Clams from the middle and upper sites presented ripe gametes (ripe ova or spermatozoa) in the late summer months followed by spawning in the Fall. However, using the method by Tomkiewicz et al. (2011), results suggest that clams from the middle and upper sites may have spawned twice between June and November (Figure 21). The percentage of gametic tissue dropping in June and November from these sites are not nearly as great as presented from the clams in the lower site, but a partial spawning event is not out of the question. Overall, the clams in the lower site undergo gametogenesis at a faster rate and may become ripe up to two months before individuals at the other two sites. By the time spawning occurred, water temperatures had begun to drop from peak levels in the summer. Overall, water temperature does appear to be a strong factor in the rate and timing of gamete production. It was unexpected to have a weak correlation between salinity and production of gonadal tissue from clams living in the lower reaches of the bayou; however, upon further examination (Figure 21), the spawning event in June followed by an increase in gonadal tissue and second spawning event in November, could be reason why gametogenesis did not correlate positively with

salinity. In contrast, salinity did correlate in a positive fashion with production of gonadal tissue in clams from the middle and upper sites. For several months, salinity in these regions remained at 0 ppt, only to increase starting in summer, and peaking in November.

A dual reproductive cycle in which bivalves release gametes more than once within a single year is not unusual, and has been reported in *Spisula solidissima* (Ropes 1968). While temperature, food abundance (Delgado and Camacho 2005), and possibly hormonal influences cause spawning in marine species (Ropes 1968), if salinity is the primary trigger for spawning in estuarine species of bivalve, then this may support why clams in the lower reaches of Johnson Bayou appeared to have spawned twice, but interestingly, at different salinity levels (i.e., salinity peaked in November).

Aside from salinity levels, food abundance may be another factor in the rate and timing of gametogenesis and spawning. The contours of the lower reaches of Johnson Bayou include a larger volume of water and more gentle slopes along the grasses compared to the middle and upper sites. It stands to reason that the lower reaches of Johnson bayou has a greater abundance of food coming in and out of the system during tidal shifts. A study by Delgado and Camacho (2005) showed that the quantity of food does not influence maturation, but does condition gonadal development. Specimens in the presence of abundant food develop gonads faster than those without as much food (Delgado and Camacho 2005). Future research should focus on abundance of phytoplankton present in the selected sites in Johnson Bayou.

Unlike Fairbanks (1963), who stated that specimens of *R. cuneata* presented gonads of different color and texture from sites in Lake Pontchartrain, gonads in specimens from Johnson Bayou were found to be a single color, and the sex could only

be determined via histological examination. Even then, if no gametes are present, or germ cells are undifferentiated, then the sex of the individual cannot be determined (Bower and Blackbourn 2003). In this study, determination of sex, particularly of clams in the spent phase, was made based on the presence of residual gametes, some outside of the follicles and lobules, presumably due to rupture or natural breakdown of a follicle or lobule. However, the eight clams whose sex could not be determined were collected at times where they should have been in the spent phase. Consequently, if the gonad is collapsed during the spent phase, then there may be no cellular material left to determine sex.

Following the ripe and partially spent phases, the presence of empty lumens suggests that any remaining gametes were in the process of being removed with granular hemocytes, and follicles should begin to shrink and eventually collapse. Collapsed gonadal tissue appears much like visceral tissue (e.g., digestive gland and muscle tissue). Other bivalve species may exhibit similar features of gonadal tissue for some time after spawning, with no obvious gonadal development occurring during this time (Afiati 2007). Given the fact that all stages of gametogenesis were observed during the ripe phase in both sexes, several annual spawning events are not unreasonable. Previous studies have reported multiple spawning events in populations in *R. cuneata* (Fairbanks 1963; Chanley 1965; Jovanovich and Marion 1989). In the current study, while it was not determined at the specific salinity level spawning is triggered, the results do provide insight into a relative range, and more importantly how clams may behave when salinity does not reach levels known to trigger spawning in other estuarine systems. In other words, salinity levels in the middle and uppermost regions of Johnson Bayou do not reach that of the lowermost region. It is very reasonable to hypothesize that clams

throughout the system are cued to their local environment (i.e., sites in Johnson Bayou) to undergo gametogenesis and spawn at a relative level of salinity at their location.

Organic matter analysis

Sediment from the lower site of Johnson Bayou was found to contain more OM than sediment from the middle and upper sites. The results are supported by the visual observation of sediment type abundant in each area. Where sediments at the lower site are composed of thick layers of silt and peat-like material, the middle contains areas of silt and clay with some areas composed of a layer of sand located beneath a thin layer of silt that accretes over time. Last, the upper parts of the bayou are characterized by large areas composed of sand and clay. During times of heavy rainfall where surface velocities can reach greater than 1 m s^{-1}, sand washes out away from the edges of the bayou toward the middle parts of the channel. It was not uncommon to see bends in the channel freshly covered with sand shortly after a storm, and then slowly covered by plant litter and silt throughout the following months. For this study, only the top level of sediment (cores of ~90 mm) was removed for OM determination, as the clams do not live at depths much greater than their shell length (max recorded = 71.3 mm) since siphon length limits the depth at which infaunal bivalves can live. Nonetheless, there was a difference in percent OM between sites and in some cases, statistically different depending on whether clams were present or absent. Percent OM was lower where clams were present versus where they were absent (average of ~3-6% versus ~4-11%, respectively).

There might be a level of OM that inhibits growth or settlement (Tenore et al. 1968); however, it may be that the physical factors of Johnson Bayou (sediment particle size, water velocity, basin shape) are more likely be attributed to where clams are present

versus where they are absent. The amount of OM, specifically in the lower reaches in Johnson Bayou, exceeds what has been reported in a few studies. For instance, in laboratory studies, Tenore et al. (1968) observed that *R. cuneata* preferred sand with high OM (1% in their study). Fairbanks (1963) reported a maximum OM of about 6% in clay in Lake Pontchartrain. The maximum recorded percentage OM from Johnson Bayou came from the lower site, heavy in silt and measured at approximately 22%. While clams were not found in this area, they were found in areas of OM as high as 18%. However, clams of either species were rarely found in sediment with OM higher than 6%. Based on these results, it appears that both *R. cuneata* and *P. caroliniana* may prefer a lower amount of OM regardless of sediment type in areas of Johnson Bayou.

Growth and survivability of the clams may be influenced by the amount of OM present in the sediments, based on previous research focused on *R. cuneata* (Fairbanks 1963; Tenore et al. 1968; Hoese 1973). A study of a population in the Pamlico River Estuary in North Carolina showed few numbers of clams were associated with a clay and silt substrate with high OM and high phosphate concentration (1% and 0.1%, respectively) (Tenore et al. 1968). These results were supported by laboratory experiments involving a range of high (1% and 0.1%) and low (0.1% and 0.001%) OM and phosphate concentrations, respectively (Tenore et al. 1968). In contrast, sand with high OM and high phosphate concentrations was found to be preferred by clams in the same study (Tenore et al. 1968; Tenore 1972). Greater growth of clams was reported from sand with high OM content compared to sand with low OM content. Clams were adversely affected in clay-silt sediment with high OM and phosphate concentration (Tenore et al. 1968). Another study conducted by Hoese (1973) found no correlation

between abundance of clams and sediment type, and reported a paucity of individuals in sediments with an organic content greater than 10%. In general, it appears that in areas where sediment is overlain with a high amount of plant detritus, the number and size of clams were much lower (Fairbanks 1963), likely due to the clam's inability to stabilize themselves in sediment containing a copious amount of plant material (Hoese 1973).

Fairbanks (1963) found that between two localities in Lake Pontchartrain, levels of OM in the water column had an effect on population density and size of clams. The population on the north shore had higher numbers of individuals, smaller and less variable sizes, heavier shells, and more eroded umbos compared to the population on the south shore. Additional factors that likely have a cause in the differences observed by Fairbanks (1963) include lower pH, greater bacterial counts, and clay and silt sediments characteristic of the north shore compared to the south shore. High organic content would potentially allow greater growth and survivability of larvae while heavier shells could result from increased calcification in response to a lowered pH; the latter produced by carbonic acid resulting from carbon dioxide released from the actions of bacteria (Fairbanks 1963). If larvae are selectively feeding on bacteria, and bacteria are abundant in sediment high in OM, then this could explain the correlation. During the summer of 1958, Fairbanks (1963) calculated a 0.53% and 6.72% OM content for sand and clay, respectively. Organic matter content in the water column was calculated at 29.4 and 23.3 mg ($KMnO_4$) for the north and south shores of Lake Pontchartrain, respectively (Fairbanks 1963).

Sediment particle size analysis

Over half the mass of sediment from the middle and upper sites indicated that these areas are composed primarily of fine sand. In contrast, samples from the lower site were not primarily composed of one dominant particle size, resulting in a more even distribution of sediment particle sizes in this site. The sediment in the lower site appears from the surface to be composed of thick, but soft mud and silt in most areas and thick peat-like material in others. Particle size analysis reveals a mixture of sand, silt, and some clay. Areas heavy in peat-like material were found where higher wave action or greater velocity was observed. The sediment in the middle of Johnson Bayou is a mix of sand, silt (dominant sediment type), and clay. Clay particles are defined as less than 0.063 mm in diameter (Wentworth 1922), and because of the small particle size, clay naturally holds on to water and has less pore space, making it difficult for organisms to move into or through it. The dominant areas of clay within the study site were located primarily in between the middle and upper collection sites. Clams of both species were found in this sediment type, but their presence was sparse. The sediment in the upper site is composed of a greater amount of sand than silt and clay; although there is some variability depending on location in the innermost parts of the bayou. In general, clams of either species studied here are more commonly found in silt compared to in sand and clay.

Burrowing behaviors per sediment type

With respect to observed burrowing behavior, closure of the siphons was not a reliable indicator of intended burrowing, because the clam may have been in the process of expelling waste material from the mantle cavity. In addition, during the burrowing process, many clams would rock or angle themselves where siphonal activity was

impossible to observe from the standpoint of the recording device. Siphons occasionally opened before complete contraction of the muscles. A more reliable indicator of intended burrowing was the rise of the animal slightly out of the sediment just prior to siphonal closure. This motion indicated swelling of the foot so it can act as an anchor while the retractor muscles contract, bringing the animal into the sediment.

After pooling the data from recordings of burrowing activity of all clams from all orientations, it was found that sediment type had a significant effect on the number of burrowing events and on the length of events. When burrowing activity results per sediment type were compared to one another using Tukey's HSD, the number and length of burrowing events undertaken by clams in sand versus clay was not statistically different. However, when comparing silt versus clay, the number of burrowing events was statistically different, while the length of burrowing events was not statistically different. It was surprising that there was not a difference in the length of burrowing events between sand and clay due to the differences in particle size. This may be due to the artificial environment in which this was conducted. While clay particles are much smaller and there is a smaller pore size between particles compared to sand and silt, the fact that multiple clams were recorded burrowing from different starting positions in the same artificial environment likely had an effect on the results. Multiple clams moving through the sediment without a lengthy time interval to allow for re-compaction would have introduced water into the sediment. The presence of an increased space between particles would have potentially altered how the clams were able to move through this type of substrate.

When analyzing the number and length of burrowing events by species, the most obvious difference was that less time was spent burrowing by *P. caroliniana* individuals. This may be due to the fact that bivalves with thinner shells and less shell inflation can burrow quicker (Seed 1980). The shell of *R. cuneata* is about four times the thickness of that of *P. caroliniana*.

At the beginning of this study, it appeared that clams were unable to successfully burrow from the V-D orientation except when in silt. However, later observations demonstrated that clams could actually burrow from this orientation, albeit with apparent difficulty. Alas, by this time, 6 of the 13 clams had completed the trials and had been returned to the bayou, and one specimen died before a successful recording of one of the five orientations was captured. As a consequence, the design was unbalanced and significance between species was not determined.

The results support observations of clam abundance and location in Johnson Bayou. Far more clams (> 32 m^2) were found in silt than in sand or clay (up to 5 m^2). The most interesting observation was that regardless of orientation, the patterns held true per sediment type. Clams undertook more burrowing events in sand and clay, but length of events were variable. This information could be useful in the development of prediction models intended to predict locations of clams within a system. Site observations support the conclusion that an area heavy in silt, with low water flow compared to the channel, and a gently sloping bank, then there is a greater chance of encountering clams. Both field and preliminary laboratory observations indicated that clams had a harder time burrowing if plant debris (e.g., sticks, decaying leaf litter) was present. Thus, while the presence of emergent and submerged grasses in Johnson Bayou had an effect on the flow

of water in some areas, if organic or inorganic debris was too thick, then clams were not present or were in reduced numbers.

Ultimately, abiotic factors such as salinity, OM, and sediment particle size have an effect on the physiological aspects of *R. cuneata*, and the presence and abundance of *R. cuneata* and *P. caroliniana* in Johnson Bayou. The results of this research may be valuable for understanding the dynamics in other systems surrounding St. Louis Bay (e.g., Jones River, Bayou Portage).

Table 1

Phases and gametic stages of clams used in the reproductive histology study

Phase	Percent gonadal to somatic tissue	Characteristics
Early active	25-50% gonadal tissue	Follicles and lobules are thin and primarily empty. The presence of oogonia and spermatogonia embedded in the follicular and lobular walls indicate an active gonad. Very few gametes are present beyond -gonia. Visceral somatic tissue and muscle bundles are abundant around the follicles and lumens.
Late active	50-75% gonadal tissue	All stages of gametes are present, but lumens are not yet enlarged or swollen with gametes. The number of ripe ova and spermatozoa begin to outnumber all other stages.
Ripe	>75% gonadal tissue	Follicles and lobules are swollen with gametes, primarily of ripe ova and spermatozoa. Very little somatic tissue is present.
Partially spawned	50-75% gonadal tissue	Lumens appear emptied of most gametes with residual or unspawned ripe ova and spermatozoa remaining. A second round of spawning is possible. Otherwise, residual gametes will undergo atresia.
Spent	<25% gonadal tissue	Follicles and lobules are empty and collapsed or have few unspawned and degenerating oocytes and sperm cells. Hemocytes are commonly found around and in the lumens.

This table is adapted from the publication by Ropes and Stickney (1965) from which was used the stages ("phases" here) and stages of the gametes per phase.

Table 2

Plants of Johnson Bayou

Scientific Name	**Common Name**
Albizian julibrissin	Pink silk tree
Alternantha philoxeroides	Alligatorweed
Ampelopsis arborea	Pepper-vine
Aster tenuifolius	Perennial salt marsh aster
Azolla caroliniana	Mosquito fern
Baccharis angustifolia	False willow
Baccharis halimifolia	Groundsel bush (sea myrtle)
Cicuta maculata	Water hemlock (spotted cowbine)
Cladium jamaicense	Saw grass
Crinum americanum	Swamp lily
Hydrocotyle umbellata	Marsh pennywort
Hymenocallis crassifolia	Spider lily
Ilex vomitoria	Yaupon
Ipomoea sagittata	Morning glory
Juncus roemarianus	Needle rush
Kosteletzkya virginica	Seashore mallow
Lemna minor	Duck weed
Lilaeopsis chinesis	Eastern lilaeopsis
Lonicera japonica	Japanese honeysuckle
Ludwigia sp.	Seedbox
Myriophyllum aquaticum	Brazilian milfoil
Phragmites australis	Common reed (Roseau cane)
Pinus taeda	Loblolly pine tree
Polygonum sp.	Smartweed
Quercus nigra	Water oak
Rubus sp.	Blackberry
Rumex verticillatus	Swamp dock
Ruppia maritima	Ditch grass (widgeongrass)
Sagitaria lancifolia	Bull-tongue (lance-leaved arrowhead)
Salvinia minima	Common salvinia (water spangles)
Scirpus robustus	Salt marsh bulrush
Scirpus validus	Softstem bulrush
Serenoa ripens	Saw palmetto
Setaria sp.	Grasses (foxtail)
Sesbania punicea	Rattlebush
Spartina alterniflora	Smooth cordgrass
Spartina cynosuroides	Big cordgrass
Triadica sebifera (*Sabium sebiferum*)	Chinese tallow
Typha latifolia	Cattail
Vigna luteola	Hairy-pod cow pea (deer pea)

This table lists the scientific and common names of identified species of emergent, submerged, free-floating, and terrestrial plants that directly impact and are impacted by Johnson Bayou.

Table 3

Invertebrates of Johnson Bayou

Scientific Name	**Common Name**
Agasicles hygrophila	Alligatorweed flea beetle
Apitasia sp.	Stripped anemone
Balanus sp.	Barnacle
Beröe ovata	Comb jelly
Callinectes sapidus	Blue crab
Chryosaora quinquecirrha	Atlantic sea nettle
Diopatra cuprea	Decorator worm
Dolomedes triton	Fishing spider
Dugesia sp.	Planarian
Ensis sp.	Razor clam
Gammarus sp.	Gammarid (amphipod)
Geukensia demissa	Ribbed mussel
Lyssomanes virids	Jumping spider
Myzobdella lugubris	Leech
Nereis sp.	Nereid (polychaete)
Neritina reclivata	Olive nerite
Palaeomonetes pugio	Grass shrimp
Polymesoda caroliniana	Marsh clam
Rangia cuneata	Wedge clam
Tagelus plebius	Stout tagelus
Uca spp.	Fiddler crabs

This table lists the scientific and common names of identified species of invertebrates in Johnson Bayou.

Table 4

Fish of Johnson Bayou

Scientific name	**Common name**
Anguilla rostrata	American eel
Archosargus probatocephalus	Sheepshead
Atractosteus spatula	Alligator gar
Cynoscion nebulosus	Spotted seatrout
Elops saurus	Ladyfish
Heterandria formosa	Least killifish
Ictalurus catus	White catfish
Ictalurus punctatus	Channel catfish
Lepisosteus sp.	Gar
Leponis macrochinus	Bluegill
Micropogonias undulatus	Atlantic croaker
Micropterus dolomieu	Smallmouth bass
Morone saxatilus	Striped bass
Pylodictis olivaris	Flathead catfish
Sciaenops ocellatus	Red drum
Trinectes maculatus	Hogchocker

This table lists the scientific and common names of identified species of fish that either inhabit or can be found at some point during the year in Johnson Bayou.

Table 5

Birds of Johnson Bayou

Scientific name	**Common name**
Accipiter cooperii	Cooper's hawk
Agelaius phoeniceus	Red-winged blackbird
Anas platyrhynchos	Wild duck (mallard duck)
Ardea alba	Great blue heron
Ardea herodias	Great egret
Aythya affinis	Lesser scaup
Aythya americana	Redhead
Aythya collaris	Ring-necked duck
Butorides virescens	Greenback heron
Egretta caerulea	Little blue heron
Elanoides farficatus	Swallow-tailed hawk
Mimus polyglottos	Mockingbird
Nyctanassa violacea	Yellow-crowned night heron
Pandion haliaetus	Osprey
Pelecanus occidentalis	Brown pelican
Phalaxcrocorax auritus	Double-crested cormorant

This table lists the scientific and common names of identified species of birds that either inhabit or migrate to and from Johnson Bayou.

Table 6

Reptiles and amphibians of Johnson Bayou

Scientific name	**Common Name**
Agkistrodon contortix	Copperhead
Agkistrodon ventralis	Cottonmouth
Alligator mississippiensis	American alligator
Chelydra serpentina	Snapping turtle
Coluber constrictor	Black racer
Hyla cinerea	American green tree frog
Lampropeltis getula holbrooki	Speckled king snake
Ophisaurus ventralis	Eastern glass lizard
Pantherophis guttatus	Corn snake
Rana sphenocephala	Southern leopard frog
Trachemys scripta	Red-eared slider

This table lists the scientific and common names of identified species of reptiles and amphibians in and around Johnson Bayou.

Table 7

Shell dimensions and whole body mass of Rangia cuneata

	Lower	**Middle**	**Upper**
Shell Length (mm)	42.2 – 69.8	47.5 – 71.3	38.6 – 60.3
Shell Height (mm)	35.7 – 61.3	38.2 – 62.7	32.4 – 44.8
Shell Inflation (mm)	30.8 – 50.6	28.9 – 54.6	25.9 – 38.7
Whole Body Mass (g)	34.1 – 173.8	39.1 – 134.1	21.7 – 70.3

This table presents the range of shell dimensions and whole body mass (shell + soft tissue) recorded from 108 collected *Rangia cuneata* from the lower, middle, and upper sites.

Table 8

Statistical comparison of shell dimensions and whole body mass of Rangia cuneata

Location Comparison	Shell Dimension	t value (q_{obt})	Significance?
Lower versus Middle	Length	2.53	Not significant
Lower versus Upper	Length	11.32	Significant
Middle versus Upper	Length	8.79	Significant
Lower versus Middle	Height	4.76	Significant
Lower versus Upper	Height	11.18	Significant
Middle versus Upper	Height	6.42	Significant
Lower versus Middle	Inflation	4.88	Significant
Lower versus Upper	Inflation	9.42	Significant
Middle versus Upper	Inflation	5.99	Significant
Lower versus Middle	whole body mass	3.50	Significant
Lower versus Upper	whole body mass	10.43	Significant
Middle versus Upper	whole body mass	6.92	Significant

A Tukey's HSD (q_{crit} = 3.36; p = 0.05) was performed with the assumption that there was a statistical difference in shell dimensions between, while a Holm-Sidak method was performed with the hypothesis that there was a statistical difference in whole body mass between sites (lower, middle, and upper).

Table 9

Ranges of abiotic factors from seasonal measurements

Dates of Measurement	pH	Dissolved oxygen (% saturation)	Water Temperature (°C)	Salinity (ppt)
October 2014	6.34 – 7.21	12.5 – 86.4	21.8 – 25.3	0 – 10
	6.30 – 7.01	8.96 – 62.5	21.8 – 24.8	0 – 10
February 2015	6.42 – 7.20	55.9 – 126.7	12.7 – 16.6	0 – 8.5
	6.32 – 7.10	30.2 – 122.9	12.6 – 15.9	2 – 12
June 2015	6.70 – 7.08	30.5 – 65.8	27.9 – 32.4	0 – 0
	6.70 – 7.10	16.5 – 61.5	26.8 – 29.9	0 – 0
October 2015	6.55 – 7.55	30.0 – 83.7	22.8 – 26.0	9.5 – 20.5
	6.77 – 7.54	23.6 – 92.0	23.0 – 24.9	15 – 22
February 2016	5.80 – 6.88	74.4 – 111.1	15.2 – 21.2	0 – 0
	5.79 – 6.84	53.6 – 98.7	14.7 – 21.2	0 – 0
May 2016	6.15 – 7.08	28.5 – 76.6	19.8 – 22.7	0 – 0
	6.05 – 6.92	21.9 – 70.0	19.5 – 21.9	0 – 0
August 2016	6.48 – 7.38	24.3 – 111.6	26.9 – 28.9	0.1 – 7
	6.30 – 7.05	24.1 – 96.2	26.4 – 31.3	0.1 – 8.4

A total of seven occasions of abiotic field measurements were undertaken, once in each of the above months. A range of values per abiotic factor are separated into surface and bottom water by a midline.

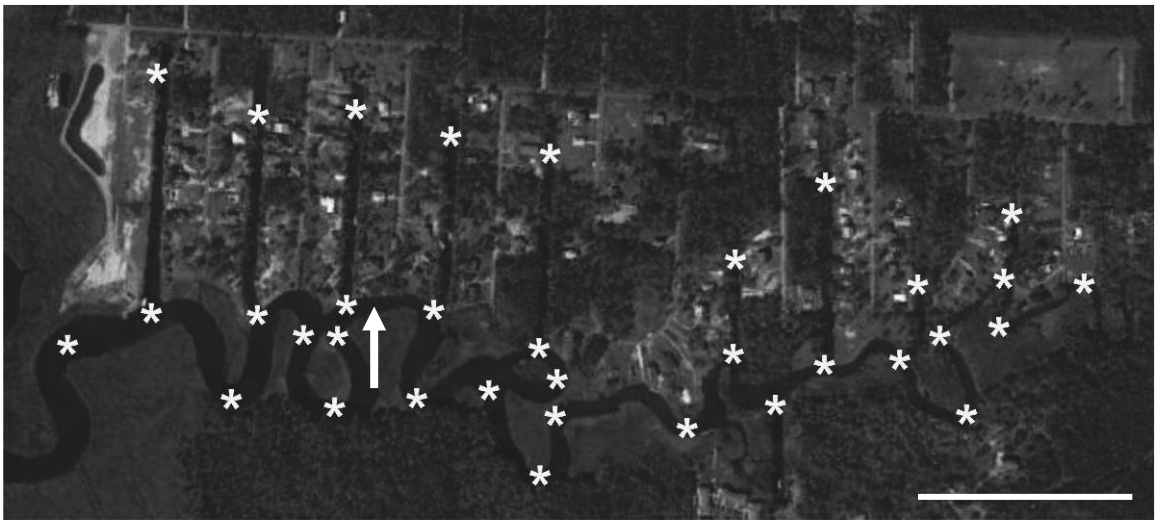

Figure 1. Seasonal sites for abiotic measurements in Johnson Bayou.

This image acquired and saved from GoogleEarth2013 shows 34 selected locations (*) in Johnson Bayou between 30°20.233'N 89°14.202'W and 30°20.274'N 89°13.419'W, at which seasonal abiotic parameters were measured (surface and bottom water) including pH, dissolved oxygen, water temperature, and salinity. The locations were selected based on the shape of the system and human development (e.g., canals and bulkheading on topmost portion of image). Arrow indicates site at which abiotic factors were measured on a near daily basis from 2014-2016. Scale bar = 0.25 km.

Figure 2. Collection sites for *Rangia cuneata* and sediment in Johnson Bayou (2016).

Specimens of *Rangia cuneata* and sediment samples were taken at the end of each month in 2016 along established salinity gradients indicated by numbered circles (1 – lower, 2 – middle, 3 – upper). Scale bar = 0.25 km.

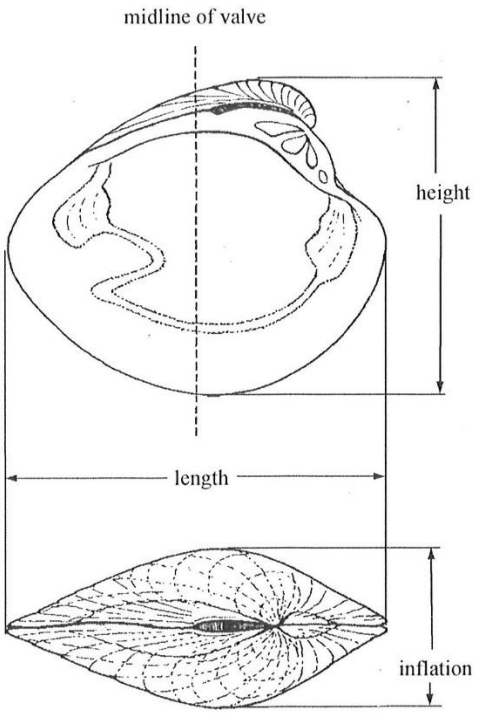

Figure 3. Shell dimensions for measuring bivalves.

Measurements include length from anterior to posterior, height from umbo (dorsal) to ventral, and inflation is determined at the thickest points of the shell. Image adapted from Leal JH. 2002. Bivalves. In: Carpenter KE, editor. The living marine resources of the Western Central Atlantic. Volume 1. Introduction, mollusks, crustaceans, hagfishes, sharks, batoid fishes, and chimaeras. FAO Identification Guide for Fishery Purposes. The Food and Agriculture Organization of the United Nations, Rome. p. 25-98. Reproduced with permission.

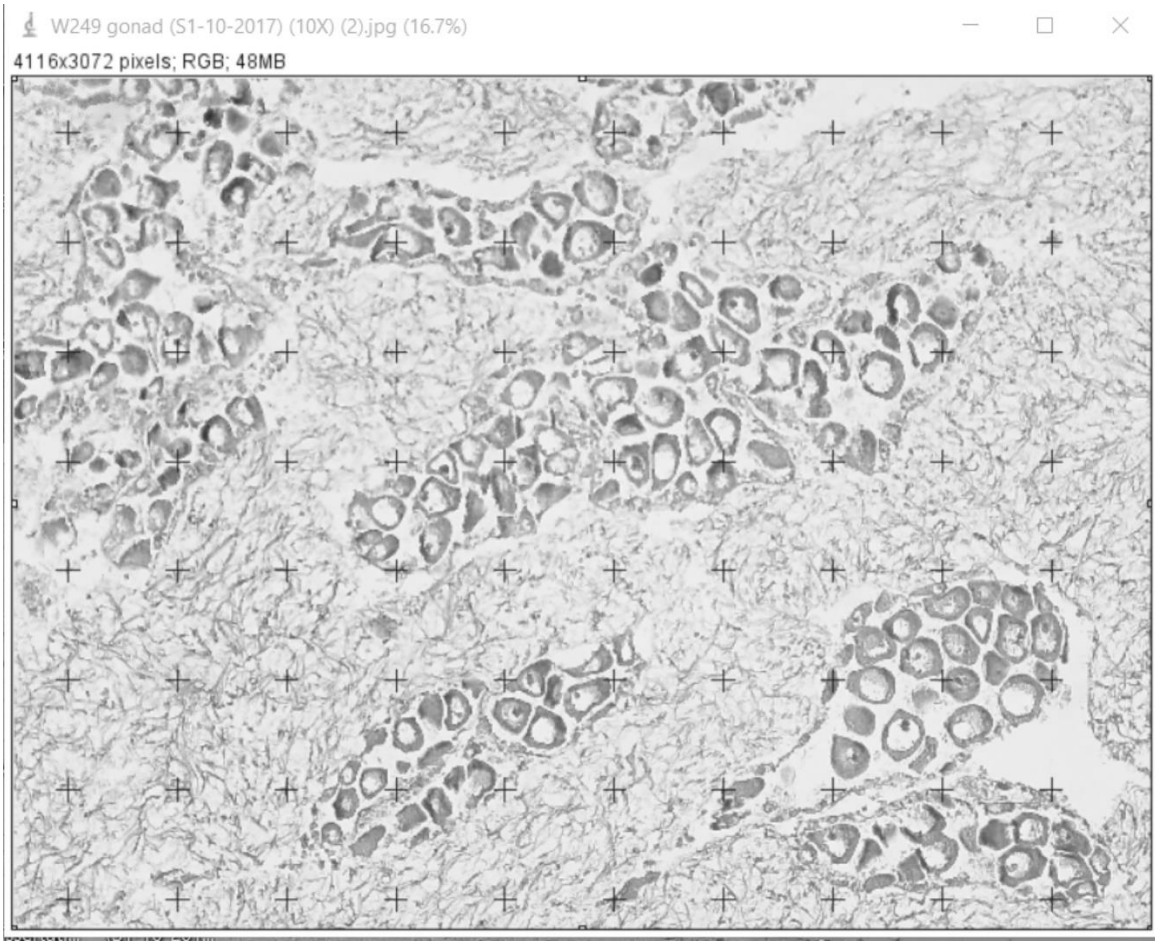

Figure 4. ImageJ analysis screenshot of gonadal tissue.

Adapted methods from Tomkiewicz et al. (2011): an image is opened into ImageJ and a series of 80 crosses are placed by the software over the image. Gonadal versus somatic tissue and the stage of gametes are recorded if it intersects a cross.

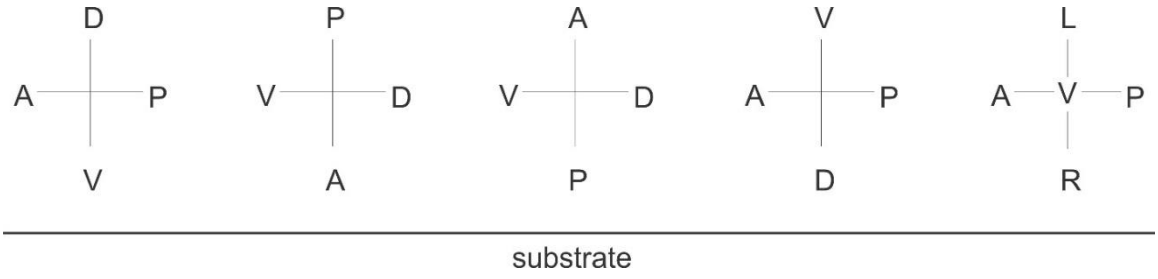

Figure 5. Starting positions and orientations for burrowing study.

These were the orientations each clam was placed in prior to recording burrowing behavior. The substrate was either sand, silt, or clay sediment. (A = anterior, D = dorsal, P = posterior, V = ventral, L = left valve, R = right valve).

Figure 6. Alligatorweed, alligatorweed flea beetle, and Brazilian milfoil.

Alligatorweed flea beetles are released by the U.S. Corps of Engineers each year (Center et al. 2009). This insect feeds exclusively on alligatorweed (a). Larvae of the beetle (arrows) hatch on the underside of the leaves and signs of consumption are indicated by holes in the leaves and stems (b). Brazilian milfoil (arrows) is associated with alligatorweed in Johnson Bayou, but is less abundant (c).

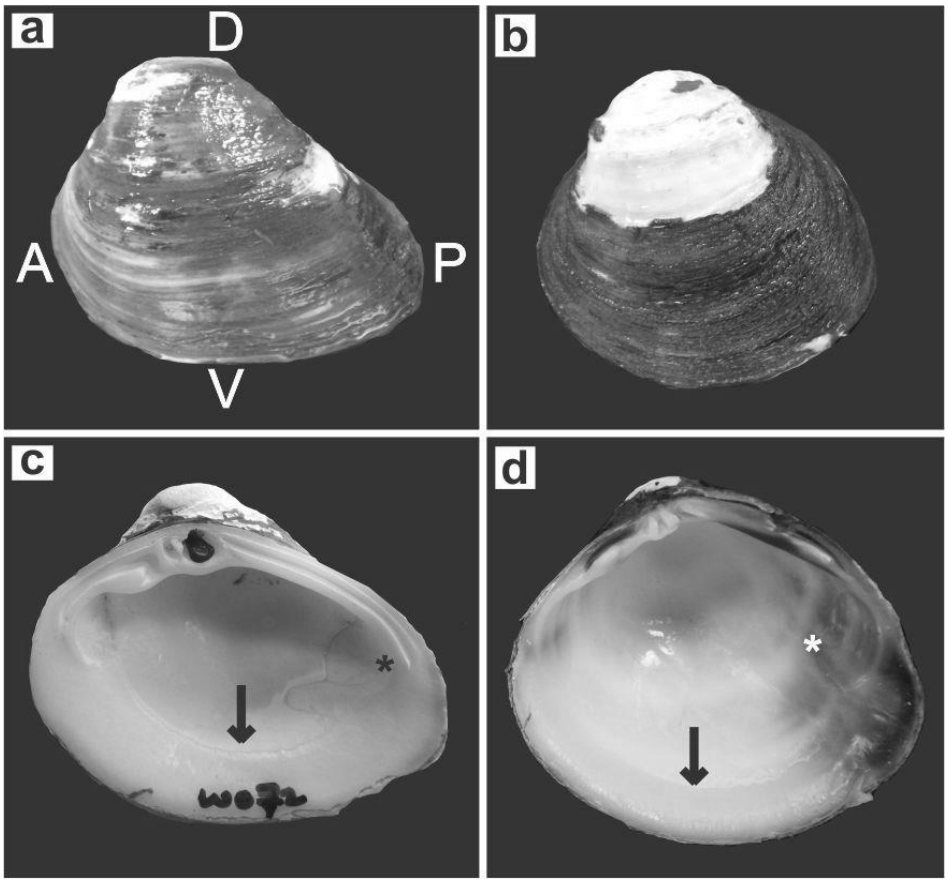

Figure 7. Shell characteristics of *Rangia cuneata* and *Polymesoda caroliniana.*

The periostracum of *Rangia cuneata* is dark, smooth, and unornamented (a). The periostracum of *Polymesoda caroliniana* is dark brown to black and ruffled (b). The nacre of *R. cuneata* is completely white, but has discernible scars where the adductor and retractor muscle (*) and the mantle tissue (arrow) are attached to the shell (c). The nacre of *P. caroliniana* is a mix of white, pink, and purple with scars that are less discernible, but mirrors those on *R. cuneata* (d). Abbreviations: A = anterior, D = dorsal, P = posterior, V = ventral). All images were oriented with respect to (a).

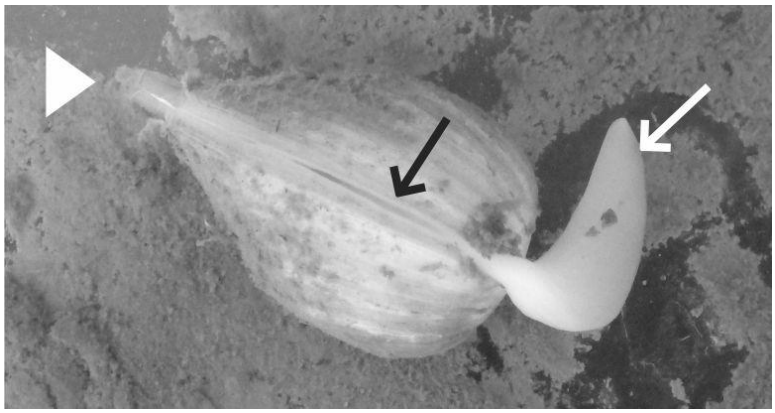

Figure 8. The foot, siphons, and pedal gape of clams.

The foot of both species (*R. cuneata* is shown here) is a pale, tongue-like structure (white arrow) that emerges from the pedal gape in the mantle tissue (black arrow). Siphons (arrowhead) indicate the posterior side of the animal.

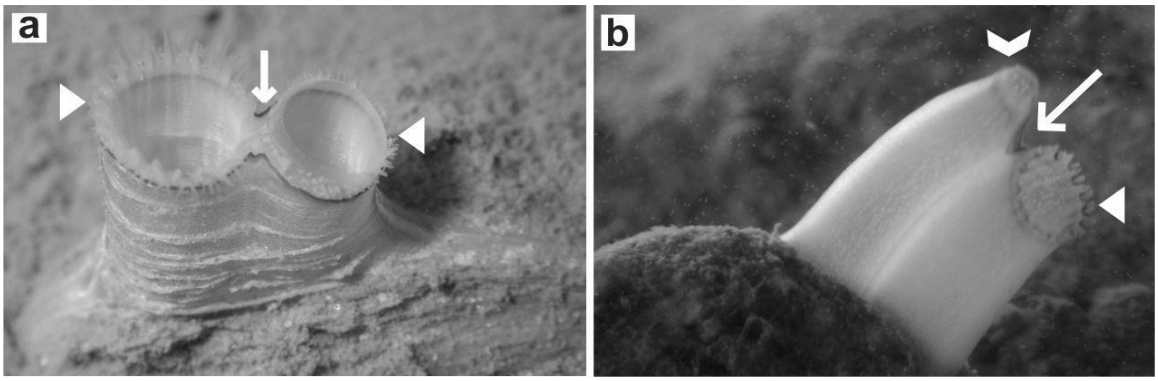

Figure 9. Siphons of *Rangia cuneata* and *Polymesoda caroliniana.*

The incurrent (left opening) and excurrent (smaller right opening) siphons are fused (arrow) in *Rangia cuneata* (a). The openings of both siphons are surrounded by a ring of tentacles, which are larger on the incurrent than the excurrent siphon. In *Polymesoda caroliniana*, the incurrent (right opening) and the excurrent (left and topmost opening) are smaller in diameter than those of *R. cuneata* and fused a few millimeters below the openings (arrow). The incurrent siphon is ringed with short, stubby tentacles (arrowhead) while the excurrent siphon is ringed with thin tissue (chevron).

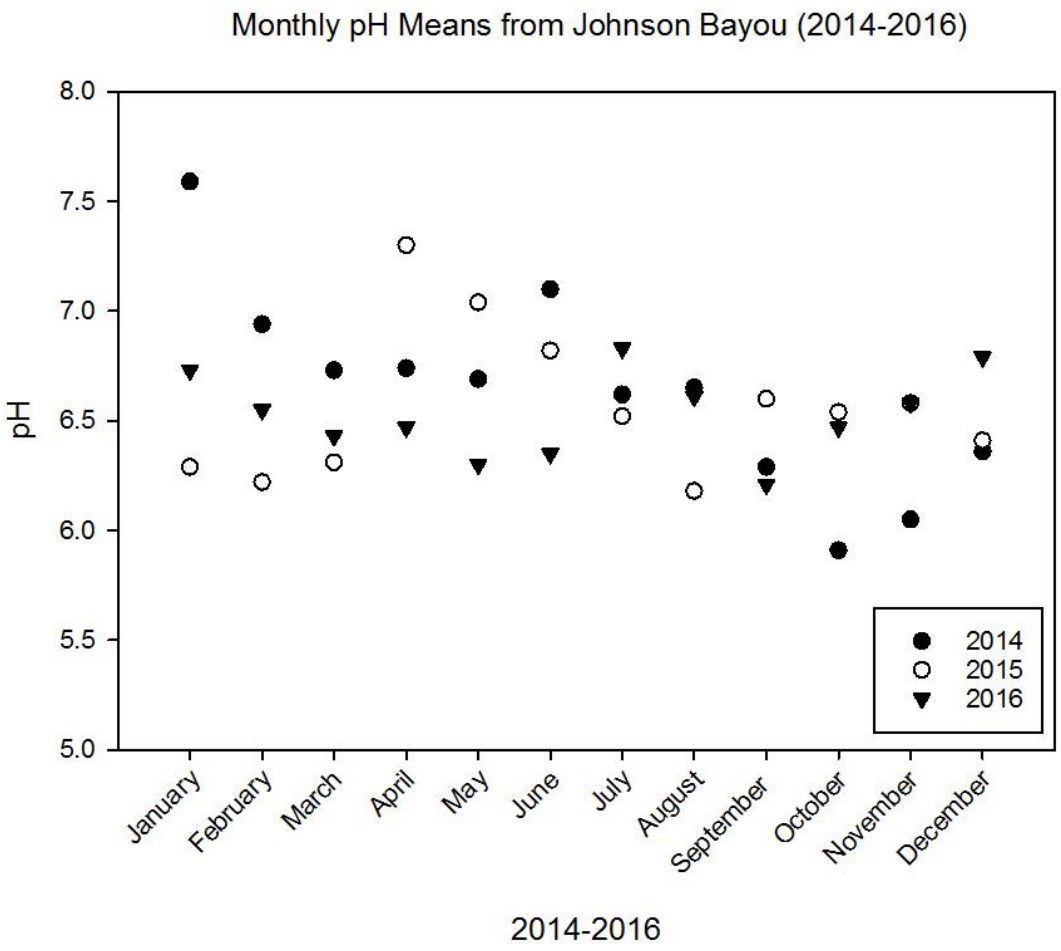

Figure 10. Monthly means of pH in Johnson Bayou (2014-2016).

pH means are presented across three years measured from a single point in Johnson Bayou. In general, average pH remained between 6.0 and 7.5 across all three years with the exception of January (pH = 7.6) and October of 2014 (pH = 5.9).

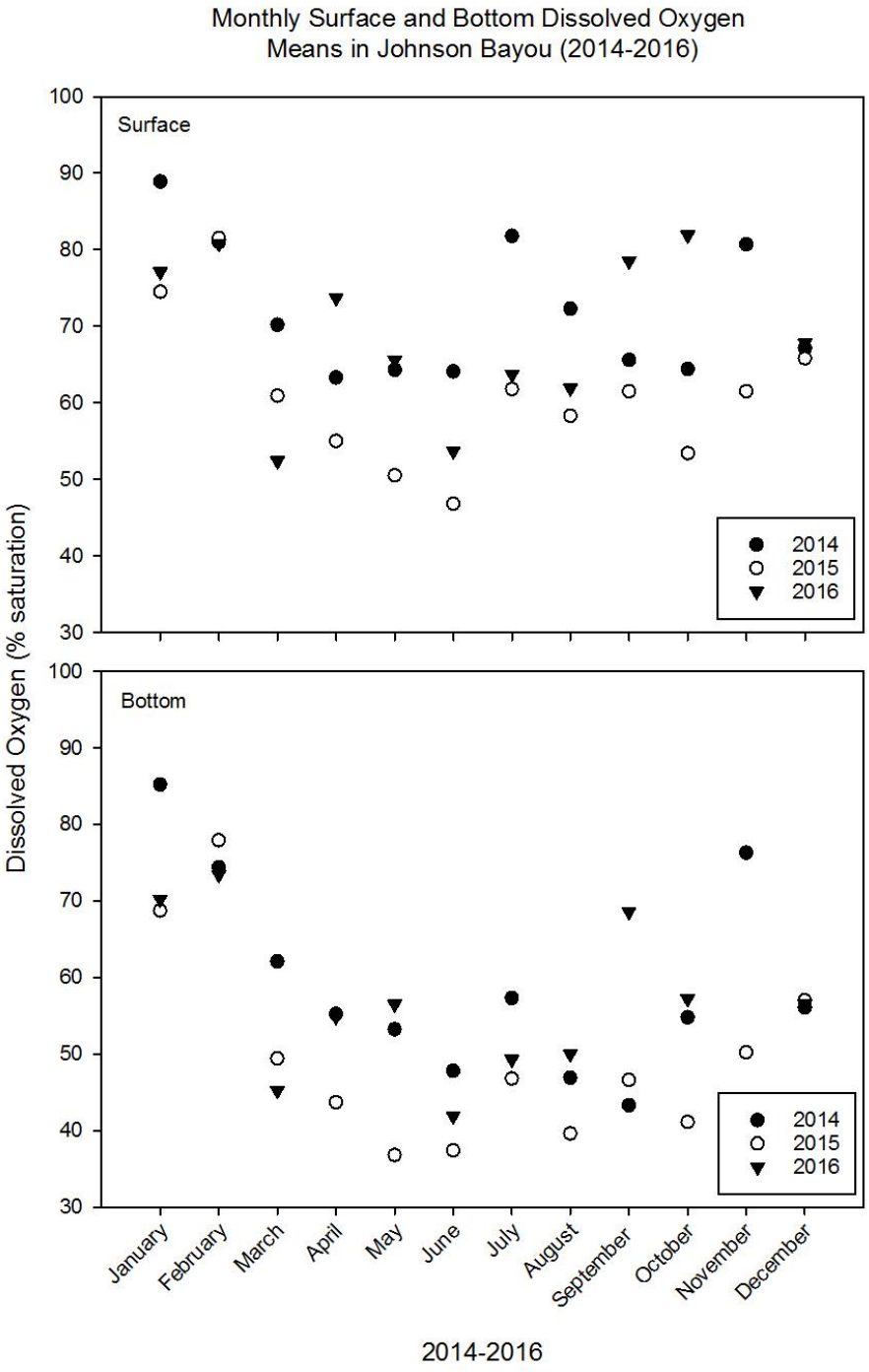

Figure 11. Monthly means of dissolved oxygen in Johnson Bayou (2014-2016).

Surface (a) and bottom (b) dissolved oxygen means are presented across three years measured from a single point in Johnson Bayou. In general, there was a lower average of dissolved oxygen on the bottom than the surface across all three years. Dissolved oxygen was highest in January and February across all years except for September and October in 2016. Averages across all three years ranged from 46.8 % saturation (2015) to 88.9 % saturation (2014) for surface and 36.8 % saturation (2015) to 85.2 % saturation (2014).

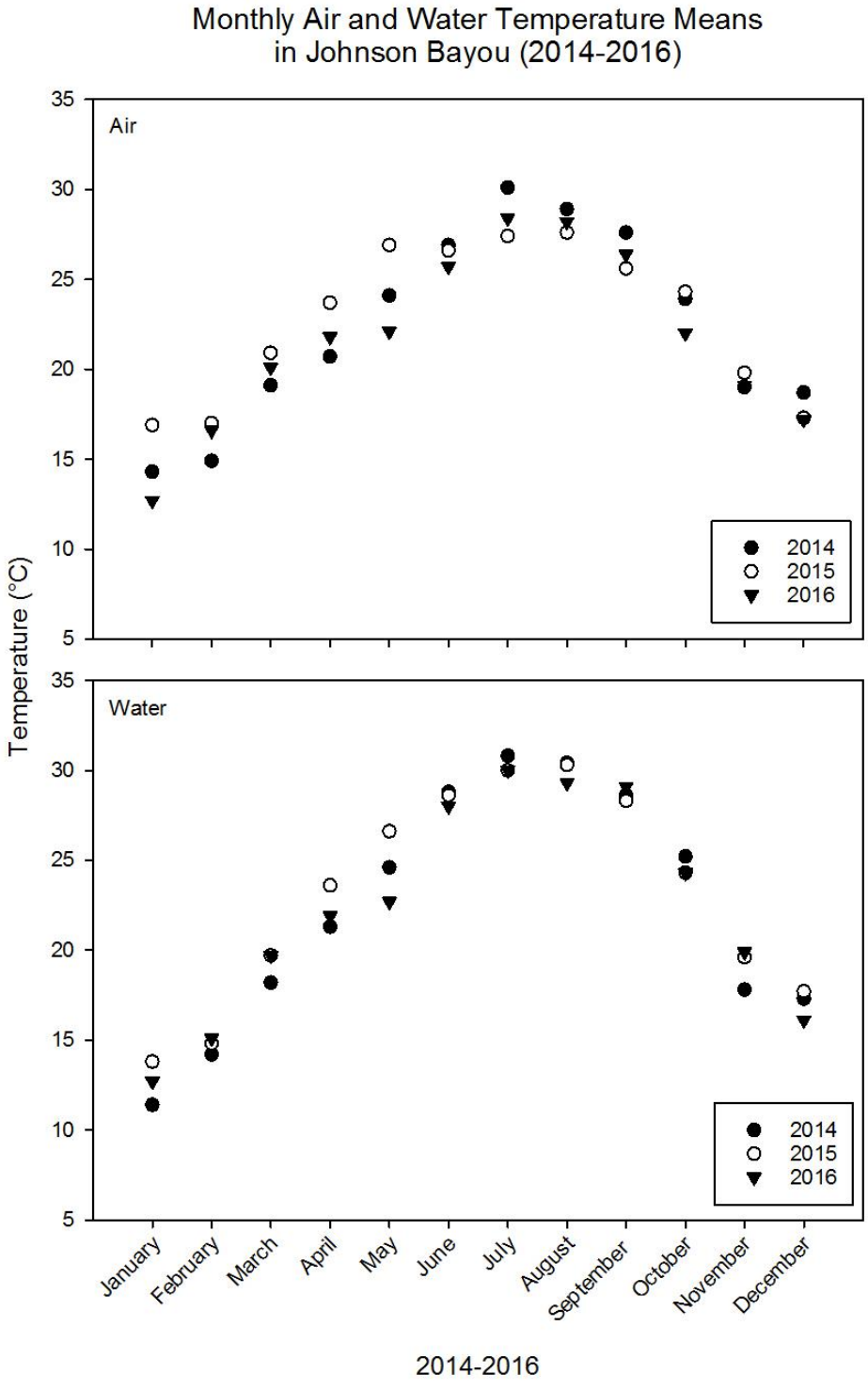

Figure 12. Monthly means of air and water temperature in Johnson Bayou (2014-2016).

Air (a) and water (b) temperature means are presented across three years measured from a single point in Johnson Bayou. Across these years, averages ranged from 12.7°C to 30.1°C for air temperature, and 11.4°C to 30.8°C for water temperature.

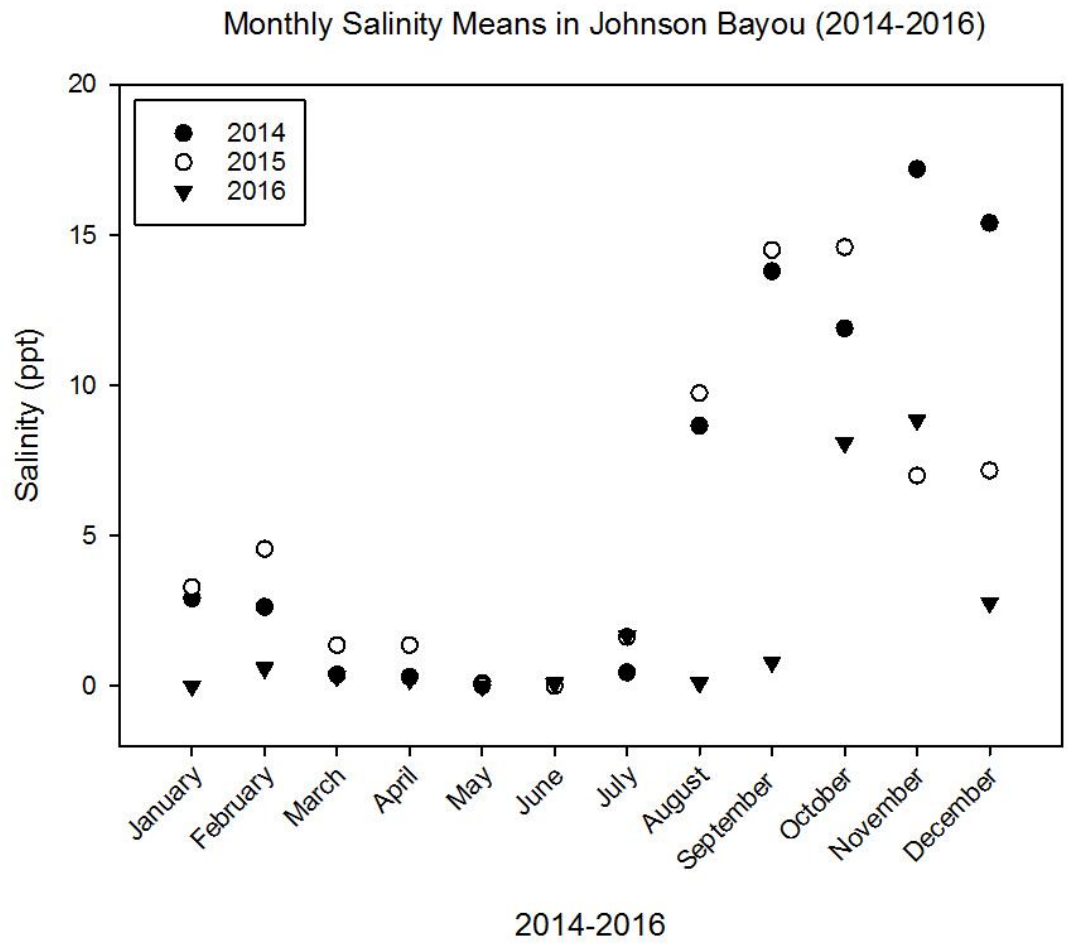

Figure 13. Monthly means of salinity in Johnson Bayou (2014-2016).

Salinity means are presented across three years measured from a single point in Johnson Bayou. For half of every year, salinity was near 0 ppt, and peaked from October to December.

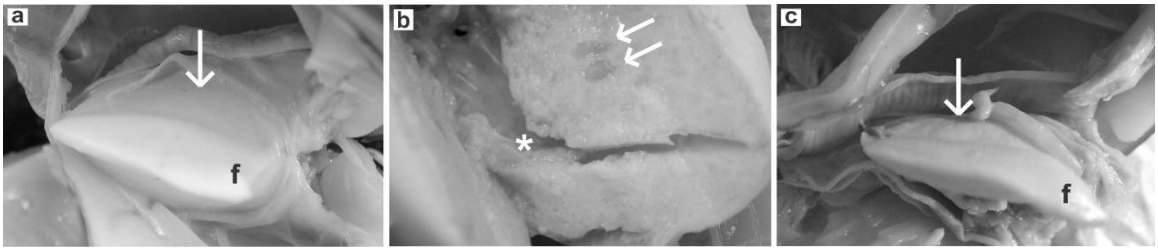

Figure 14. Gross morphology of the gonad and foot of *Rangia cuneata.*

The gonad is part of the visceral mass (arrow) flanked by the demibranchs and dorsal to the foot (f) (a). A section through a ripe gonad reveals digestive tissue (arrows) and the crystalline style (*) surrounded by gonadal tissue (b). In partially spawned and spent clams, the gonad is nearly absent (arrow) and the visceral mass is shrunken almost as thin as the foot (f) (c).

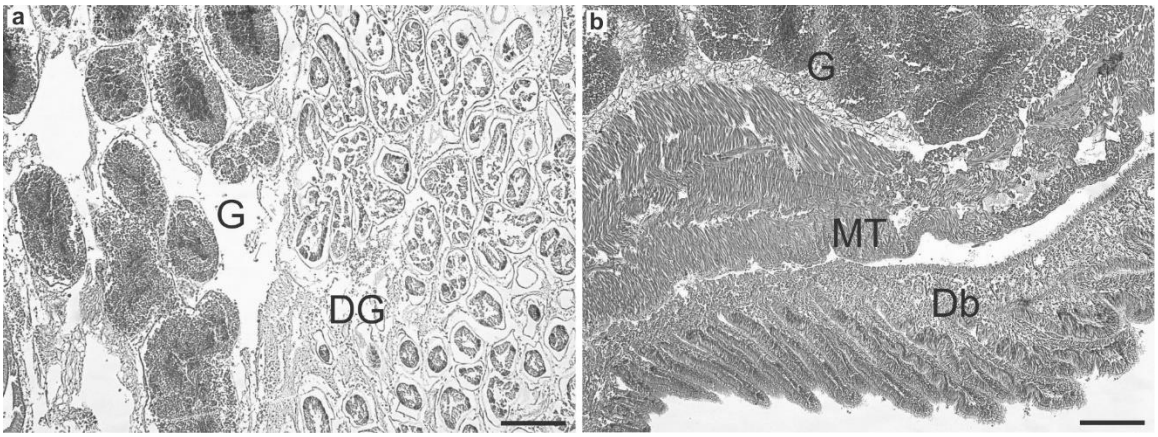

Figure 15. Photographs of H&E stained sections through the visceral mass of *Rangia cuneata*.

The gonad (G) grows in the vicinity and around the digestive gland (DG) (a). A thick muscular layer (MT) normally surrounds the gonad. The demibranchs (Db) lie just outside this muscle layer (b). Scale bars = 100 µm.

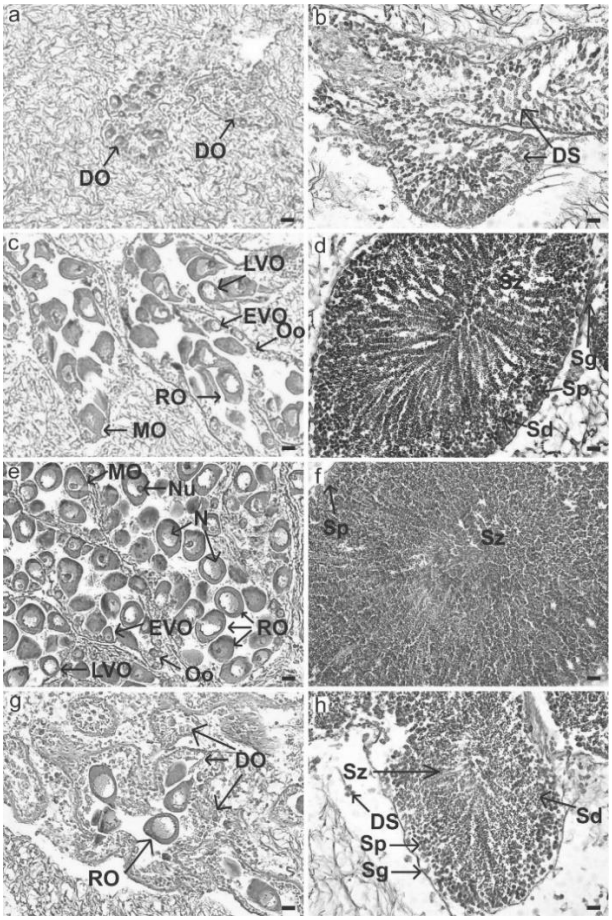

Figure 16. High magnification photographs of H&E stained female and male gonadal tissue of *Rangia cuneata*.

At the beginning of each year, gonadal tissue is characterized by collapsed or near empty follicles with degenerating oocytes and lobules with degenerating sperm cells (a, b). Early and late active phases (c, d) are characterized by the presence of enlarged oogonia and spermatogonia embedded in the follicular and lobule walls. All stages of gametes can be present at this time, including early and late vitellogenic oocytes indicated by increasing amounts of yolk and vitellogenin, but attached to the follicular walls, mature oocytes with a thin stalk, and a few ripe ova free in the lumen (c). In males, this includes spermatocytes in clusters along the outer lumen, spermatids further in the lumen, but smaller in size, and finally spermatozoa in the central lumen with the characteristically eosinophilic tails oriented toward the center (d). The ripe phase in both sexes is indicated by swollen follicles and lobules, and reduced somatic tissue (e, f). All stages of gametes may be present, but at the peak before spawning, the lumens are dominated by ripe ova with large nuclei and darker stained nucleoli (e) and spermatozoa (f). Last, partially spawned clams show a highly reduced number of ripe ova and spermatozoa (g, h), some of which do not get released. If no further spawning events can occur, degeneration of oocytes and sperm cells will occur. (Abbreviations: DO = degenerating oocyte; DS = degenerating sperm; EVO = early vitellogenic oocyte; LVO = late vitellogenic oocyte; MO = mature oocyte; N = nucleus; Nu = nucleolus; Oo = oogonia; RO = ripe ova; Sd = spermatids; Sg = spermatogonia; Sp = spermatocytes; Sz = spermatozoa). Scale bars = 10 µm.

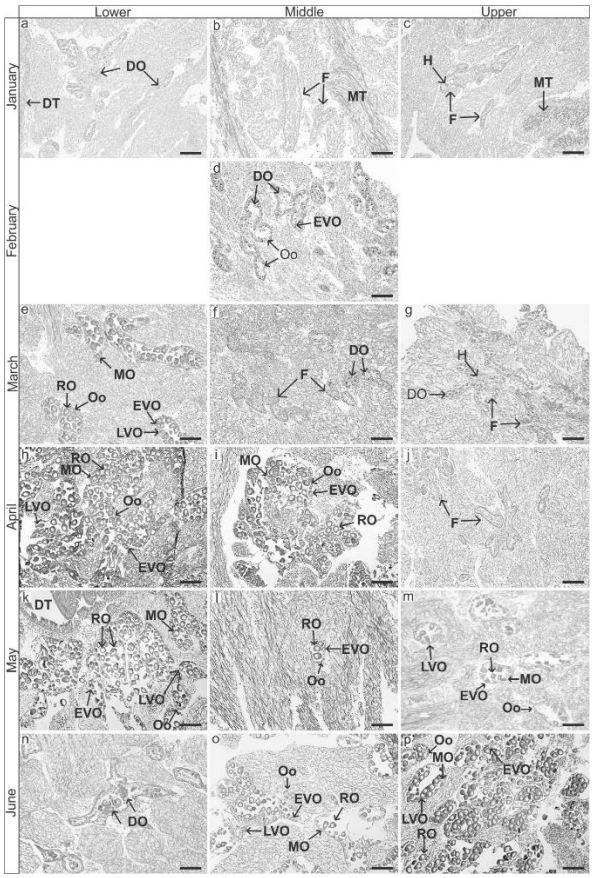

Figure 17. Photographs of H&E stained female gonadal tissue of *Rangia cuneata* taken from the lower, middle, and upper sites of Johnson Bayou from January to June 2016.

In January across all sites, spent clams had small, shrunken follicles containing degenerating oocytes and hemocytes. Digestive tissue (a) and muscle tissue (b, c) were commonly observed in sections. In February, clams from the middle section were spent with degenerating oocytes, but some presented oogonia and early vitellogenic oocytes along the follicular walls (d). In March, clams from the lower site were in the early active phase, producing early and late vitellogenic oocytes, and a few mature and ripe ova (e). Some clams from the middle and upper sites all contained residual or degenerating oocytes, but some produced early vitellogenic oocytes (f, g). In April, clams from the lower and middle sites were in the ripe (h) and late active phases (i), respectively. Many clams from the upper site still appeared spent or were producing few early vitellogenic oocytes (j). In May, clams from the lower site appeared to be spawning with a majority of mature or ripe ova in enlarged follicles against digestive tissue (k). Clams from the middle site were producing ripe ova (l), but remained in the early to late active phase. Clams from the upper site were in the early active phase producing early and some late vitellogenic oocytes (m). By June, clams from the lower site were partially spawned or spent with unspawned and degenerating oocytes in the follicles (n). Clams from the middle and upper sites were between the late active and ripe phases (o, p). Blank panels indicate no female clams were collected. (Abbreviations: DO = degenerating oocytes; DT = digestive tissue; EVO = early vitellogenic oocyte; F = follicle; H = hemocyte; LVO = late vitellogenic oocyte; MO = mature oocyte; MT = muscle tissue; Oo = oogonia; RO = ripe ova). Scale bars = 100 µm.

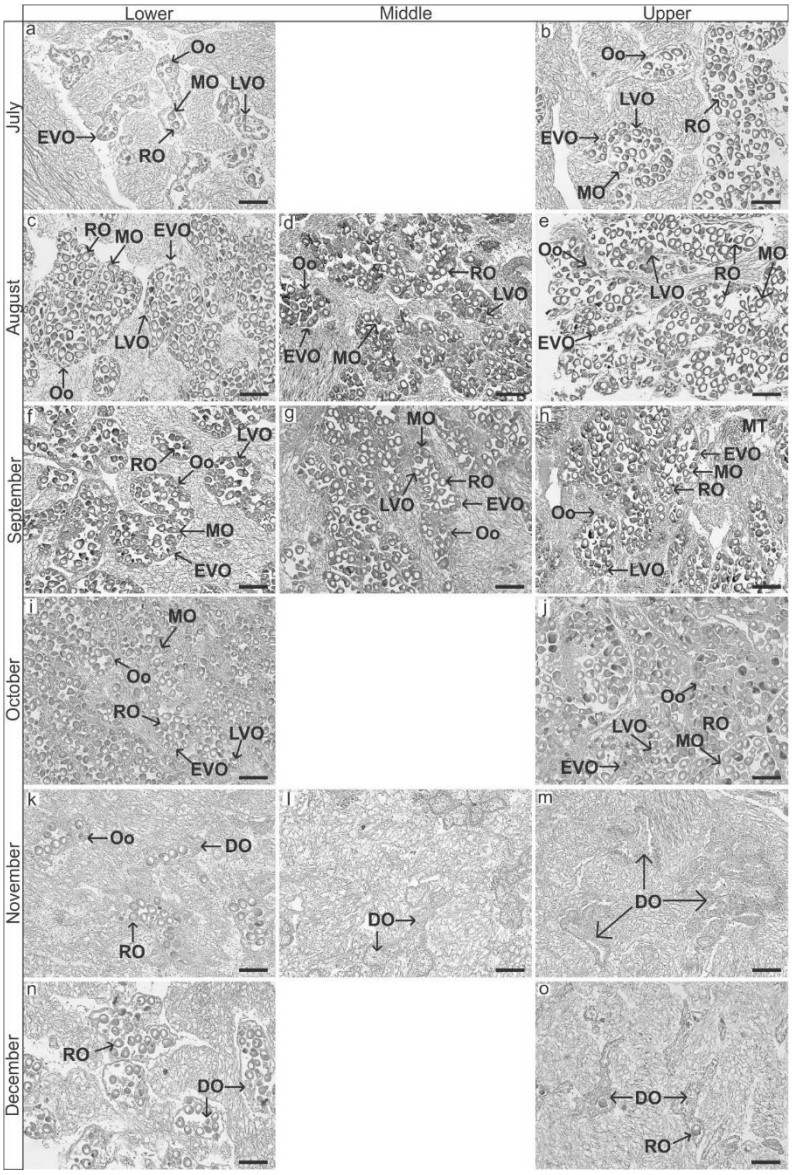

Figure 18. Photographs of H&E stained female gonadal tissue of *Rangia cuneata* taken from the lower, middle, and upper sites of Johnson Bayou from July to December 2016.

In July, clams from the lower site were in the early active phase, producing early and late vitellogenic oocytes, and some mature and ripe ova (a). Clams from the upper site were progressing from the early to late active phase (b). From August to September, clams across all sites progressed through the late active phase (c-h). By October, clams from the lower and upper sites were ripe, indicated by swollen follicles and an abundance of ripe ova (i, j). By November, all clams were spent (k-m) with a few remaining unspawned ripe ova (k). In December, clams from the lower and upper sites had some unspawned ripe ova and degenerating oocytes (n, o). Blank panels indicate no female clams were collected. (Abbreviations: DO = degenerating oocytes; DT = digestive tissue; EVO = early vitellogenic oocyte; F = follicle; H = hemocyte; LVO = late vitellogenic oocyte; MO = mature oocyte; MT = muscle tissue; Oo = oogonia; RO = ripe ova). Scale bars = 100 µm.

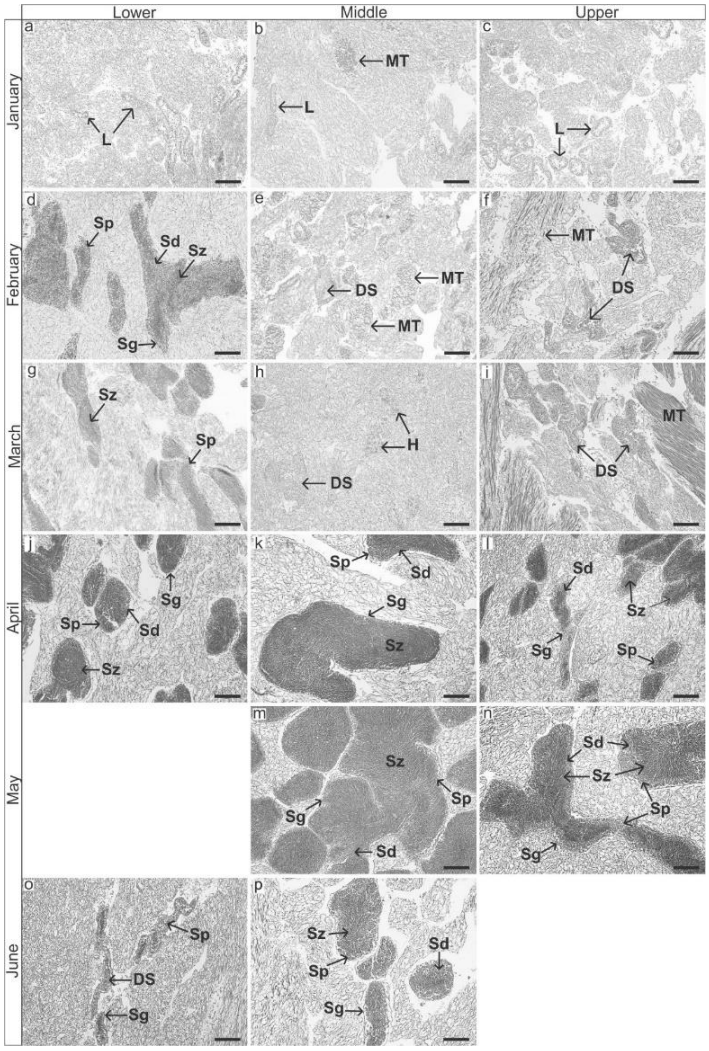

Figure 19. Photographs of H&E stained male gonadal tissue of *Rangia cuneata* taken from the lower, middle, and upper sites of Johnson Bayou from January to June 2016.

In January, all clams were in the spent phase with small, shrunken lobules (a-c). Muscle tissue was commonly observed in these sections (b). In February, clams from the lower site were in the early active phase, producing gametes of all stages, primarily spermatocytes (d). Clams at the middle and upper sites were spent with degenerating sperm cells present. Muscle tissue was commonly observed (e, f). Clams remained in the same phases in March as they were in February (g-i). In April, clams from the lower site progressed into the late active phase with increasing numbers of spermatids and spermatozoa (j). Clams from the middle site were in the early to late active phase (k). Clams from the upper site were in the early active phase (l). In May, clams from the upper site progressed into the late active phase (n). In June, clams from the lower site had partially spawned or were spent indicated by few spermatocytes and degenerating sperm cells (o). Clams from the middle site appeared partially spawned, but still produced gametes of all stages (p). Blank panels indicate no male clams were collected. (Abbreviations: DS = degenerating sperm; H = hemocyte; L = lobule; MT = muscle tissue; Sd = spermatids; Sg = spermatogonia; Sp = spermatocyte; Sz = spermatozoa). Scale bars = 100 µm.

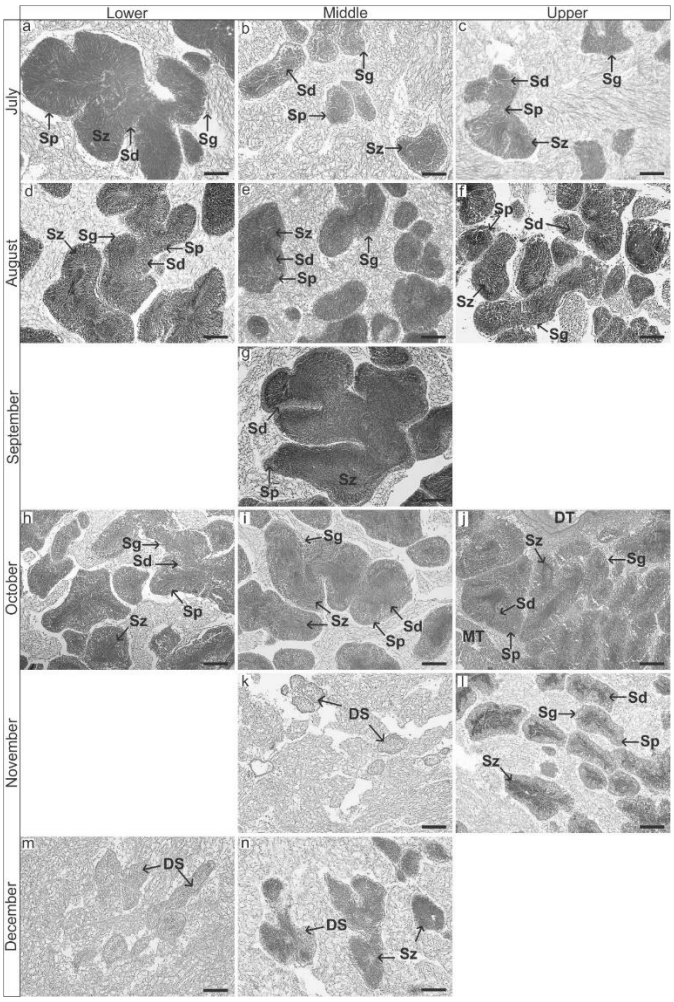

Figure 20. Photographs of H&E stained male gonadal tissue of *Rangia cuneata* taken from the lower, middle, and upper sites of Johnson Bayou from July to December 2016.

In July, clams from the lower site were in the late active and ripe phases with enlarged lobules filled with primarily spermatozoa (a). Clams at the middle site were partially spawned, indicated by smaller lobules and sparse amounts of spermatozoa, but numerous spermatocytes and spermatids (b). Clams at the upper site were in the late active phase (c). In August, clams from the lower site were ripe (d), while clams in the middle and upper sites were in the late active to ripe phases (e, f). In September, clams from the middle site were ripe (g). In October, clams from the lower site were partially spawned (h), indicated by an increasing amount of space in the lumens of the lobules and less spermatozoa than in ripe clams. Clams from the middle and upper sites were ripe with very little somatic tissue present (i, j). In November, clams from the middle site were spent with degenerating sperm cells present in the lumens (k). Clams from the upper site were partially spawned, indicated by increasing amount of somatic tissue and less spermatozoa in the lumens (l). In December, clams from the lower site were spent with unspawned spermatozoa and degenerating sperm cells present (n). Blank panels indicate no male clams were collected. (Abbreviations: DS = degenerating sperm; H = hemocyte; L = lobule; MT = muscle tissue; Sd = spermatids; Sg = spermatogonia; Sp = spermatocyte; Sz = spermatozoa). Scale bars = 100 µm.

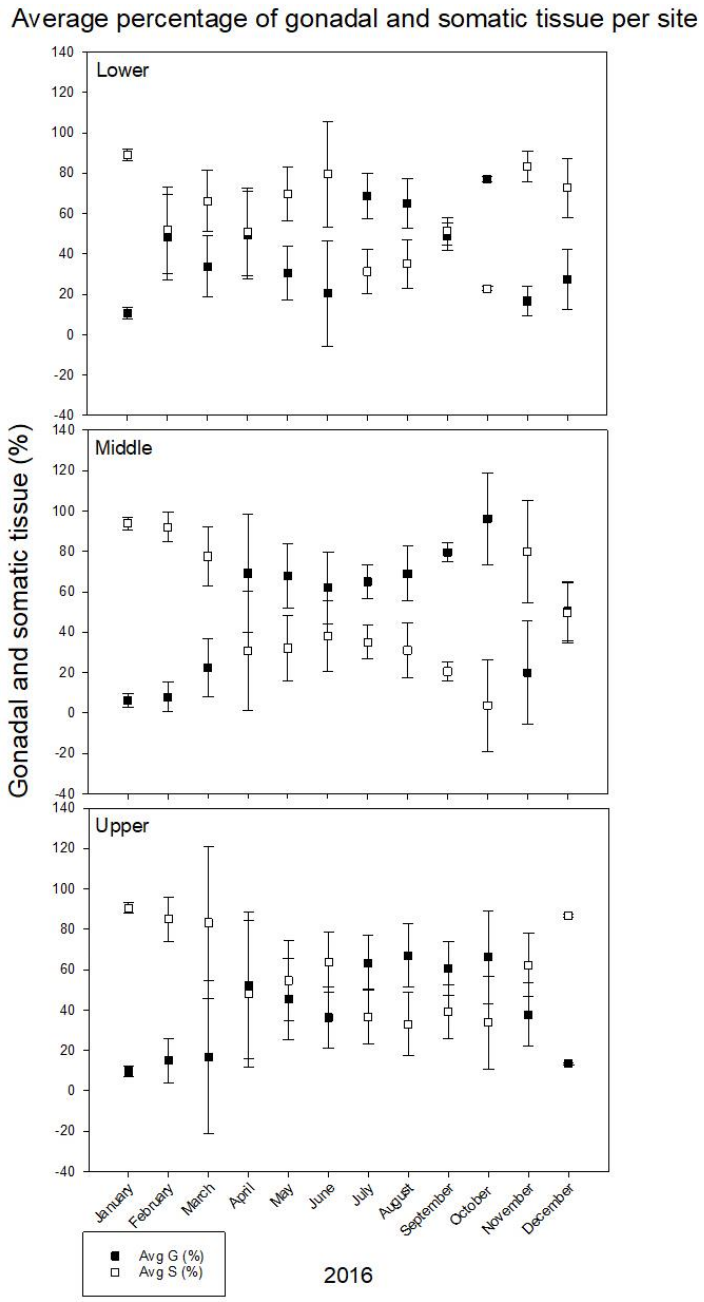

Figure 21. Average percentage of gonadal versus somatic tissue across all sites from January to December 2016.

The average percentage of gonadal and somatic tissue was determined by pooling data from all clams collected from each site (lower, middle, and upper) at the end of each month in 2016. Clams from the lower site produced nearly equal percent gonadal to somatic tissue by summer, and greater than 50%, peaking in October. Clams from the middle site produced greater than 50% gonadal tissue by April and peaked at greater than 95% gonadal tissue in October. Clams from the upper site reflect those from the middle site, but did not produce as much gonadal tissue. Error bars indicate standard deviation.

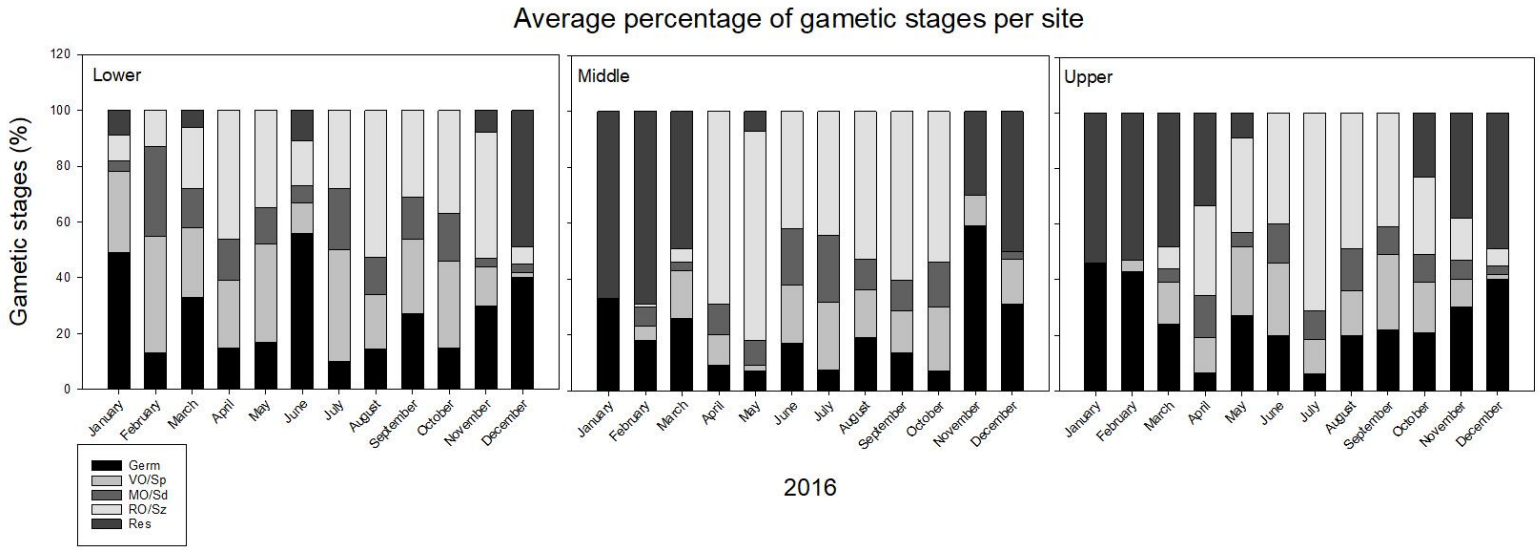

Figure 22. Average percentage of gametic stages of male and female clams from all sites collected from January to December 2016.

Gametic stages were pooled and averaged into a percentage based on data from three clams collected per site (lower, middle, and upper) at the end of each month in 2016. Germ cells (oogonia and spermatogonia) accounted for 50% twice in January and June in clams from the lower site and once in clams from the middle. Germ cells generally accounted for 10-30% across all sites throughout the year. Vitellogenic oocytes (VO; including early and late vitellogenic oocytes) and spermatocytes (Sp) accounted for nearly 20% or less in clams from the lower site, and at 5% or less in June and December. These stages in clams from the middle and upper sites peaked between May and June, but varied from 0-20% across all months. The percentage of mature oocytes (MO) and spermatids (Sd) varied in clams across all sites throughout the year, anywhere from 0% to nearly 25% (lower site, February). Based on increasing and subsequent decreasing levels of ripe ova (RO) and spermatozoa (Sz), clams from the lower and middle sites may have spawned twice, around April and May and again between August and October. Clams from the upper site spawned once after July. Residual gametes (Res) accounted for 0% to greater than 50% (December) in clams from the lower site. Residual gametes accounted for over 60% in clams from the middle site in January and February and over 50% in December, with 0% to ~5% between March and November. No residual gametes were counted in April and between June and September in these clams. Residual gametes in clams from the upper site decreased from over 50% in January to 0% by June, but increased from October to December to approximately 50%.

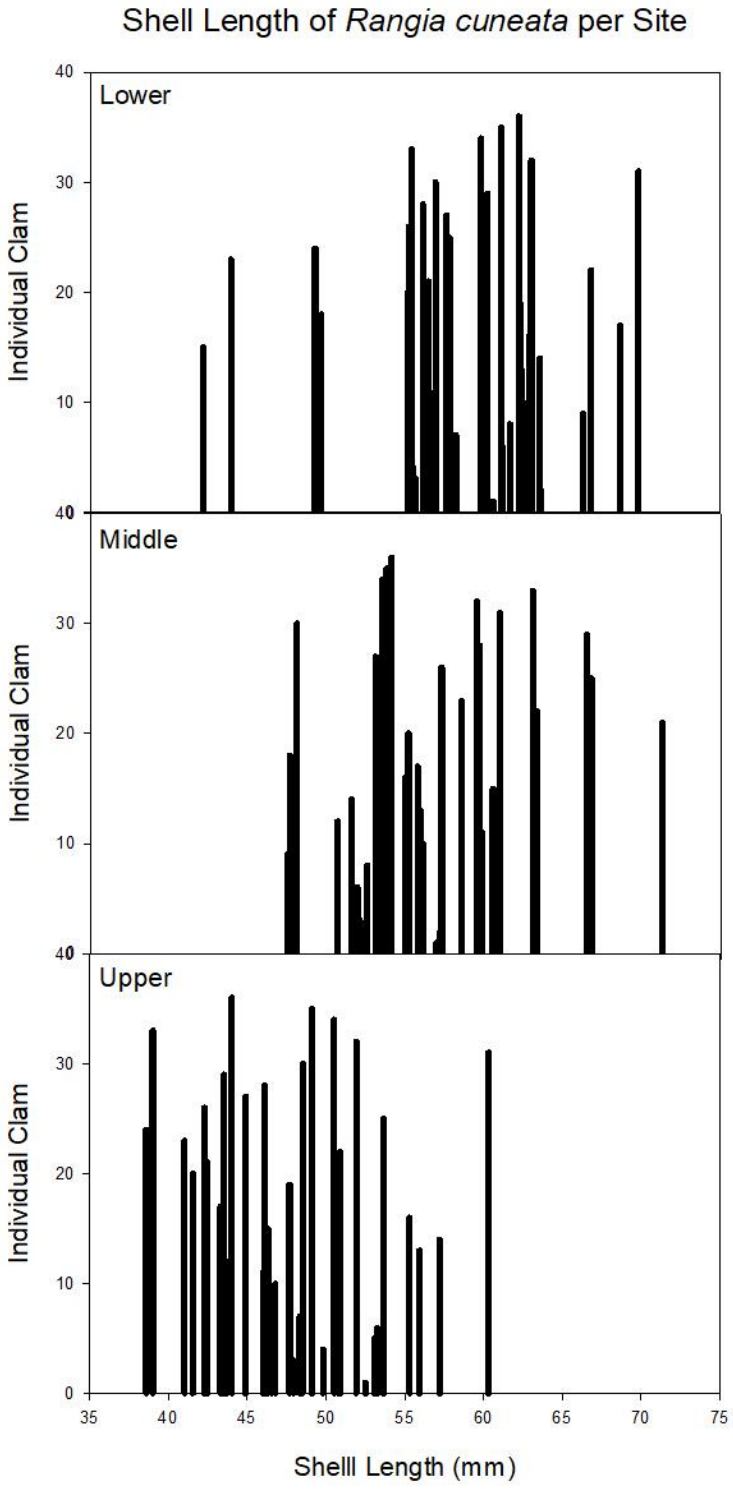

Figure 23. Shell length of *Rangia cuneata* per site.

The shell lengths of *Rangia cuneata* (N = 108) were measured and graphed based on location. Average shell length per site was 58.5, 56.1, and 47.9 mm, respectively.

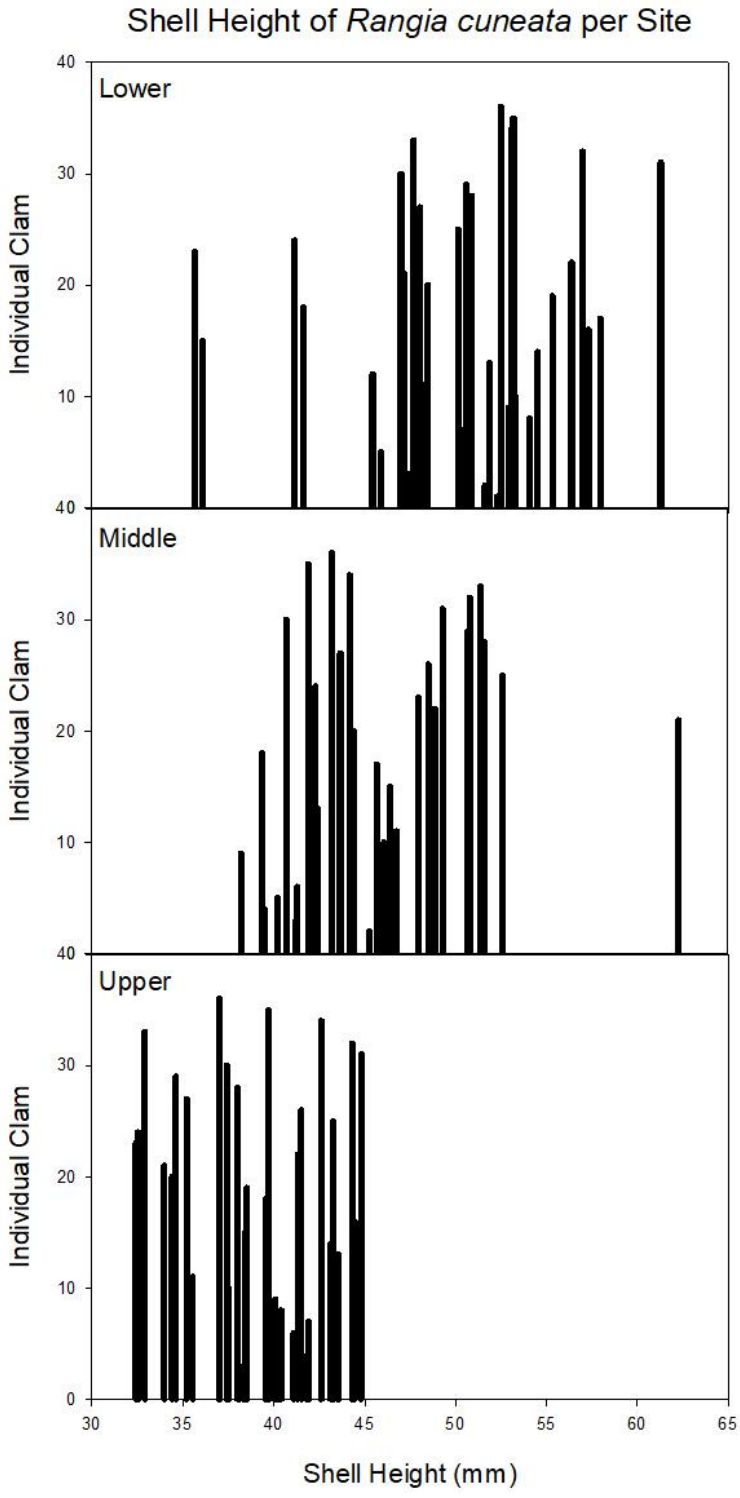

Figure 24. Shell height of *Rangia cuneata* per site.

The shell heights of *Rangia cuneata* (N = 108) were measured and graphed based on location. Averages shell height per site was 50.1, 45.3, and 38.9 mm, respectively.

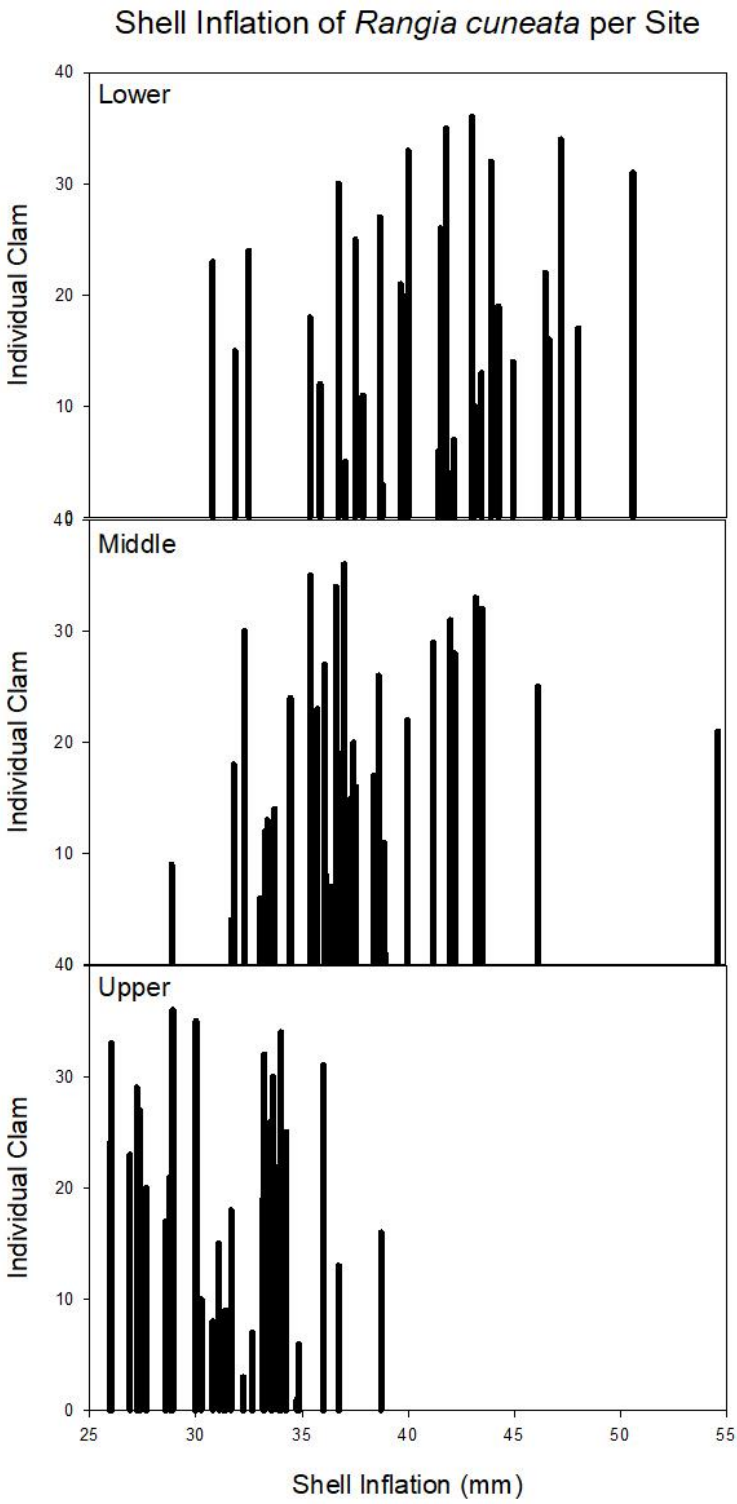

Figure 25. Shell inflation of *Rangia cuneata* per site.

The shell inflations of *Rangia cuneata* (N = 108) were measured and graphed based on location. Averages shell inflation per site was 40.8, 37.4, and 31.4 mm, respectively.

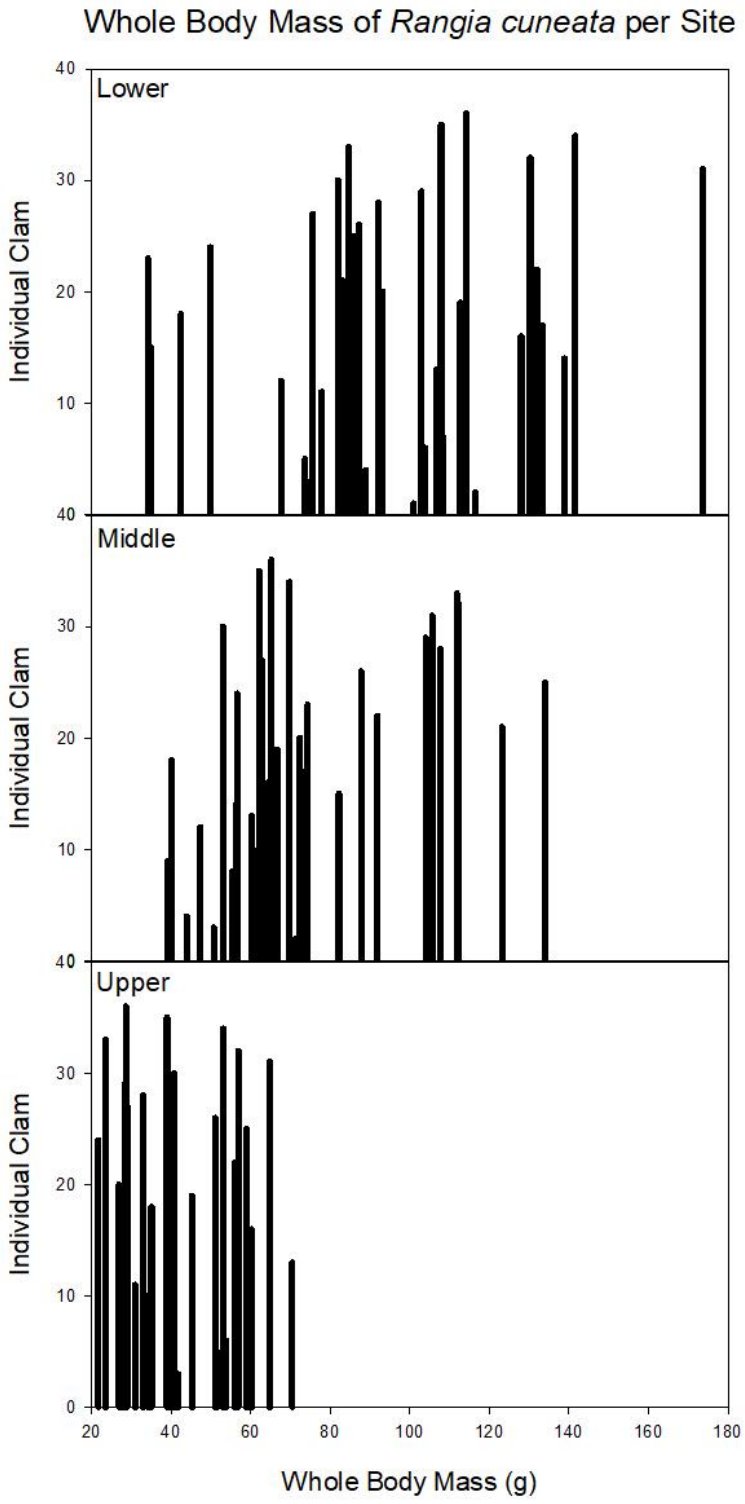

Figure 26. Whole body mass of *Rangia cuneata* per site.

The whole body mass of *Rangia cuneata* (N = 108) were measured and graphed based on location. Average whole body mass per site was 97.5, 72.9, and 42.1 mm, respectively.

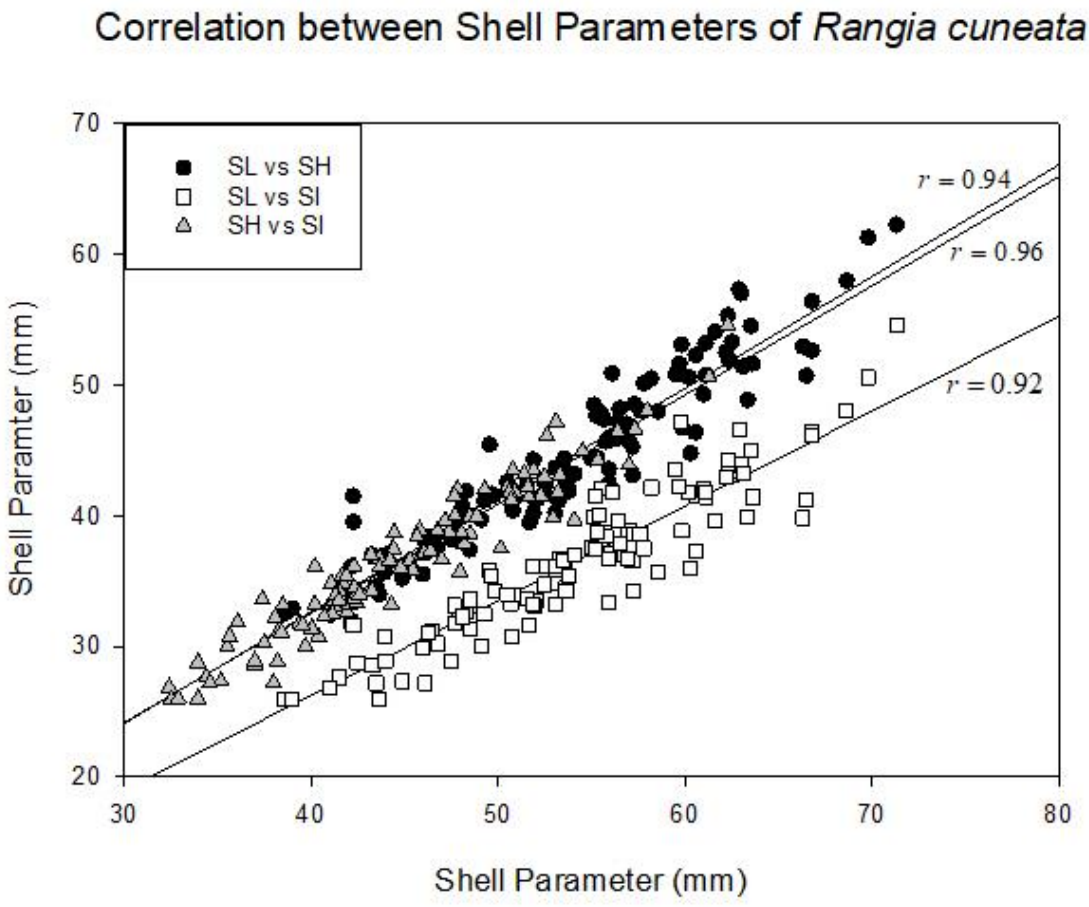

Figure 27. Correlation analysis between shell parameters of *Rangia cuneata*.

A Pearson correlation (simple linear) was performed between shell parameters (shell length – SL; shell height – SH; and shell inflation – SI) measured from collected specimens of *Rangia cuneata* (N = 108). All parameters were strongly and positively correlated with one another as indicated by the Pearson coefficient (r).

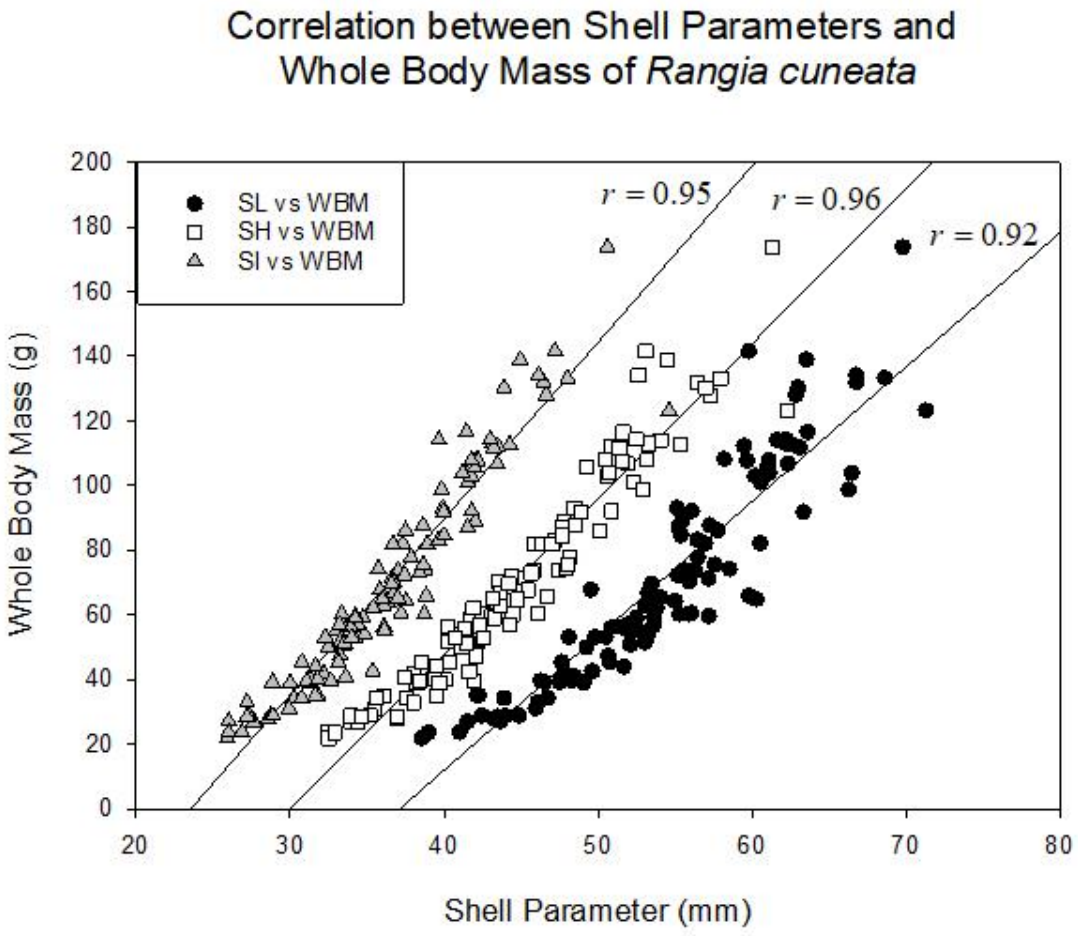

Figure 28. Correlation analysis between shell parameters and whole body mass of *Rangia cuneata*.

A Pearson correlation (simple linear) was performed between individual shell parameters (shell length – SL; shell height – SH; and shell inflation – SI) and whole body mass measured from collected specimens of *Rangia cuneata* (N = 108). All parameters were strongly and positively correlated with whole body mass as indicated by the Pearson coefficient (r).

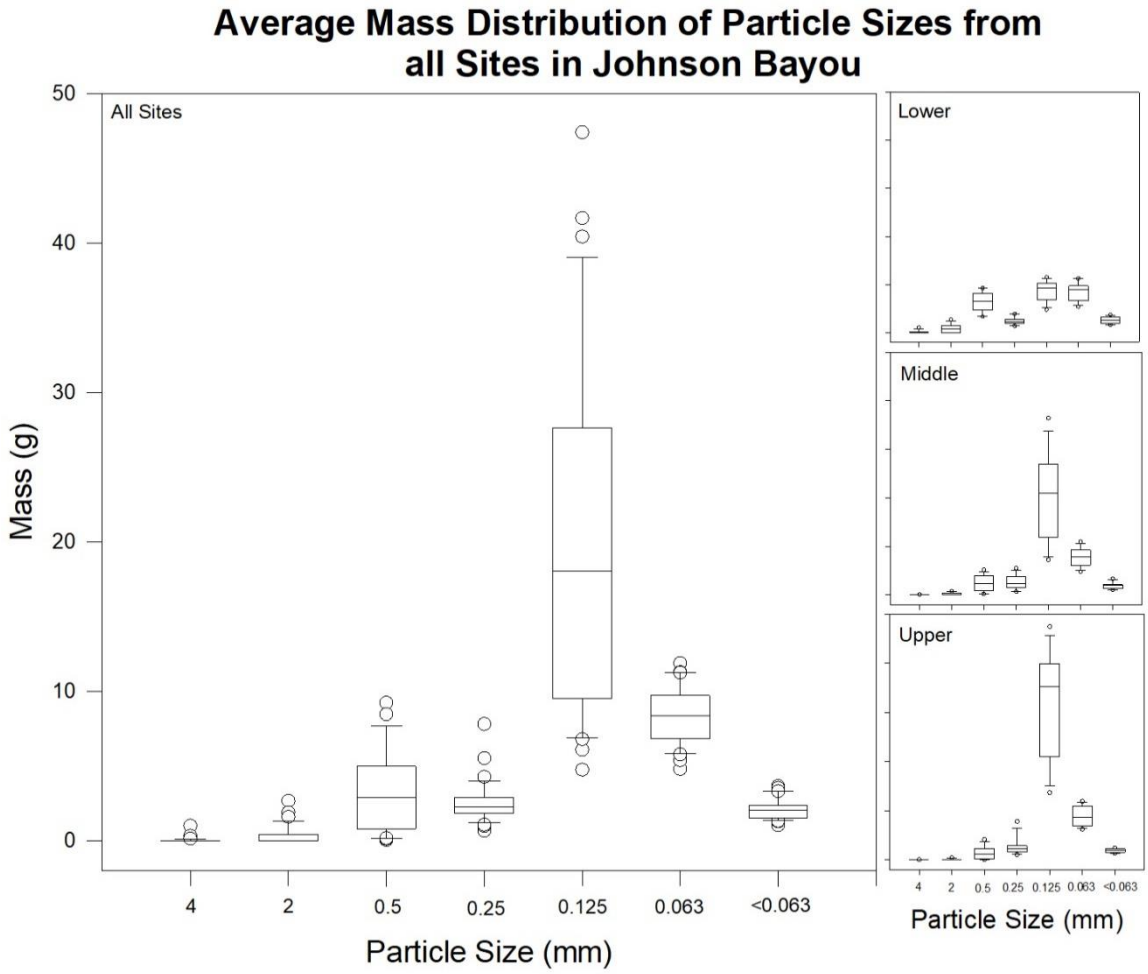

Figure 29. Average mass distribution of particle sizes from all sites in Johnson Bayou.

The mass distributions of all particle sizes were averaged and plotted from all sites, then separated based on location (lower, middle, upper). Based on mass, there was little sediment greater than 4 mm, majority of sediment between 0.125 and 0.25 mm, and intermediate amounts of remaining particle sizes. There was no one majority of sediment particle size from the lower site. The majority of particle size was between 0.125 and 0.25 mm in diameter from the middle and upper sites. The central line represents the median. The box interquartile range is between the first and third quartiles and the whiskers (error bars) above and below represent the 95^{th} and 5^{th} percentiles. Outliers are indicated as individual points.

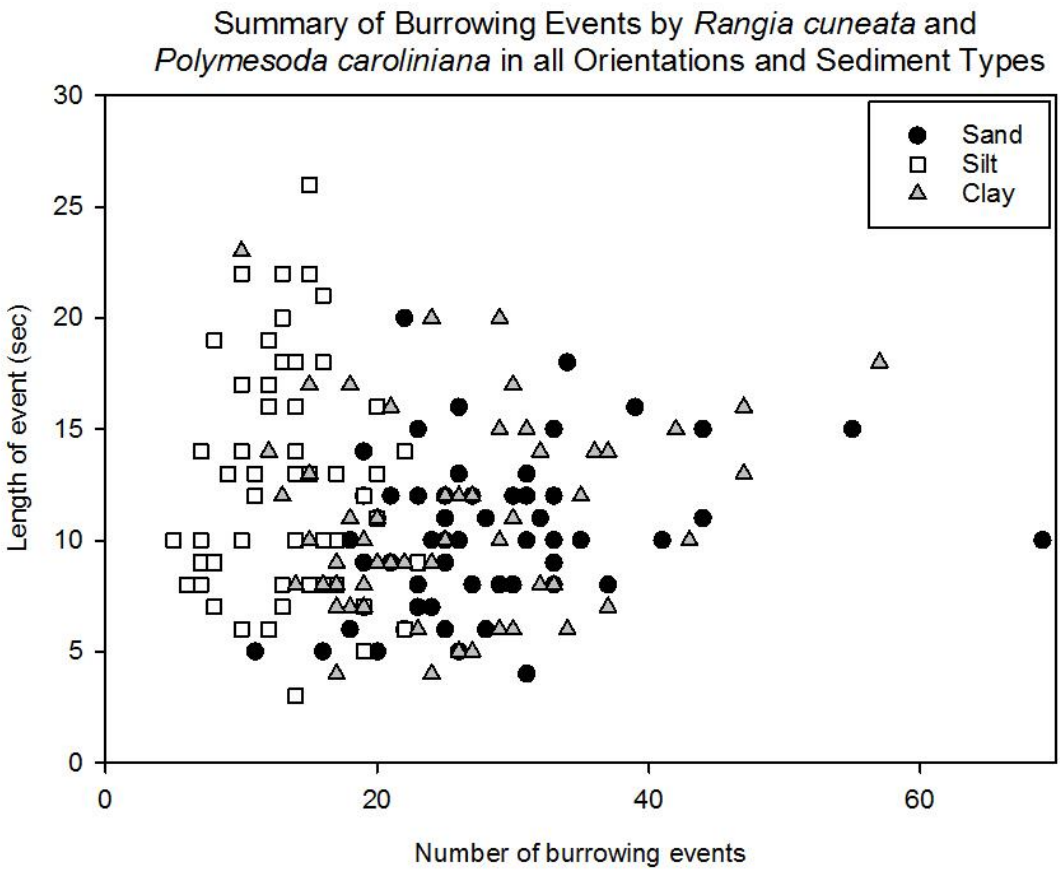

Figure 30. Summary of burrowing events by *Rangia cuneata* and *Polymesoda caroliniana* in all orientations in sand, silt, and clay.

The number of burrowing events of *Rangia cuneata* and *Polymesoda caroliniana* from all orientations in sand ranged from 11 to 69. The length of events ranged from 1 to 20 seconds. The number of burrowing events of *R. cuneata* and *P. caroliniana* from all orientations in silt ranged from 5 to 23. The length of events ranged from 2 to 26 seconds. The number of burrowing events of *R. cuneata* and *P. caroliniana* from all orientations in clay ranged from 10 to 57. The length of events ranged from 2 to 23 seconds.

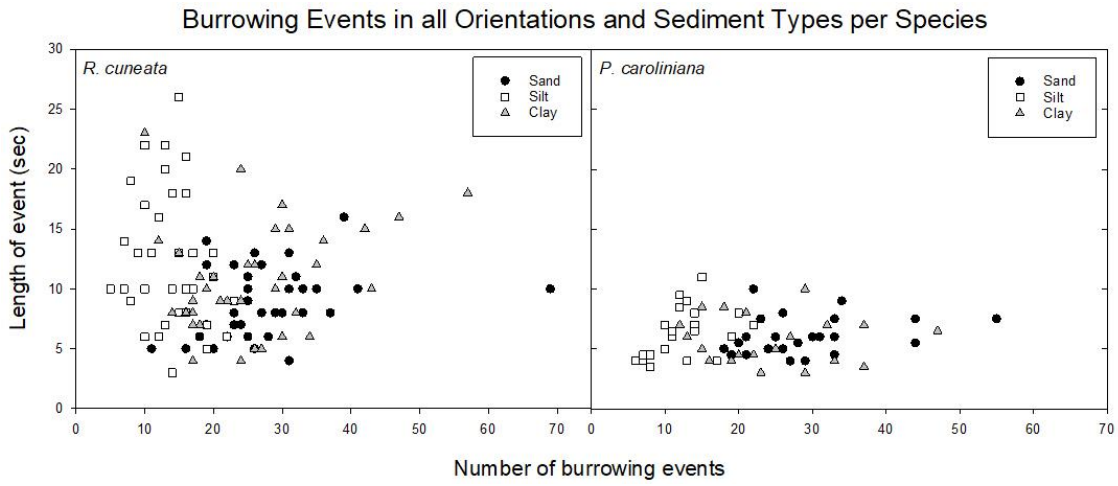

Figure 31. Burrowing events in all orientations in sand, silt, and clay, separated by species.

The number of burrowing events of *Rangia cuneata* versus *Polymesoda caroliniana* in sand ranged from 11 to 69 and 18 to 55 events, respectively. The length of events by *R. cuneata* and *P. caroliniana* ranged from 1 to 16 seconds and 1 to 20 seconds, respectively. The number of burrowing events of *R. cuneata* versus *P. caroliniana* in silt ranged from 5 to 23 and 6 to 22 events, respectively. The length of events by *R. cuneata* and *P. caroliniana* ranged from 2 to 26 seconds and 2 to 22 seconds, respectively. The number of burrowing events of *R. cuneata* versus *P. caroliniana* in clay ranged from 10 to 57 and 12 to 47 events, respectively. The length of events by both species ranged from 2 to 23 seconds.

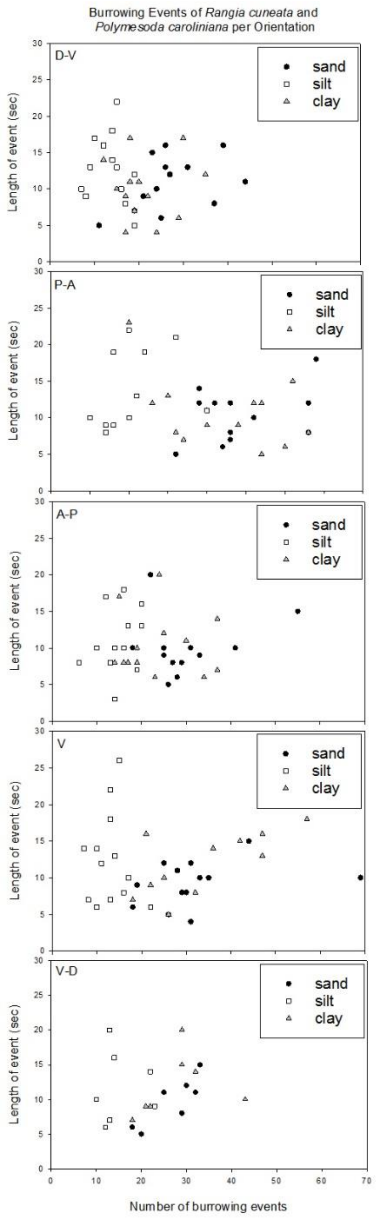

Figure 32. Burrowing events of *Rangia cuneata* and *Polymesoda caroliniana* in sand, silt, and clay separated by orientation.

The two longest burrowing events in sand occurred in the V-D and V orientations with 33 and 69, respectively. The average number of events per orientation were 27 (D-V), 24 (P-A), 30 (A-P), 33 (V), and 27 (V-D) (N = 13, 13, 13, 13, 7, respectively). The two longest burrowing events in silt occurred in the D-V and V-D orientations with 19 and 23, respectively. The average number of events per orientation were 13 (D-V), 10 (P-A), 14 (A-P), 13 (V), and 15 (V-D) (N = 13, 13, 13, 13, 7, respectively). The two longest burrowing events in clay occurred in the P-A and V orientations with 33 and 57, respectively. The average number of events per orientation were 21 (D-V), 22 (P-A), 24 (A-P), 34 (V), and 28 (V-D) (N = 13, 13, 13, 12, 7, respectively). (Abbreviations: D-V = dorsal-ventral; P-A = posterior-anterior; A-P = anterior-posterior; V = ventral; V-D = ventral-dorsal).

References

Abbott RT, Morris PA. 1995. A field guide to shells: Atlantic and Gulf Coasts and the West Indies. 4th ed. New York. Houghton Mifflin Company.

Afiati N. 2007. Gonad maturation of two intertidal blood clams *Anadara granosa* (L.) and *Anadara antiquata* (L.) (Bivalvia: Arcidae) in Central Java. J Coast Dev. 10(2):105-113.

Andrews J. 1971. Seashells of the Texas Coast. Austin. University of Texas Press.

[ANZECC] Australian and New Zealand Guidelines for Fresh and Marine Water Quality. 2000. National water quality management strategy: The guidelines. 1: paper no. 4.

Bower SM, BLackbourn J. 2003. Geoduck clam (Panopea abrupta): anatomy, histology, development, pathology, parasites and symbionts: normal histology – reproductive system [Internet]. Canada: DFO; [cited 2015 November 25].

Cain T. 1972. The reproductive cycle and larval tolerances of *Rangia cuneata* in the James River, Virginia. [Dissertation]. [Charlottesville (VA)]: University of Virginia. p. 121.

Cain TD. 1975. Reproduction and recruitment of the brackish water clam *Rangia cuneata* in the James River, Virginia. Fish Bull. 73(2):412-430.

Center TD, Cuda, JP, Grodowitz MJ. 2009. Alligatorweed flea beetle *Agasicles hygrophila* Selman and Vogt (Coleoptera: Chrysomelidae: Halticinae). Entomology and Nematology Department, UF/IFAS Extension. EENY 462.

Chanley P. 1965. Larval development of the brackish water mactrid clam, *Rangia cuneata*. Chesap Sci. 6(4):209-213.

Delgado M, Camacho AP. 2005. Histological study of the gonadal development of *Ruditapes decussatus* (L.) (Mollusca: Bivalvia) and its relationship with available food. Sci Mar. 69(1):87-97.

Duobinis-Gray EM, Hackney CT. 1982. Seasonal and spatial distribution of the Carolina marsh clam *Polymesoda caroliniana* (Bosc) in a Mississippi tidal marsh. Estuaries. 5(2):102-109.

Fairbanks LD. 1963. Biodemographic studies of the clam *Rangia cuneata* Gray. Tulane Stud Zool. 10(1):3-47.

Hoese HD. 1973. Abundance of the low salinity clam, *Rangia cuneata* in southwestern Louisiana. P Natl Shellfish Assoc. 63:99-106.

Hopkins SH, Andrews JD. 1970. *Rangia cuneata* on the East Coast: thousand mile range extension, or resurgence? Science, New Series. 167(3919):868-869.

Jovanovich MC, Marion KR. 1989. Gametogenic cycle of *Rangia cuneata* (Mactridae, Mollusca) in Mobile Bay, Alabama, with comments on geographic variation. Bull Mar Sci. 45(1):130-138.

Leal JH. 2002. Bivalves. In: Carpenter KE, editor. The living marine resources of the Western Central Atlantic. Volume 1. Introduction, mollusks, crustaceans, hagfishes, sharks, batoid fishes, and chimaeras. FAO Identification Guide for Fishery Purposes. The Food and Agriculture Organization of the United Nations, Rome. p. 25-98.

Loosanoff VL. 1969. Maturation of gonads of oysters, *Crassostrea virginica*, of different geographical areas subjected to relatively low temperatures. The Veliger. 11:153-163.

Marelli DC. 1987. Processes controlling intertidal zonation in an estuarine soft-bottom bivalve assemblage. [Dissertation]. [Ann Arbor (MI)]: The Florida State University.

Olsen LA. 1976a. Reproductive cycles of *Polymesoda caroliniana* (Bosc) and *Rangia cuneata* Gray, with aspects of desiccation in the adults, and fertilization and early larval stages in *P. caroliniana*. [Dissertation]. [Tallahassee (FL)]: Florida State University.

Olsen LA. 1976b. Ingested material in two species of estuarine bivalves; *Rangia cuneata* Gray and *Polymesoda caroliniana* (Bosc). P Natl Shellfish Ass. 66:103-104.

Pfitzenmeyer HT, Drobeck KG. 1964. The occurrence of the brackish water clam, *Rangia cuneata*, in the Potomac River, Maryland. Chesap Sci. 5(4):209-212.

Richards, HG 1962. Animals of the seashore. Boston (MA): Humphries Inc.

Ropes JW. 1968. Reproductive cycle of the surf clam, *Spisula solidissima*, in offshore New Jersey. Biol Bull. 135(2):349-365.

Ropes JW, Stickney AP. 1965. Reproductive cycle of *Mya arenaria* in New England. Biol Bull. 128(2):315-327.

Schneider P, Smolowitz R, Smith C, Degiorgis J, McCafferty M. 1997. Comparison of three techniques for evaluating seasonal gametogenesis in *Spisula solidissima*. Dev Cell Mol Biol. 193:233-234.

Seed R. 1980. Shell growth and form in the Bivalvia. In: Rhoads DC, Lutz RA, editors. Skeletal growth of aquatic organisms: Biological records of environmental change. New York (NY): Plenum Press. p. 23 – 67.

Steinman AD, Lamberti GA. c1996. Biomass and pigments of benthic algae. In: Hauer FR, Lamberti GA, editors. Methods in Stream Ecology. San Diego (CA): Academic Press.

Swingle HA, Bland DG. 1974. Distribution of the estuarine clam *Rangia cuneata* Gray in coastal waters of Alabama. Ala Mar Resour Bull. 10:9-16.

Tenore KR. 1972. Macrobenthos of the Pamlico River estuary, North Carolina. Ecol Monogr. 42(1):51-69.

Tenore KR, Horton DB, Duke TW. 1968. Effects of bottom substrate on the brackish water bivalve *Rangia cuneata*. Chesap Sci. 9(4):238-248.

Tiner RW, Rorer A. 1993. Field guide to coastal wetland plants of the Southeastern United States. Amherst (MA): University of Massachusetts Press.

Tomkiewicz J, Kofoed TMN, Pedersen JS. 2011. Assessment of testis development during induced spermatogenesis in the European eel *Anguilla anguilla*. Mar Coast Fish. 3(1):106-118.

Wakida-Kusunoki AT, MacKenzie Jr. CL. 2004. Rangia and marsh clams, *Rangia cuneata*, *R. flexuosa* and *Polymesoda caroliniana*, in Eastern Mexico: distribution, biology and ecology, and historical fisheries. Mar Fish Rev. 66(3):13-20.

Wentworth CK. 1922. A scale of grade and class terms for clastic sediments. J Geol. 30(5):377-392.

Woodburn KD. 1962. Clams and oysters in Charlotte County and vicinity. St. Petersburg (FL): Board of Conservation Marine Laboratory.

CHAPTER III - A COMPARATIVE STUDY ON THE GROSS MORPHOLOGY AND ULTRASTRUCTURE OF THE FOOT OF *RANGIA CUNEATA* AND *POLYMESODA CAROLINIANA*

Introduction

Use of microscopy on foot tissue

There have been several studies on the basic morphology of the foot of bivalves, but few rigorous and thorough examinations of the morphology and ultrastructure using microscopic methods. Mores studies need to take place on the ultrastructure and histological composition of infaunal bivalves to provide better insight into comparative studies between species and families. With increased information, we may also be able to infer how different species are able to burrow or have adapted to living in specific sediment types.

Using different microscopical techniques allows for investigation into multiple aspects of foot morphology and ultrastructure. In this study, scanning electron microscopy (SEM) is used to produce a 3D gross morphological image of foot tissue. The use of diagnostic histological stains (hematoxylin and eosin; H&E), provides an ultrastructural view of tissue sections. Histochemical methods, where specific stains bind primarily to one type of structure or compound, are used to help determine the presence or absence of those specific structures or compounds not possible under H&E protocols. For instance, in this study, Alcian blue and periodic-acid Shiff stains were used to determine the composition of the glandular material in the subepithelium region of the foot of *R. cuneata* and *P. caroliniana*.

Alcian blue and periodic-acid Shiff can be used separately or in combination when determining polysaccharide type and composition. Alcian blue is a copper phthalocyanine compound with a high affinity for polyanionic substances such as glycosaminoglycans (Quintarelli and Dellovo 1966). Given its stability at low pH and its high degree of specificity, it has been widely used in histochemical and cytochemical protocols. The density or darkness of the stain may indicate a more concentrated area of substrate, or more than one type of substrate. Certain molecules, such as hyaluronate, can bind more stain than others such as chondroitin 4-sulfate (Whiteman 1973). Another important staining protocol is the periodic acid-Schiff, comprised of periodic acid and the Schiff stain. Periodic acid is an oxidizing agent used in histochemical and electron microscopy methods. Periodic acid cleaves certain saccharide rings producing aldehyde and ketone groups in the fixed section. When the Schiff reagent is added, it binds to the aldehyde groups producing a magenta color when reacted with water. Thus, this protocol provides an indication of the type of carbohydrate present in a sample, which is primarily used as an indicator of glycogen or mucus in a sample.

Images obtained through the use of transmission electron microscopy (TEM) supports what can be examined under light microscopy, but provides a higher resolution and higher magnification on thin sections (90-100 nm) of tissue. The standard staining protocol for TEM is uranyl acetate and lead citrate for binding and staining to nucleic acids and proteins, respectively. The fixative, osmium tetroxide (OsO_4), is also a stain, because it is electron dense and binds to lipid moieties (e.g., plasma membranes).

Research aims

No research on the foot morphology or ultrastructure has been published on either *R. cuneata* or *P. caroliniana*. The focus of this research was to not only characterize the gross morphology and ultrastructure of both species, but compare the results between two species from two different bivalve families. This was purely a descriptive study, using electron microscopy methods, and histological and histochemical staining protocols for light microscopy examination. Results revealed largely similarities between the foot of both species, but also some interesting differences. Notably, the type of mucopolysaccharides produced appears to be dissimilar. Descriptive measures from light micrographs supported visual observations between species. Last, foot tissue obtained from a fixed specimen (i.e., after collection, the clam is opened and fixed in 100% EtOH) is contracted tissue. A relaxed foot protocol was performed in order to examine any differences in ultrastructure, primarily of the musculature and the size and distribution of glandular material, providing an internal view of how the foot changes between contraction and relaxation, and inferring how the clam adjusts the foot for anchoring and burrowing in the substrate.

Methodology

Scanning electron microscopy

Specimens for pedal morphological and ultrastructural analysis were randomly collected from Johnson Bayou (N = 8; 4 of each species). The posterior or anterior adductor muscle was severed using a razor blade placed between the two shell valves and, if the specimens were not to undergo a relaxation protocol, then clams were immediately placed in 100% EtOH. For relaxation of the foot, clams were placed in 7%

$MgCl_2$ until valves were agape and the foot observably relaxed. Following fixation for a minimum of 48 hours, the contracted foot of some specimens was removed from the visceral mass and cut either longitudinally or in cross-section. A longitudinal section was necessary to examine the sides of the foot and to accommodate the scanning electron microscopy (SEM) stub. The cross-section was performed to visualize internal morphology. Remaining tissues were placed in 100% EtOH for storage and archiving at the University of Southern Mississippi Gulf Park Campus, Long Beach, MS.

Sections of the foot taken for analysis were excised and fixed in 2.5% glutaraldehyde in 0.1 M sodium cacodylate buffer (pH 7.4) for 2 hours at 4°C. Following three rinses in buffer, samples were postfixed in 1% osmium tetroxide in buffer for 2 hours at 4°C. Samples were rinsed three times in buffer before undergoing a graded ethanol (EtOH) dehydration series (50, 70, 90, 95, 2 x 100% EtOH) for 10-15 minutes each. Samples were placed in propylene oxide for 10 minutes before being mounted on aluminum stubs. Samples were sputter coated with gold at a thickness of 10-20 nm (Desk II Denton, Denton Vacuum, Incorporated, Moorestown, NJ) and viewed under SEM (Hitachi SU3500, Hitachi High-Technologies, Corporation, Chiyoda-ku, Tokyo, Japan) at an accelerating voltage of 5 kV.

Light microscopy

In order to examine the major structures and layers of the foot and gain insight into its composition, radial, longitudinal, and sagittal sections of tissue from both species were stained and imaged under light microscopy. Hematoxylin and Eosin (H&E) staining served as the control for all histological experiments due to the ease of the protocol, reliability, and its broad use for determining acidophilic and alkalinic structures. An

Alcian blue and periodic-acid Schiff (AB-PAS) protocol was used to determine where acidic polysaccharides and non-acidic mucopolysaccharides (e.g., glycogen, glycoproteins) were located in the foot tissue. Acidic polysaccharides (e.g., glycosaminoglycans, substituted mucopolysaccharides) were localized with AB (pH 2.5 for carboxylated acidic proteoglycan) (Norenburg and Ferraris 1990; Calabro et al. 2005) whereas non-acidic polysaccharides (e.g., unsubstituted mucopolysaccharides, glycoproteins) are localized by PAS. All sample preparations occurred at the USM Gulf Park campus; however, sectioning and staining were performed at GCRL and imaged using a Digital Eclipse DXM 1200 Nikon with ACT-1 software (Nikon Corporation, Konan, Minato-ku, Toyko).

Transmission electron microscopy

The protocol for TEM followed Park et al. (2012), Cohen and Tamburri (1998), Bairati et al. (2000) and Bairati and Gioria (2008). Sections of the foot were fixed in 2.5% glutaraldehyde in 0.1 M sodium cacodylate buffer (pH 7.4) for 2 hours at 4°C. Following three rinses in buffer, samples were postfixed in 1% osmium tetroxide in buffer for 2 hours at 4°C. Samples were rinsed three times in buffer before undergoing a graded ethanol dehydrate series (50, 70, 90, 95, 2 x 100% EtOH) for 10-15 minutes each. Pre-embedment of tissue occurred with a 1:1 ratio of 100% EtOH and Spurr's resin and rotated overnight. Tissues were then embedded in 100% Spurr's resin and cured at 70°C for 36 hours (Thermo Scientific Precision drying oven, Model 658, Marietta, OH). Sections were cut with a diamond knife to a thickness of 90-100 nm, placed on copper grids, stained with uranyl acetate and lead citrate (Reynolds 1963) and viewed using a Zeiss900 TEM (Carl Zeiss SMT, Peabody, MA) at an accelerating voltage of 50 kV.

Data analysis

All qualitative data (e.g., images and figures) were edited and formatted in CorelDraw X8 (Corel Corporation, Ottawa, Ontario, Canada). Image J version 1.48 was used to scale and measure select features (e.g., diameter of muscle fibers) based on recorded images. Quantitative data included dimensions of foot tissue examined under light microscopy (LM) and TEM (e.g., dimensions of muscle tissue). All quantitative data were recorded and analyzed in Sigmaplot 13.0 (Systat Software, Incorporated, San Jose, CA).

Results

A gross morphological to internal ultrastructural examination was performed on both species using SEM for a large scale (whole foot) observation, light microscopy with histological staining techniques to determine composition of the foot, and TEM for a higher magnification and verification of what was observed under light microscopy.

Scanning electron microscopy

Scanning electron micrographs of both species revealed a ciliated epithelium and an internal cross-section of the subepithelial region and internal musculature, as well as the presence of a hemolymph sinus. Prominent features of the foot of *R. cuneata* included a strongly pointed toe (Figure 33a), ill-defined heel (Figure 33b), and deep villi of epithelial cells with cilia that appeared to increase in density and length progressing from the dorsal to the ventral portion of the foot (Figure 33c-e). A cross-section revealed inner muscle fibers in various orientations surrounding the hemolymph sinus (Figure 34a, b). The internal musculature was not sharply separated from the thick subepithelial region (Figure 34c, d). This cross-section also showed that the ventral portion of the foot was

strongly tapered into a V-shape (Figure 34d). Not all of these features observed in *R. cuneata* were the same as seen in *P. caroliniana*.

The foot of *P. caroliniana* had a rounded toe and well-defined heel (Figure 35a). The ventral portion of the foot and villi had a very rugose or wrinkled appearance. The epithelium was very similar to that of *R. cuneata* with deep villi, and cilia on the epithelial cells increasing in density and length in a dorsal to ventral direction (Figure 35b-d). A cross-section showed a similar morphology to that in *R. cuneata*: dense inner musculature surrounding the hemolymph sinus (Figure 36a, b), thick subepithelial region, not sharply separated from the internal musculature (Figure 36c, d), but an overall rounded pedal shape (Figure 36d). Returning to the epithelium, a thick line of mucilaginous-like material was observed on the outside of the foot of both species in some scanning electron as well as light micrographs. In addition, material such as phytoplankton (e.g., diatom frustules and dinoflagellates) were observed trapped in or on this material when viewed under SEM (Figure 37). Particular points of further interest from the scanning electron micrographs included the subepithelial composition, orientation of muscle fibers, and the hemolymph sinus. While scanning electron micrographs provided high resolution of the foot's gross morphology and some internal ultrastructure, light microscopy and histochemical staining provided better contrast and a clearer picture of the ultrastructure.

Light microscopy

Stained H&E sagittal sections of *R. cuneata* and *P. caroliniana* contracted foot tissue revealed several characteristics (Figures 38, 39). Similar to observations under SEM, the toe was composed of a thin epithelium, subepithelial region, and internal

musculature (Figure 38a). Epithelial cells transitioned from simple cuboidal with short cilia to simple columnar cells with long cilia from the visceral mass (dorsal) to the bottom of the foot (ventral). A dense layer of basal bodies on the apical portion of these epithelial cells were evident. Within the epithelia cells, single nuclei were located near the basal portion of the cells. Beneath the epithelium, the subepithelium was composed primarily of large polysaccharide-producing cells (mucocytes) compacted in amorphous glands (Figure 38a, b). In H&E stained micrographs, these glands (3.8 – 33.2 µm diameter, average = 9.8 ± 6.2 µm, n = 25) were grayish in color and comprised of mucocytes (0.8 – 4.3 µm in diameter, average = 1.9 ± 0.9 µm, n = 33) separated by thin membranes. If in section, each mucocyte appeared to have a single nucleus (Figure 38b). The thickness of this subepithelial region increased towards the ventral margin and toe (thickness from ~95 – 153 µm). As was reported by Park et al. (2012) through observations of *G. veneriformis*, and observations from SEM reported here, no clear delineation between the subepithelial (i.e., connective tissue) layer and the muscular layer in *R. cuneata* and *P. caroliniana* was observed (Figures 38, 39). The muscular layer dominates the inside of the foot in both species. It is comprised of bundles of muscle fibers, oriented dorsal-ventrally, longitudinally, and in cross-section (Figure 38c). When relaxed, these fibers become string-like and the spaces between bundles of muscle fibers is reduced (Figure 38d). Diameter of muscle fibers bundles ranged from 0.19 – 17.6 µm (avg = 4.9 ± 4.6 µm, n = 73). Length was not measured given variability in section thickness. The hemolymph sinus was visualized in a radial section (dorsal to ventral) of the posterior end of the foot (Figure 38e, f) approximately 100 µm in diameter, supporting observations from scanning electron micrographs. Dorsal-ventral and

longitudinally oriented muscle fibers surrounded this sinus. A longitudinal section of the foot of *P. caroliniana* revealed the hemolymph sinus in cross-section, ringed by ciliated columnar cells with laterally positioned nuclei (Figure 39). In the same micrograph, it can be seen that the musculature is internal to the thick subepithelial region all around the foot. The subepithelial region normally contains gland whose composition can be either homogeneous or heterogeneous.

In order to determine if the composition was homogenous or heterogeneous, sections of contracted and relaxed foot tissue were stained with H&E as a control for staining nuclei and cytoplasmic material, Alcian blue (AB) against acidic mucopolysaccharides, periodic-acid Schiff (PAS) against non-acidic mucopolysaccharides, and an AB-PAS protocol (Figure 40) to support observations from the individual staining protocols. H&E stained micrographs show the ciliated epithelial cells external to grayish-blue to pale colored glands comprised of single-nucleated mucocytes in both species (Figure 40a-d). The presence of acidic mucopolysaccharides in both species was indicated by positive staining with AB (Figure 40e-h); however, only non-acidic mucopolysaccharides were positively stained with PAS in *R. cuneata* (Figure 40i, j). No structure in sections from *P. caroliniana* was positively stained with PAS (Figure 40k, l). The combined staining protocol (AB-PAS) revealed co-localization of acidic and non-acidic (in *R. cuneata*) mucopolysaccharides, indicating a heterogenous composition (Figure 40m, n), but only localization and homogeneous composition of glandular material in *P. caroliniana* (Figure 40o, p). Background staining of light blue and light magenta was an artifact of nonspecific staining and failure of the rinsing steps to fully remove the stains. Observing stained sections of contracted and relaxed foot

tissue from both species provided a comparison of ultrastructure; however, there was no large difference in the size or distribution of the glands and mucocytes, as originally hypothesized. Interestingly, the material stained by AB showed a heavily granular appearance (Figure 40o, p), which was further examined in higher resolution electron micrographs from TEM.

Transmission electron microscopy

Sections of the epithelium and subepithelial material from both species were imaged under TEM. Tissue was stained with OsO_4, uranyl acetate (against nucleic acids), and lead citrate (against proteins and other cytoplasmic components). The micrographs showed heavily ciliated columnar cells outside of the thick subepithelium (Figures 41, 42). In *R. cuneata*, the cilia were rooted with electron dense basal bodies. As observed in light micrographs, the epithelial cells had a single nucleus located near the basal portion of the cell. Some glandular material from the subepithelium was observed in between the epithelial cells, presumably in the act of secretion to the outside environment (Figure 41a). A basement membrane was observed beneath the epithelial cells (Figure 41b), not observable from SEM or light microscopy micrographs. Beneath this membrane and in the subepithelium, there was a clear indication of heterogeneity in the glands, presumed to be sites for producing and storing mucus (Figure 41c, d). Portions of the glands were electron opaque, while other areas were not. Some glands in their entirety were not electron opaque, but still appeared granulated and nucleated (Figure 41d).

The epithelium of *P. caroliniana* is comparable to that of *R. cuneata*, with long cilia in a standard 9+2 arrangement (Figure 42a, b). Location of the glands were primarily beneath the epithelium, but mucocytes were occasionally observed between epithelial

cells, presumably in the act of secreting its product to the external environment. However, the glands appeared more homogenous in *P. caroliniana* (Figure 42c, d). The mucocytes were nucleated, weakly granular, and divided by thin membranes, while bundles of muscle fibers were observed randomly surrounding the glands (Figure 42d).

Discussion

This is the first report on the gross morphology and ultrastructure of the foot of *R. cuneata* and *P. caroliniana* using SEM, histological and histochemical staining techniques with light microscopy, and TEM. The information gathered from this research revealed a similar composition of the foot between two species of estuarine clams within two different families. Overall, the foot had a sharply pointed (*R. cuneata*) or rounded toe (*P. caroliniana*) leading posteriorly to an undefined or well-defined heel (Figures 33, 35). From light micrographs, there was no clear indication of a basement membrane beneath the epithelium, but instead an indistinct transition to the subepithelium with muscle fibers, primarily dorsal-ventral in orientation (Figure 33). The subepithelium increased in thickness and in abundance of glandular material as it progressed towards the ventral portion of the foot (Figures 33, 34). Single-nucleated structures that comprised the glands were presumed to be mucocytes, that produced specific type(s) of polysaccharides (i.e., acidic or nonacidic mucopolysaccharides) indicated by the intensity of a specific stain.

The most interesting observation regarding the subepithelial region and associated material is the fact that *P. caroliniana* does not appear to produce nonacidic polysaccharides, as indicated by the negative staining reaction with PAS, but does produce acidic polysaccharides, as indicated by positive staining with AB (Figure 40). In *R. cuneata*, there was a clear co-localization of AB and PAS in the subepithelium,

meaning acidic and non-acidic mucopolysaccharides were produced in the same glands. The material in the subepithelium was highly granular in both species, evidenced by how strong the stain bound material present in the glands. There was greater heterogeneity in the glands in *R. cuneata*. It was hypothesized that the heavily granulated material, as stained by AB, would have appeared as the most electron opaque material under TEM. This was not the case based on micrographs compared between *R. cuneata* and *P. caroliniana* (Figures 41, 42). It must be emphasized that tissue was stained with lead citrate, and so future research will have to undertake trials of varying stain protocols, in order to eliminate possible error in interpreting presence and location of proteins versus acidic polysaccharides. AB has been used in electron microscopy, but for reasons unknown, it was not entirely successful in this study and led to perplexing results (i.e., thick bands of artifacts through the subepithelium) (data not shown).

It is not clear whether the observed "glands" are true single glands in *R. cuneata* and *P. caroliniana*, nor might they possess single nucleated mucocytes, because the sections (~5 µm for LM and ~100 nm for TEM) obtained in this research cannot provide the entire ultrastructure of these glands and mucocytes without 3D reconstruction. In some species of bivalve (e.g., *M. edulis*) (Lane and Nott 1975), there is more than one type of gland present, each producing a different product. However, this occurs primarily in epifaunal bivalves in which the material produced and secreted are involved in byssal thread formation (Norenburg and Ferraris 1990). Based on histological and histochemical analyses, *R. cuneata* and *P. caroliniana* do not produce different types of glands, because the subepithelium only changed in thickness from dorsal to ventral, and did not change in the intensity of staining with AB or PAS. A possible step for support of the results from

R. cuneata and *P. caroliniana* would be examination with fluorescent stains under laser-scanning confocal microscopy, aimed at locating nuclei (with DAPI), proteins (aminofluorescein), and polysaccharides (concanavalin A) (Holloway and Cowen 1997). An additional examination into discerning the type of glycosaminoglycan or substrate is by changing the pH of a working AB solution. If testing with AB in fluid, a higher pH (5.6-5.8) may be necessary; however, at this pH, the effect of AB on substrate is severely diminished because proteins and glycoproteins may become weakly ionized and form a complex with AB (Whiteman 1973). Thus, based on the results here, a pH of 2.5 was successful.

Mucocytes, or cells that produce and secrete mucus, are common in molluscan tissues such as the gills, digestive gland, mantle, and foot (Fiala-Médioni and Métivier 1986, Morton 1986). The extracellular material observed in some electron and light micrographs (e.g., mucilaginous material and phytoplankton) could lend credence to the hypothesis of pedal feeding (Marelli 1987). Detritus and phytoplankton from the sediment may become trapped in the mucus released from the subepithelial region. If this is then followed by movement of the aggregate via ciliary action into the mantle cavity sorting and digestion can then take place. Live imaging or fixation of an active secretion would be the next step to observe how glandular material from the subepithelium is released and in what quantity at given time. Further research is required to determine the specific function(s) of the pedal glands and the molecular structure their products.

Internally to the subepithelium, three major muscle orientations were observed in any and all sections of pedal tissue. Trueman and Brown (1985) determined that this was not the case in other bivalves, such as *Donax serra*, where the entire internal

ultrastructure is dominated by one orientation of muscle fibers in any one section of pedal tissue. Orientations of muscle fibers could be very informative for studying pedal flexibility as well as limits imposed by its morphology and ultrastructure. Two of the three muscle fiber orientations in *R. cuneata* and *P. caroliniana* surrounded, and presumably formed the hemolymph sinus. This large opening or tube-like structure observed in scanning electron micrographs and histologically stained tissue was identified as a hemolymph sinus by Park et al. (2012) in *G. veneriformis*. Hemolymph is thought to originate from a hemocoel associated with mantle tissue that is used as storage for hemolymph waiting to be transported and inflate tissue, such as the foot, when needed (Morton 1980). This was not observed in the current study in either species; thus, it remains open to further research as to the placement of such a hemocoel and origin of the hemolymph pumped into the pedal sinus.

Most of the research performed on both clams was conducted on contracted pedal tissue. Relaxed pedal tissue was examined in order to provide insight into how the foot ultrastructure may appear compared to contracted (i.e., when the foot is retracted into the shell) and when the foot is relaxed (i.e., when the foot is extended past the ventral shell margins). Relaxed pedal tissue was imaged under SEM (data not shown); however, the results showed no large differences in morphology as compared to contracted tissue. The only observable difference under light microscopy, was that the musculature changed from tight bundles of muscle fibers to string-like, wavy bundles. Full relaxation was sometimes not possible. One specimen perished during the relaxation procedure. Another sample partially contracted once placed in buffered glutaraldehyde. This was possibly due to an effect of osmolarity. While the concentrations of fixatives and buffers remained

the same for all tissues for each respective microscopy technique, there may be a need for further research into optimizing a protocol that can reduce this effect of osmolarity on the tissue. Nonetheless, this was the first comparative study on the pedal morphology and ultastructure of *R. cuneata* and *P. caroliniana,* and the first to examine relaxation of pedal tissue for light microscopic analysis. Future research comparing the ultrastructure and composition of glandular material in the foot between infaunal species within and between families could provide insight into how species have adapted to their environments and reveal how closely related species are on a morphological and ultrastructural scale.

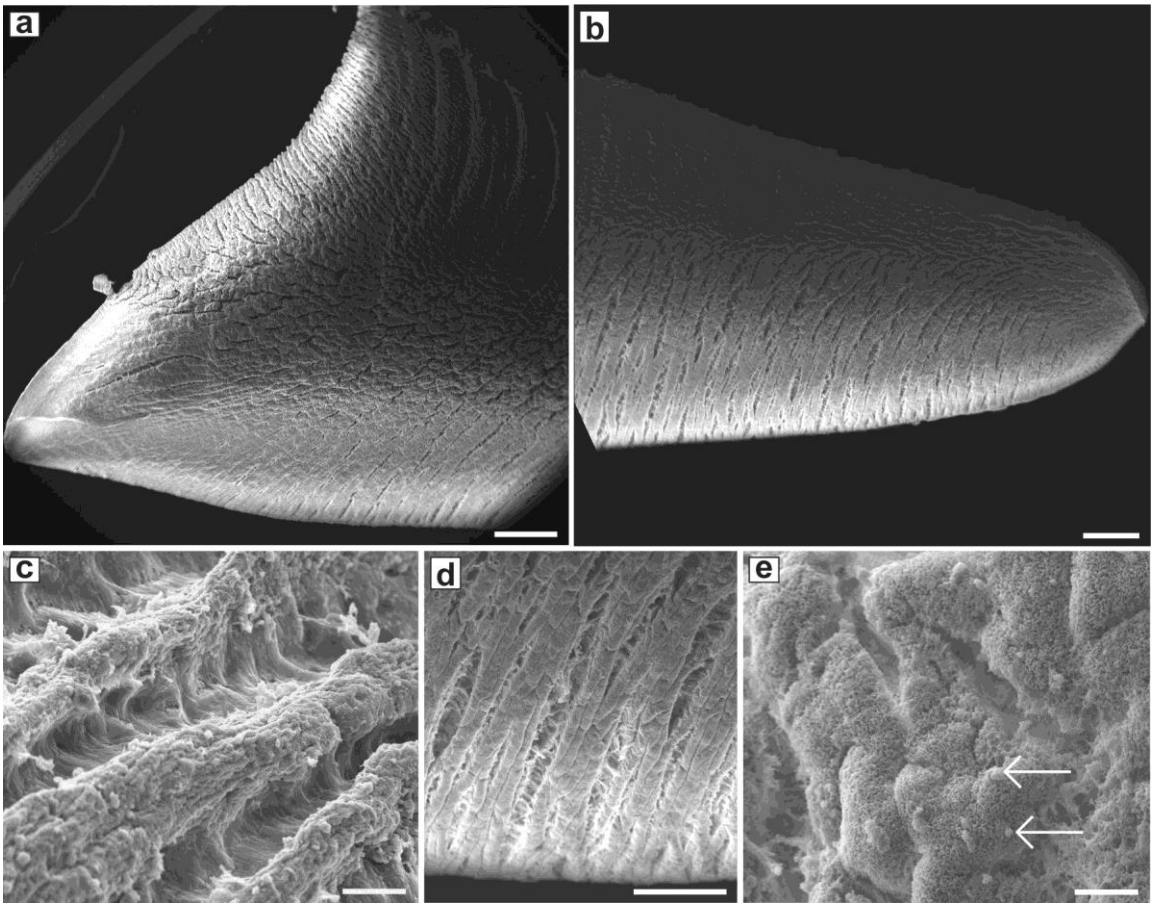

Figure 33. SEM micrographs of the foot of *Rangia cuneata*.

The foot of *Rangia cuneata* under SEM has a well-defined toe (a) leading toward a rounded heel (b). A high magnification image taken from the dorsal portion (top) of the foot reveals an epithelium with deep villi, but is not strongly ciliated (c). The ventral portion of the foot has deep villi (d) and is heavily ciliated (arrows; e). Scales bars = 500 µm (a, b), 250 µm (d), 25 µm (c, e).

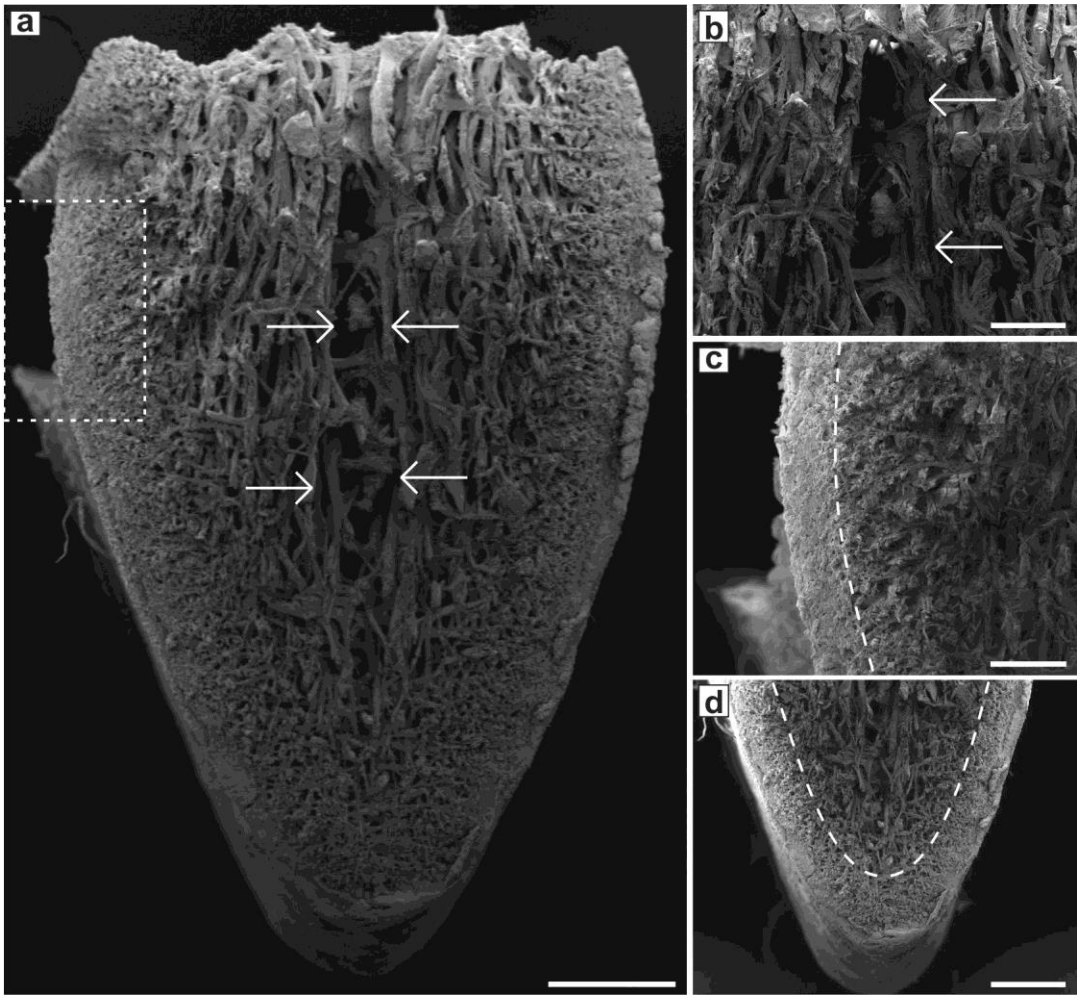

Figure 34. SEM micrographs of a cross-section through the foot of *Rangia cuneata*.

A cross-section of the foot of *Rangia cuneata* reveals inner muscle fibers surrounding the hemolymph sinus (arrows, a, b). A higher magnification of the epithelium and subepithelial regions (box in a) indicated that they are not strongly separated from the internal musculature (to the right of the dashed line, c). The ventral portion of the foot is tapered in a V-shape with a dense subepithelial region (below and outside of the dashed line, d). Images are oriented with dorsal (top) and ventral (bottom). Scale bars = 500 µm (a, d), 250 µm (b, c).

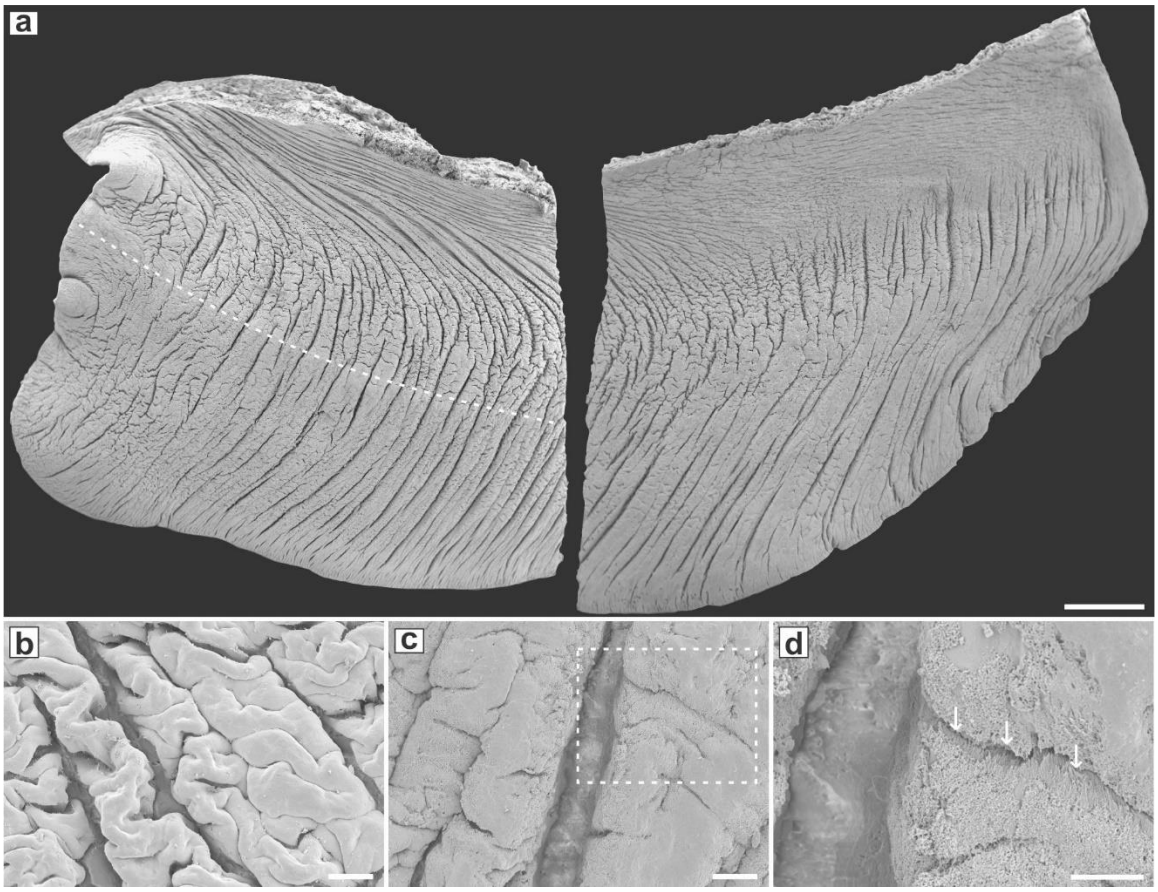

Figure 35. SEM micrograph of whole foot of *Polymesoda caroliniana*.

The whole foot of *Polymesoda caroliniana* was cut in half to accommodate SEM mounts. The foot has a large, rounded toe that curves to a small heel (from left to right) (a). Higher magnification images reveal a somewhat smooth, but wrinkled epithelium (b) imaged from above the dotted line in (a). The epithelium becomes more flattened with deep villi (c) and is heavily ciliated (arrows, d, inset from c) towards the ventral portion of the foot. Scale bars = 1 mm (a), 50 µm (b, c), 25 µm (d).

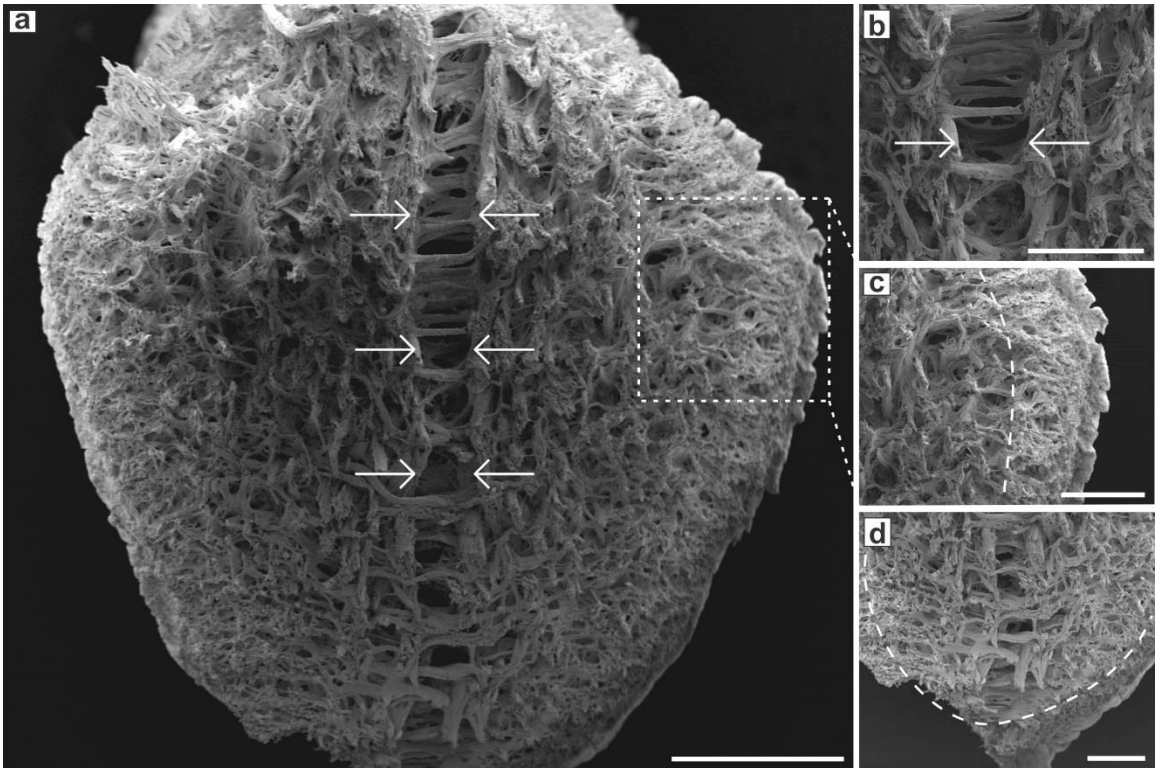

Figure 36. SEM micrographs of a cross-section through the foot of *Polymesoda caroliniana*.

A cross-section of the foot of *Polymesoda caroliniana* reveals inner musculature surrounding the hemolymph sinus (arrows, a, b). A higher magnification of the epithelium and subepithelial regions (box in a) indicated that they are not strongly separated from the internal musculature (to the right of the dashed line, c). The ventral portion of the foot is not tapered as strongly as that of *R. cuneata* (Figure 28), but does have a dense subepithelial region (below and outside of the dashed line, d). Images are oriented with dorsal (top) and ventral (bottom). Scale bars = 500 µm (a, d), 250 µm (b, c).

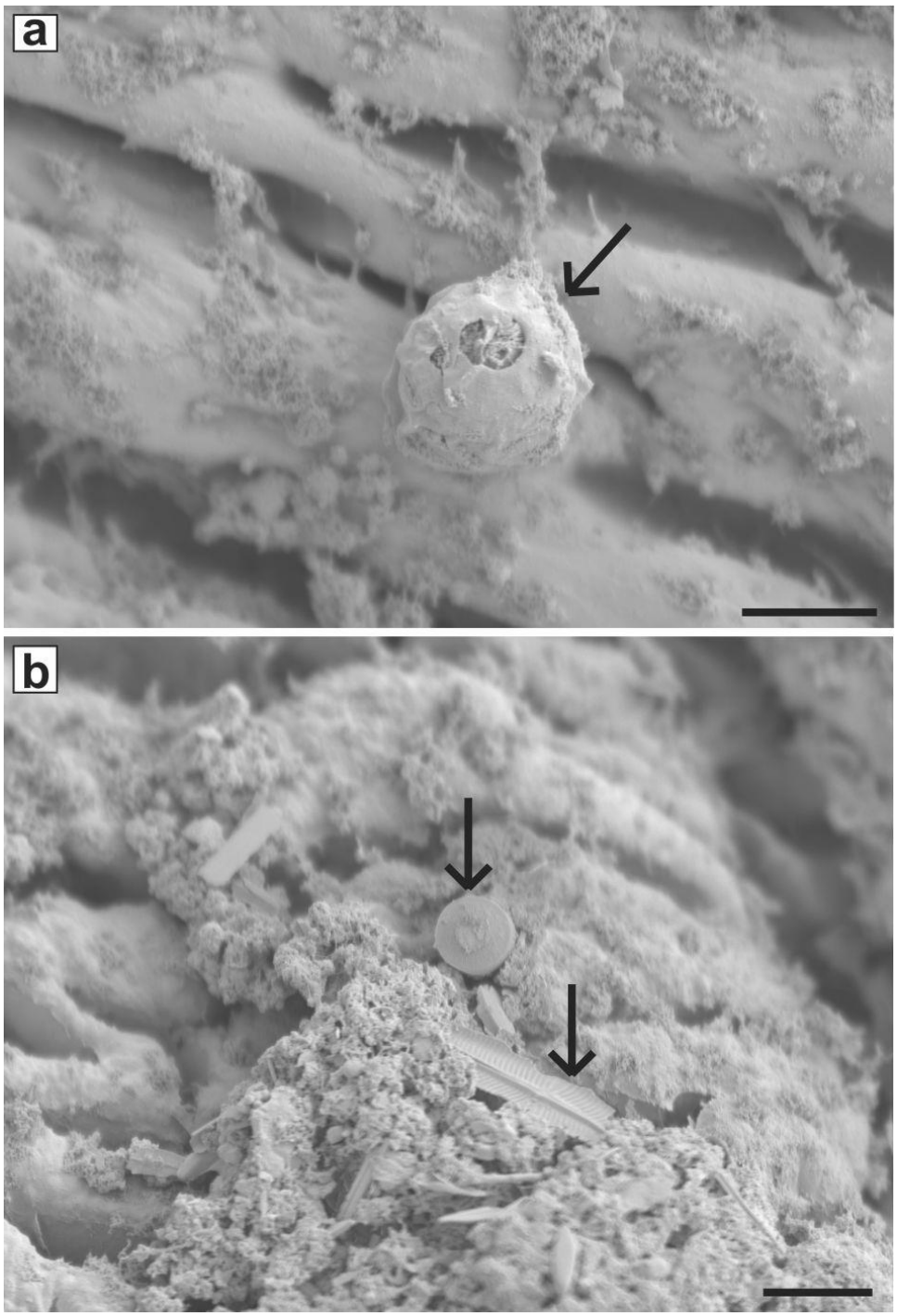

Figure 37. SEM micrograph of extracellular material on the epithelium of the foot.

Several observations of the epithelium of the foot of *Rangia cuneata* and *Polymesoda caroliniana* included mucilaginous secretions with fragments or whole cells of phytoplankton (e.g., dinoflagellate (arrow in a); diatoms (arrows in b)). Scale bars = 25µm.

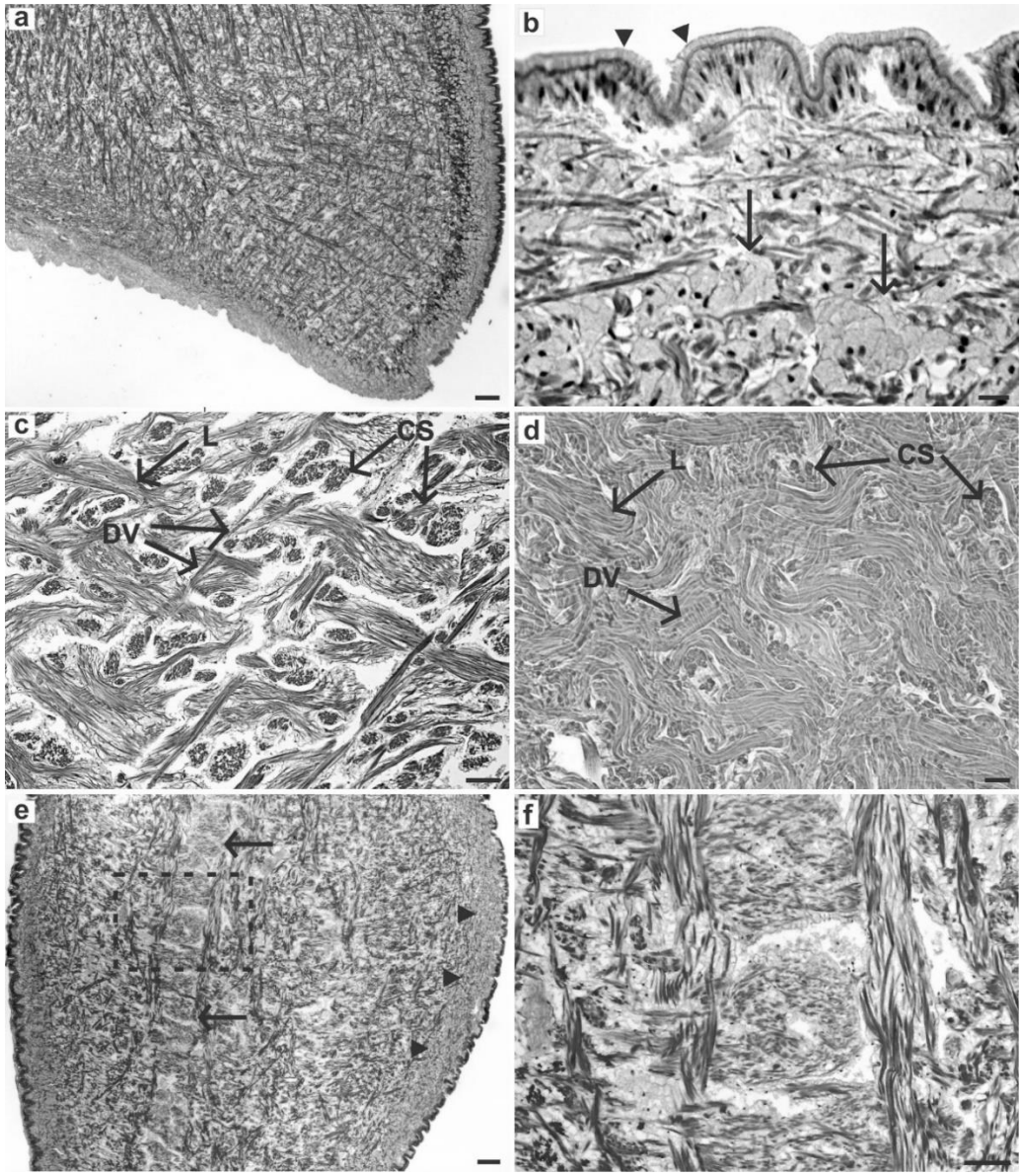

Figure 38. H&E stained foot tissue of *Rangia cuneata*.

H&E stained photographs were acquired of the toe of *Rangia cuneata* present an epithelium, subepithelial region, and inner musculature (a). Ciliated, simple cuboidal to columnar cells comprise the epithelium (arrowheads, b). Nuclei (dark punctate coloration) are laterally to basally located in these cells. The subepithelium is of gray coloration (arrows in b). The muscle fibers are positioned in three major orientations: longitudinal (L), cross-section (CS), and dorsal-ventral (DV) (c). Under relaxation, the muscle fibers become string-like and the volume increases substantially, making it more difficult to see the separate orientations of the fibers (d). A cross-section through a contracted foot of *R. cuneata* from the posterior side of the foot reveals the ciliated epithelium and thick subepithelial region (arrowheads, g), and internal musculature surrounding the hemolymph sinus (arrows) (g). (h) is a higher magnification image from (g; box). Scale bars = 100 µm (a, g), 50 µm (b, e, h), 10 µm (c, f), 5 µm (d).

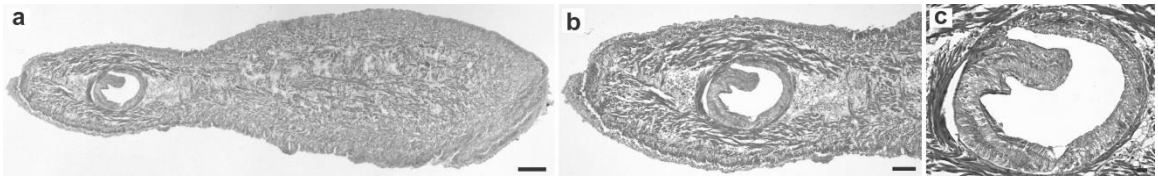

Figure 39. Longitudinal section through the foot of *Polymesoda caroliniana*.

A longitudinal section of a contracted foot of *Polymesoda caroliniana* from the posterior to anterior (left to right orientation) shows the epithelium surrounding a subepithelial region and inner musculature. The hemolymph sinus is a circular tube near the posterior end of the foot (a, b). The tube is lined with simple columnar, ciliated cells with laterally placed nuclei (c). Scale bars = 100 µm (a), 50 µm (b), 10 µm (c).

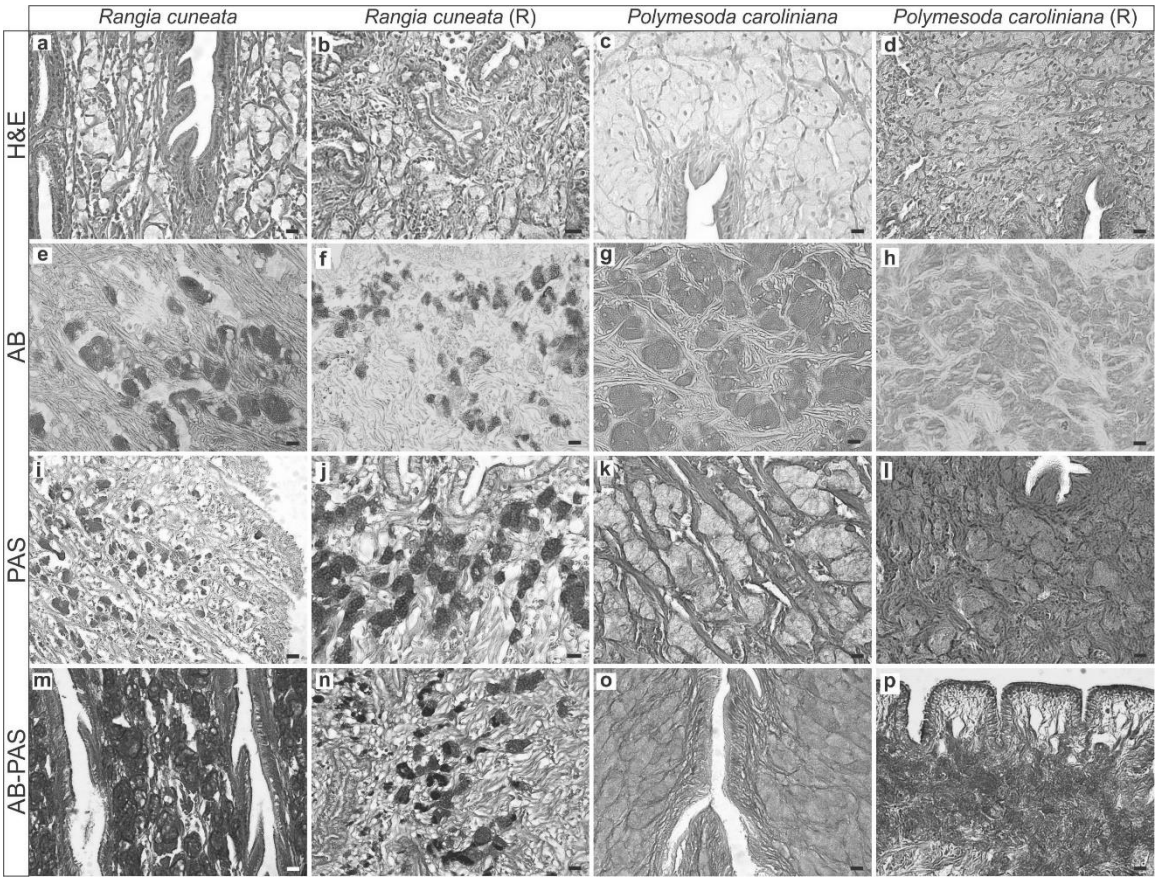

Figure 40. High magnification images of histochemically stained foot tissue of *Rangia cuneata* and *Polymesoda caroliniana*

High magnification images of contracted and relaxed (R) foot tissue of *Rangia cuneata* and *Polymesoda caroliniana* were compared based on staining with hematoxylin and eosin (H&E) (a-d), Alcian blue (AB) (e-h), periodic-acid Schiff (PAS) (i-l), and a combined Alcian blue-periodic-acid Schiff (AB-PAS) protocol (m-p). General ultrastructure of the epithelium, subepithelial region, and muscle fibers were observed under standard H&E staining. Hematoxylin (dark coloration) stains DNA, revealing lateral to basally located nuclei in the ciliated, columnar cells and mucus-producing cells (mucocytes) comprising the subepithelium. Eosin stains cytoplasm and muscle fibers (a-d). Glycosaminoglycans or acidic polysaccharides were localized in the subepithelial region in both species via AB staining (dark coloration, e-h). Only *R. cuneata* showed positive PAS staining, indicating production of non-acidic polysaccharides (deep magenta, i-j), whereas no localization of this material was observed in *P. caroliniana* (light coloration indicating nonspecific staining, k-l). This is further supported with co-localization of AB-PAS in *R. cuneata* (m, n) and in *P. caroliniana* (positive AB staining only; o, p). Scale bars = 10 µm.

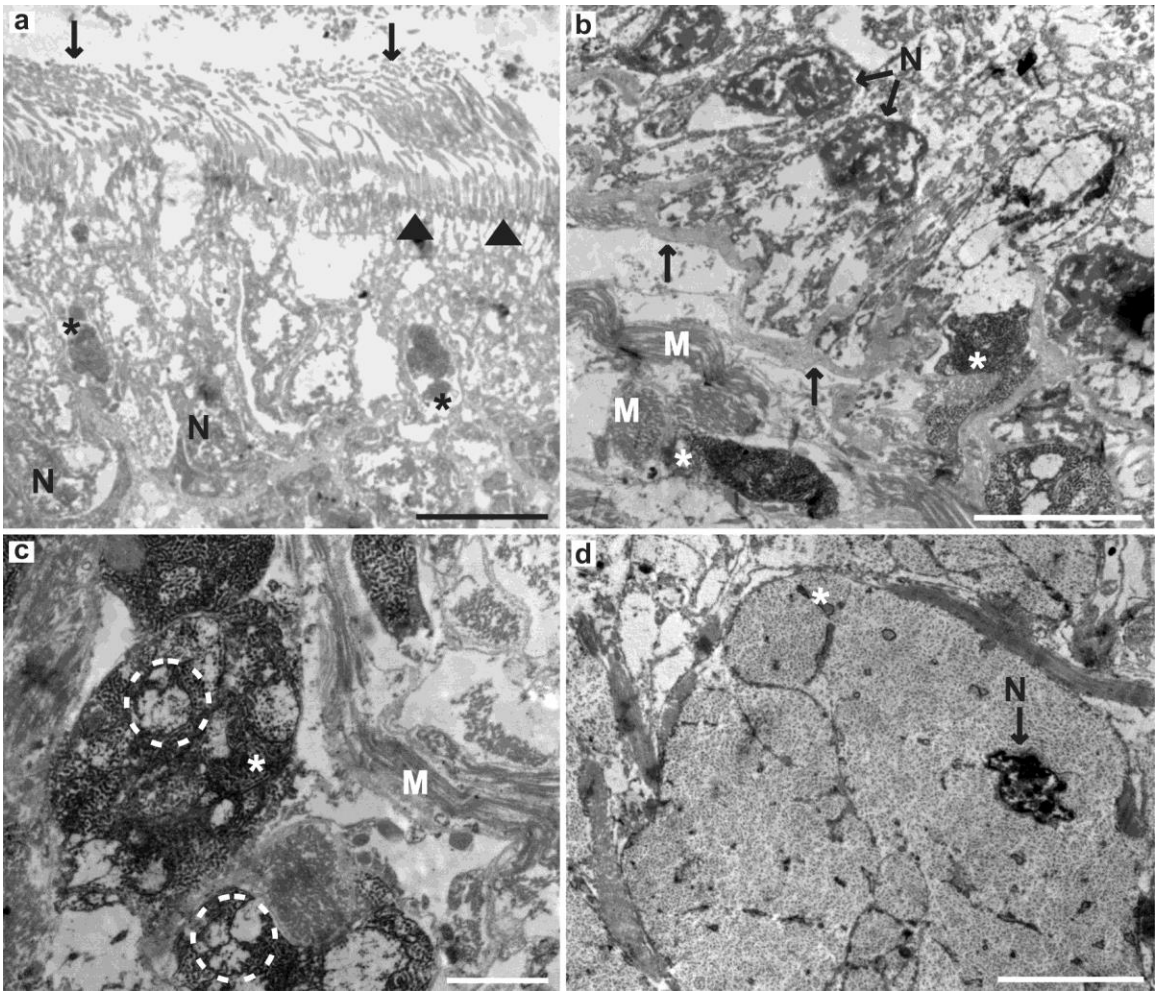

Figure 41. TEM micrographs of foot tissue of *Rangia cuneata*.

High magnification images were acquired from sections of the epithelium and subepithelium of the foot of *Rangia cuneata*. Epithelial cells have long cilia (arrows) emerging from electron dense basal bodies (arrowheads). The nucleus (N) of each cell is lateral to basally located. In between some epithelial cells can be seen subepithelial electron dense granular material (*), possible indicating the presence of goblet cells (a). The epithelial cells sit on a thick basement membrane (arrows) above a large concentration of subepithelial material (*), the latter surrounded by muscle fibers (M) (b). The subepithelial material appears heterogeneous with different compositions based on how electron dense the material is (dashed circles indicate a different polysaccharide composition). Muscle fibers were also present here surrounding the glands. The darker, granular material (*; c) is likely what was stained with AB in histology images. Not all subepithelial material is composed of large, electron dense, granular material. A light, speckled appearance is also common, where nuclei may be observed; each indicating a single mucocyte. No other cytoplasmic organelles were observed (d). Scale bars = 5 µm (a-b, d), 2 µm (c).

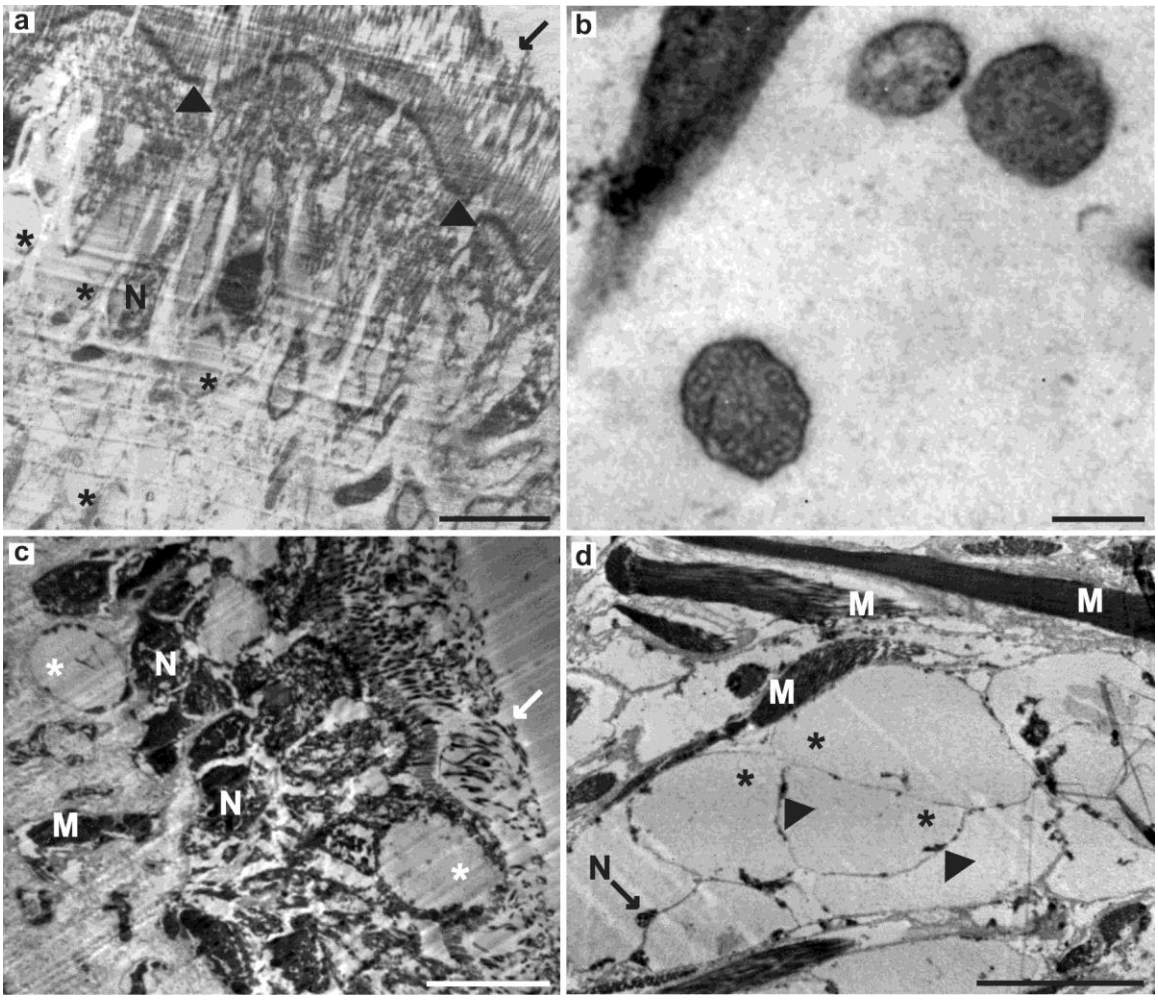

Figure 42. TEM micrograph of foot tissue of *Polymesoda caroliniana*

High magnification images were acquired from sections of the epithelium and subepithelium of the foot of *Polymesoda caroliniana*. Epithelial cells have long cilia (arrows) emerging from electron dense basal bodies (arrowheads). The nucleus (N) of each cell is lateral to basally located. Subepithelial glands or goblet cells (*) can be seen beneath the epithelium (a). A cross-section of a cilium reveals a standard 9+2 arrangement (b). The glands in the subepithelium appear homogeneous with unstained internal material (*) and surrounded by some muscle fibers (M) (c). The glands are composed of presumably numerous, amorphous mucocytes (*) with small nuclei. The glands are surrounded by muscle fibers. No other cytoplasmic organelles were observed (d). Scale bars = 10 µm (c), 5 µm (a, d), 1 µm (b).

References

Bairati A, Comazzi M, Gioria M. 2000. An ultrastructural study of connective tissue in mollusc integument: I. Bivalvia. Tissue Cell. 32(5):425-436.

Bairati A, Gioria M. 2008. An ultrastructural study of cell junctions and the cytoskeleton in epithelial cells of the molluscan integument. J Morphol. 269(3):319-331.

Calabro C, Albanese MP, Martella S, Licata P, Lauriano ER, Bertuccio C, Licata A. 2005. Glycoconjugate histochemistry and nNOS immunolocalization in the mantle and foot epithelia of *Tapes philippinarum* (bivalve mollusc). Folia Histochem Cyto. 43(3):151-156.

Cohen WD, Tamburri MN. 1998. Distinctive cytoskeletal organization in erythrocytes of the cold-seep Vesicomyid clam, *Calyptogena kilmeri*. Biol Bull. 194(1):7-13.

Fiala-Médioni A, Métivier. 1986. Ultrastructure of the gill of the hydrothermal vent bivalve *Calyptogena magnifica*, with a discussion of its nutrition. Mar Biol. 90:215-222.

Holloway CF, Cowen JP. 1997. Development of a scanning confocal laser microscopic technique to examine the structure and composition of marine snow. Limnol Oceanogr. 42(6):1340-1352.

Lane DJW, Nott JA. 1975. A study of the morphology, fine structure and histochemistry of the foot of the pediveliger of *Mytilus edulis* L. J Mar Biol Assoc UK. 55:477-495.

Marelli DC. 1987. Processes controlling intertidal zonation in an estuarine soft-bottom bivalve assemblage. [Dissertation]. [Ann Arbor (MI)]: The Florida State University.

Morton BS. 1980. The anatomy of the 'living fossil' *Pholadomya candida* Sowerby 1823 (Bivalvia: Anomalodesmata: Pholadomyacea). Copenhagen (Denmark): Dansk Naturihistorisk Forening. p. 101.

Morton B. 1986. The functional morphology of the organs of feeding and digestion of the hydrothermal vent bivalve *Calyptogena magnifica* (Vesicomyidae). J Zool Lond A. 208:83-98.

Norenburg JL, Ferraris JD. 1990. Cytomorphology of the pedal aperture glands of *Mya arenaria* L. (Mollusca, Bivalvia). Can J Zool. 68:1137-1144.

Park JJ, Lee JS, Lee, YG, Kim JW. 2012. Micromorphology and ultrastructure of the foot of the equilateral venus *Gomphina veneriformis* (Bivalvia: Veneridae). Cell Biol. 1:11-16.

Quintarelli G, Devollo MC. 1966. Age changes in the localization and distribution of glycosaminoglycans in human hyaline cartilage. Histochemie. 7(2):141-167.

Reynolds ES. 1963. The use of lead citrate at high pH as an electron-opaque stain in electron microscopy. J Cell Biol. 17:208-212.

Trueman ER, Brown AC. 1985. Dynamics of burrowign and pedal extension in *Donax serra* (Mollusca: Bivalvia). J Zool Lond A. 207:345-355.

Whiteman P. 1973. The quantitative measurement of Alcian blue-glycosaminoglycan complexes. Biochem J. 131:343-350.

CHAPTER IV – SHELL ULTRASTRUCTURE OF *RANGIA CUNEATA* AND *POLYMESODA CAROLINIANA*

Introduction

Shell layers and growth pattern

The shells of both species are prosogyrous, meaning the umbo curves toward the anterior end of the shell. The umbo is the dorsal-most, and oldest part of the bivalve shell, and the ventral margin is the youngest (Figure 43). Bivalve shells are composed of layers of aragonite or calcite ($CaCO_3$) (Lutz and Rhoads 1980). The number of layers may differ between species and may include inner, middle, and outer layers (Fritz et al. 1990). The innermost layer that comes into direct contact with the soft body tissue is the nacre. In many species, such as *R. cuneata*, attachment of soft tissue such as the adductor muscles and mantle forms a scar along the nacre (i.e., adductor muscle and pallial scars). The inner and middle layers are composed of prismatic crystals of aragonite or calcite (Lutz and Rhoads 1980). The outer shell layer is where the growth bands, examined for age determination and in population dynamics studies, are present and these bands offer visualization of the clam's growth pattern. Thick growth bands indicate warm water temperatures, while narrow, tightly packed growth bands indicate cold water temperatures at the time of shell deposition (Lutz and Rhoads 1980; Fritz and Haven 1983; Fritz et al. 1990). The outermost layer of bivalve shells is the periostracum, an organic layer not considered a true shell layer. A radial section through the maximum axis of growth (Figure 44a, b – D to V) provides a visual of the shell layers and the growth pattern.

Research aims

While much research has investigated shell morphology and ultrastructure (i.e., shell layers and composition) on several bivalve species, including *R. cuneata*, this was the first comparative study on that of *R. cuneata* and *P. caroliniana* from a system in Mississippi. The goals of this research were to provide the first description and analysis of the shell ultrastructure of *P. caroliniana* and to provide an assessment of the shell layers, and visualization of any growth breaks in both *R. cuneata* and *P. caroliniana*. Last, it was of interest to determine the elemental composition of the shells from sympatric species in an estuarine environment of MS.

The age of various species of bivalves has been published in the literature, but age using shells was not a research aim in this study. Age can be difficult to determine due to changes in the bivalve's habitat (i.e., seasonal or large-scale ecological disturbances) or physiological responses (e.g., spawning, compaction of rings with increasing age). It was of interest to compare the shell ultrastructure of *R. cuneata* to studies that have performed on this species, but from other systems (e.g., Delaware River; Fritz et al. 1990). In addition, no study has been performed on the shell ultrastructure of *P. caroliniana*. Due to the thinness of this species' shells, it was hypothesized that visualization of shell layers and any growth pattern would be more problematic compared to *R. cuneata*. Shells from live clams were used in this study. Empty shells found in the study site were in poor condition, greatly eroded, and too fragile for sectioning and subsequent examination. The gross morphology and ultrastructure were analyzed under light and scanning electron microscopy, and X-ray microanalysis was used to detect elements in various pieces of shell. It was hypothesized that elements including C, Ca, O ($CaCO_3$) would be detected,

as well as Mg, Sr, and Si. The latter three are commonly detected in biomineralized tissue of many different organisms.

Methodology

Shell morphology and ultrastructure

For visualization of shell morphology and ultrastructure (i.e., shell layers), four valves from *R. cuneata* (shell length = 23.2 – 54.5 mm) and two shells from *P. caroliniana* (SL ≈ 44 mm), collected as live individuals from random areas in sites from the middle and lower reaches of Johnson Bayou, were cut along the dorsal to ventral margin (i.e., along the maximum axis of growth) or longitudinally (anterior to posterior). Shells were cut using a RIDGID 15 Amp table saw in the Polymer Science Department in Hattiesburg, MS. Once the shells were cut, a 3 µm and 1 µm diamond paste was used to polish the section edges. Shells were then placed in Mutvei solution (1% acetic acid, 25% glutaraldehyde, 1-2 g Alcian blue (AB)) for a minimum of 1 hour at 4°C to etch and add contrast to the shell layers via the selective binding of AB to substituted polysaccharides (e.g., glycosaminoglycans; Quintarelli and Devollo 1966) in the organic matrix within the shell. Following removal from the Mutvei solution, sections were rinsed with distilled water and allowed to air dry. Images were captured before and after staining in Mutvei solution using a Pentax GPS-4 camera (Ricoh Imaging Americas Corporation, Denver, CO).

Elemental analysis via EDS

Examination of shell morphology and microanalysis required that shells be broken as whole shell examination was not possible under SEM due to size limitations. Shells were broken by wrapping them in thick paper packaging and using a hammer to

break the valves. Fragments were handled with nitrile gloves, sonicated several times for a few minutes in distilled water, and allowed to air dry before mounting on an aluminum stub. The periostracum, nacre and adductor muscle scar, and prismatic layers were examined under SEM (Hitachi SU3500, Hitachi High-Technologies, Corporation, Chiyoda-ku, Tokyo, Japan) at an accelerating voltage of 3 kV. An accelerating voltage of 15 kV was required for X-ray microanalysis, also referred to here as Energy Dispersive X-ray Spectroscopy (EDS). Map (region-of-interest (ROI)) and line spectra were obtained from shell fragments and analyzed using AZtecEnergy EDS software v2.3 (X-max 150 detector, Oxford Instruments NanoAnalysis, Buckinghamshire, UK).

Data analysis

All quantitative data (e.g., thickness of prismatic layers) was acquired using Image J version 1.48. All qualitative data (e.g., images and spectra) were edited and formatted in CorelDraw X8 (Corel Corporation, Ottawa, Ontario, Canada).

Results

Shell morphology and ultrastructure

The periostracum is a dark and thin organic layer on the outside of the shells. It is smooth on *R. cuneata*, but ruffled on *P. caroliniana* (Figure 43a, b). The nacre is completely white in *R. cuneata* with strong scars indicating attachment sites for the adductor and retractor muscles and mantle tissue (pallial line). The pallial sinus is a continuation of the pallial line, formed by the siphons which are fused sections of the mantle (Figure 43c). The nacre on the inside of *P. caroliniana* shells is a mix of white, pink, and purple coloration with little to no discernible muscle or pallial scars (Figure 43d). The periostracum and nacre layers are less than 100 µm in thickness. The shells of

R. cuneata were approximately 2.5 times thicker than those of *P. caroliniana* examined regardless of where on the shell the measurement was taken.

The first observation during and after sectioning was the breaking of shell sections at an observed transition between prismatic layers (Figure 44a, b). The break was a smooth separation of shell layers indicating differences in crystalline structure or orientation. After polishing, the greatest difference between species was the presence of four shell layers in *R. cuneata* and three layers in *P. caroliniana*, the latter lacking a middle prismatic layer. A compact and white internal section was identified as the inner homogenous layer composed of stacked nacre layers in both species. In *R. cuneata* above the inner homogenous layer was the middle layer, separated from the outer layer by the pallial myostracum (Figure 44c, d). The middle layer was lighter, but thicker than the other layers before it terminated with the inner layer about halfway to two-thirds the length of the shell towards the ventral margin (Figure 44b, c, g). The outer layer dominated the ventral margin and was where the more easily observable growth bands used in research are visualized. The thin periostracum commonly flaked and fell off of sections of both species during handling.

There were three to four distinct wedge-shaped sections of shell comprising the umbo of *R. cuneata* (Figure 44c, d). These are the concentric ridges of early growth in bivalves. If the results support observations by Fritz et al. (1990), then these wedges would indicate the first few years of ontogeny. The opaque, narrow growth bands indicate growth during the winter months, and the light, broad regions indicate growth from spring to fall (Figure 44d) (Lutz and Rhoads 1980; Fritz and Haven 1983; Fritz et al. 1990). Narrow and somewhat opaque bands indicate possible growth in the next

winter or a change in growth pattern. The length of the concentric ridges from shells of *R. cuneata* measured 2.7 – 5 mm. The width of growth bands, including some from the ridges were < 100 µm up to ~500 µm.

There are four distinct layers of shell in *R. cuneata*: a white inner homogenous layer likely formed on thick, compact sheets of nacre, a thick, somewhat translucent middle layer, a pallial myostracum, and outer layer beneath the periostracum. The inner homogenous and middle layers do not continue beyond about halfway towards the ventral margin (Figure 44c).

The shell layers ranged in thickness. Averages at the thickest point for inner homogenous, middle, myostracum, and outer layer were 0.96, 1.14, 0.002, and 1.31 mm, respectively. The outer layer was thinner in the middle of the shell (between umbo and ventral margins), but thickened at the ventral margin (Figure 44b, c, e). Averages at the thickest point of the inner, myostracum, and outer shell layer in *P. caroliniana* were 0.05, 0.002, and 1.14 mm, respectively.

Staining with Mutvei solution revealed better resolution of shell layers and growth bands. The inner homogenous layer was lightly stained, if at all, indicating little organic matrix and tightly compacted shell material. The middle and outer layers had several, but variable thin and thick layers of heavily stained organic matrix (Figure 44e). Some regions that were heavily stained could indicate growth breaks, possibly due to storm events or spawning (Figure 44f). A U-shaped notch in the growth bands beneath the periostracum along the outermost regions of the outer layer in *R. cuneata* was noted, likely indicating a storm break. Ridges along the outer layer and associated periostracum could indicate spawning breaks (Figure 44f).

The shell layers of *P. caroliniana* were more difficult to analyze due to the thinness and fragility of the shell. However, it could be discerned that the growth pattern is similar to that of *R. cuneata* in that the umbo is constructed of concentric ridges before recurving into presumably a mature stage of growth. Termination of the inner layer occurs approximately midway down the shell, similar to what occurs in *R. cuneata* (Figure 44g). Growth bands that comprise the outer layer curve perpendicularly from the inner side of the shell. Light microscopic images and SEM micrographs revealed that, along with the outer periostracum and the inner nacre, only three prismatic layers were evident in *P. caroliniana* (Figure 44h). Based on their appearance, two of the three prismatic layers varied in composition, and were separated by the pallial myostracum. Alcian blue revealed some growth bands in the outer layer, but individual bands were still difficult to examine (Figure 44e).

A longitudinal section through shells of *R. cuneata* and *P. caroliniana* revealed a thick inner homogenous layer, the pallial myostracum, and growth increments in the outer layer (Figure 45). The inner layer was interrupted by the adductor muscle (Figure 45a-c). Growth increments did not curve as strongly in *P. caroliniana* (Figure 45d) as those in *R. cuneata*. Alcian blue selectively bonded and stained the organic matrix within and between growth bands (Figure 45c, d). The thickness and presence of the organic matrix indicated by AB was highly variable between specimens in both species.

High magnification images acquired via SEM revealed the innermost layer of nacre to be very thin and situated beneath (internal to) the stacked, older layers of nacre comprising the inner homogenous layer (Figure 46). In both species, the outer layer is aragonitic crossed lamellar crystals. The outer layer, as well as the middle layer (*R.*

cuneata) is composed of aragonitic cone complex crossed lamellar crystals (Lutz and Rhoads 1980) (Figure 47a-d). First- (1°) and second-order (2°) lamellae of the outer layer grow in an alternating pattern of near uniform thickness (10-15 µm) (Figure 47b). The crystals making up the middle layer are randomly oriented (Figure 40c, d), while the nacre is uniform and unornamented (Figure 47e). The pallial myostracum was imaged after fracturing a shell into two pieces, effectively removing the bottom half of the shell (middle and inner layers). The myostracum is thin in some areas depending on the arrangement of the crystals comprising the outer shell layer. Small pore-shaped regions are indicative of organic matrix (Figure 47f).

Elemental analysis via EDS

Elemental analysis of the periostracum of both species (Figure 48a-d) showed it to be primarily composed of C, O, and Si. Additional elements included Na, Mg, P, S, Cl, K, Ca, Ti, and Fe. Counts (i.e., indicating the relative amount of an element present in the ROI) of Si were far greater than from any other spectra on any other shell layer or section, while counts of Ca were the lowest (Figure 48e, f). A line spectrum across the nacre and adductor muscle scar of *R. cuneata* indicated a transition from low to high counts of Ca, with an increase in the level of Na, Mg, P, S, and Si across the scar (Figure 49a, b). A map (ROI) spectrum of the nacre revealed uniform counts of elements (C, O, Ca, Na, Mg, S, P, Sr, and Cl) (Figure 49c). A map (ROI) spectrum of the adductor muscle scar supported results from the line spectra (i.e., lower levels of Ca, and higher levels of all other elements detected), but Sr and Cl were not detected (Figure 49d). A comparative line spectrum of nacre to the adductor muscle scar in *P. caroliniana* reflected observations from that of *R. cuneata*, but no Si or P was detected (Figure 50). A drop in

the detection of Ca occurred across the transition between nacre and scar. At this transition, the levels of C, Na, Mg, S, and Cl increased, but all except C dropped in detection levels again across the adductor muscle scar (Figure 50c). A line spectra across the outer and middle layers and the pallial myostracum of *R. cuneata* (Figure 51a) showed prominent peaks for C, H, O, and Ca, but with a drop in Ca levels across the myostracum (Figure 51b). Aluminum was not removed in all spectra, but can be discounted as X-ray analysis detects the Al from the stub upon which the sample is mounted.

Discussion

The current study compared shell morphology and ultrastructure between two venerids, from different families, that coexist in Johnson Bayou. *Rangia cuneata* and *Polymesoda caroliniana* may look very similar at first glance. The key indications for separating them are based on the periostracum, in which that of *P. caroliniana* is darker in color and ruffled, and an elongated posterior end produced by *R. cuneata* (Figure 43a, b). Internally, coloration and presence of strong scars on the nacre are the most obvious distinguishing characteristics. *Rangia cuneata* presents an entirely white nacre with distinct and sharply set scars indicating previous attachment of soft tissue (adductor muscle and mantle). The nacre is of mixed coloration from white to purple in *P. caroliniana*, and unless the shell is dried out, scars may not be discernible (Figure 43c, d). General shell morphology is not informative enough for estimating growth patterns or age. Examination of the internal shell ultrastructure via sectioning and polishing was required.

The thinnest sections attainable were approximately 0.5 cm in width, making visualization through sections with transmitted light impossible without sectioning with a thin, diamond-tipped blade. Nonetheless, visualization of shell layers and growth bands was made possible with polishing of the cut edges, and further by etching and staining with Mutvei solution. Several shells, particularly of *P. caroliniana*, broke during sectioning. A procedure to fully embed shell might reduce this occurrence; however, if necessary, removal of the shell fragments from the embedding media might cause the fragile sections to still fall apart. A partial embedding procedure was attempted with standard caulk and cement glue. Removal of fragments and sections from these materials was very time consuming and did not prevent many fragments from breaking. When cutting shells with the table saw, the point at which most sections broke was along the pallial myostracum (Figure 44b). Given how thin the myostracum is in the shells, it is not surprising this was a weak point. The use of a 3 µm and 1 µm diamond paste provided enough polish to observe a difference in shell layers and the presence of growth bands with the unaided eye.

Shells of *R. cuneata* indicated that deposition of shell material occurred in wedge-shaped concentric ridges before drastically shifting and depositing shell outward, and steadily increasing shell inflation. Based on shell growth in *M. mercenaria*, the shift from concentric ridges to recurved growth increments at a near right angle to previous shell deposition infers sexual maturity (Pannella and MacClintock 1968). Thus, if each concentric wedge indicates a year of growth, this population of *R. cuneata* may become sexually mature in 3-4 years. Ontogenetic studies may aid in answering how shell deposition specifically occurs during this early timeframe of life.

Growth breaks were difficult to examine without a larger sample size. In addition, without knowing all ecological or physiological events at the time of the examined breaks, interpretations may be suppositions. However, staining with Mutvei solution enhanced growth bands and helped identify changes in growth patterns. In *R. cuneata*, the growth break that is likely a storm break would likely have been caused by sediment particles trapped within the extrapallial sinus between the mantle tissue and shell, altering mineralization in that region. The ridges along the periostracum and outermost regions of the outer prismatic layer may indicate spawning events (Figure 47f). In this case, the clams cease growing for a time, likely in order to shunt energy into gametic production and spawning (Shumway and Parsons 2006). Spawning breaks in the shell ultrastructure are common and have even been observed in shells of bivalves that live >1000 m (Lutz and Rhoads 1980). Large and deep depressions (Figure 44f) may be considered breaks; however, the ones observed more likely indicate an outside force (e.g., predatory attack) imposed on the clam, erosion, or growth against another object. For instance, some clams were observed to live within sediment inundated with debris (e.g., sticks and logs, metal plates, or trash).

It is thought that an increased amount of organic matrix present among growth bands may be indicative of slower growth, cessation, or shell dissolution (Lutz and Rhoads 1977). This is logical given the function of the organic matrix is to control biomineralization through nucleation and inhibition of crystal growth. It is unclear whether or not growth cessation or shifts in growth patterns occurred in the examined specimens of *R. cuneata* or *P. caroliniana* from Johnson Bayou. According to Fritz et al. (1990), dark growth bands indicate winter growth. The dark colored bands indicate not

only greater organic material, but a change in shell deposition (e.g., dissolution, growth breaks, amount of shell laid down). Clark (1979) observed no distinct marks indicating winter cessation in specimens of *M. mercenaria* from Georgia.

If shell deposition was affected, then this is a reflection that the physiology of the clam was affected during this time. The "after-the-fact" observation is informative for looking at how clams respond to a specific disturbance. For example, low temperatures and salinity levels are known to retard growth in bivalves (Navarro 1988). For *M. mercenaria*, a water temperature of approximately 25°C is the upper limit for shell growth (Ansell 1968). It is hypothesized that such conditions could retard growth or cause a shift in growth patterns in *R. cuneata* and *P. caroliniana* in Johnson Bayou. In January 2015, water temperature was measured at 6°C for several days. At low tide during this time, sheets of ice were observed covering exposed banks where these clams exist. It would not be surprising if a population dynamics study revealed growth breaks due to cold shocks and mass mortality recorded during this time. Only six shells were examined in this study, four of *R. cuneata* and two of *P. caroliniana*. In contrast, nearly 500 specimens of *R. cuneata* were collected and examined by Fritz et al. (1990). One could estimate recruitment events and how successful a spawning event was in previous years by examining the growth bands of shells, based on methods and results from Fritz et al. (1990).

Lower and upper environmental limits that may affect shell growth in *R. cuneata* or *P. caroliniana* have not been determined or was not found in the literature that encompass all populations across their range. If these limits exist for the populations in Johnson Bayou, then it would be informative to observe fluctuations or changes in shell

growth, and perhaps any resulting physiological effects. It must be noted that this study only examined shell ultrastructure in a few shells from either species. Any observable differences in shell growth may not reflect the entire population. Large sample sizes are required to discern population shell growth (Fritz and Haven 1983). Nonetheless, even a few shells provided insight into elemental composition via X-ray microanalysis (i.e., elemental dispersive X-ray spectroscopy, EDS).

Elemental analysis via EDS

Growth bands can be used in the production of paleoproxies, similar to how researchers utilize ice core samples or tree rings. However, analysis via X-rays is required to first understand what elements are incorporated into the shells. The analysis from EDS provided information on the elemental composition of the shells from both species. Expected elements included C, O, and Ca ($CaCO_3$). Some additional elements that were detected, and have been detected in published research on biomineralizing organisms (Mackinder et al. 2010; Matsko et al. 2010; Drescher et al. 2012) included Na, Mg, Sr, Si, Cl, and K. The elements Na, Cl, and K could be an artifact of handling or from the environment.

Magnesium was low in spectra in both species of clam. This was expected, because highly selective ion transport systems are well known to be utilized in processes of biomineralization (Mackinder et al. 2010). If species produce shell out of calcite, then the presence of Mg can be expected in the shell, because the spacing in the crystal lattice is smaller than that in aragonite, and the ionic radius of Mg is smaller than that of Ca (Rosenberg 1980).

Strontium was another element detected in shell fragments of both species. Unlike Mg however, the ionic radius is larger than Ca. There is also more room in the crystal lattice of aragonite than calcite (Rosenberg 1980). Thus, it was not surprising to detect Sr in shell here. As a result of Mg and Sr being commonly incorporated and subsequently detected in biomineralized material (Lutz and Rhoads 1980), these elements can be used as indicators of elemental concentrations, using more sensitive methods, in the external environment of the calcifying organism under study.

Strontium has been reported to co-localize with Ca in some animals and protists, such as corals and coccolithophores (Grovenor et al. 2006, Schöne and Gillikin 2012). The Sr/Ca ratio in calcitic structures is dependent on the Sr/Ca ratio in seawater. As reported in calcifying algae, deposition of Sr into calcitic structures may be used as a record in growth variations and indicate changes in the geochemistry of the water column (Stoll and Schrag 2000, Schöne and Gillikin 2012). If research into the use of Sr in development of paleoproxies is beneficial, then the Sr/Ca ratio in the studied water column must be known. This data might be compared to the ratio or percentage of Sr in shells acquired from sediment. Incorporation of such elements such as Sr has been exploited in developing paleoproxies (Rickaby et al. 2002); however, research that has focused on Sr/Ca ratios is mainly based on correlations of Sr/Ca ratios with rates of carbon fixation and calcification. Consequently, calcifying photosynthetic organisms might be easier to use as paleoproxies, because you can hypothetically correlate growth rates with calcification in these organisms (Rickaby et al. 2002). No inference can be made with respect to the data acquired here without further study on the elemental composition of the water column as changes in abiotic factors progress and at times of

specimen collection. Regardless, shells from *R. cuneata* and *P. caroliniana* may still be valuable in sclerochronological research.

A third element of interest that was detected in some spectra was silicon, primarily from the periostracum (Figure 48). Silicon is a component in the cuticle of crustaceans and cyanobacteria that produce calcitic material, primarily at sites of growth or the laying down of biomineral material (Matsko et al. 2010); thus, the presence of Si here may infer a role in an as yet undiscovered organic matrix that regulates bivalve shell production. Presumably, Si is thought to be an important component of organic matrices or protein complexes, in which chains of Si act as "containers" for ions (e.g., Ca, P) that are required for crystal nucleation (Matsko et al. 2010).

Elements that were not expected, but detected in nearly all samples included S, P, Fe, and Ti. These elements are likely not contaminants from methodology. Care was taken to minimize contamination from external sources and were only cleaned using distilled water under sonication. Other methods, such as use of HNO_3^-, dissolves shell to be used in inductively coupled plasma mass spectrometry (Cathey et al. 2012). This method was not employed in this study. The first two elements, S and P, could be part of the periostracum's composition, as this is a proteinaceous layer on shells. Sulfates in the marine environment are up to 1000X concentrated when compared to freshwater systems. Thus, with salt water intrusion, sulfur is brought into wetland habitats. Sulfate is reduced to sulfide under microbial action (Schoepfer et al. 2014). Similarly, Fe originating from erosional processes and insoluble in freshwater systems in the form of Fe(III), is reduced once in estuarine systems under the actions of microbes. Sulfide and Fe(II) binds and forms FeS, forming the characteristic black coloration and distinct smell of anaerobic

soils (Schoepfer et al. 2014). Both species of clam in this study are infaunal organisms, directly in contact with the soils. It is not surprising that some level of S and Fe were detected in the shell fragments. Titanium was detected in the periostracum from both species of clam (Figure 48). A plant owned by DuPont located in Pass Christian, MS along the shores of St. Louis Bay produces titanium dioxide. Thus, given the proximity to Johnson Bayou, it is not surprising Ti was detected in both species. No other heavy metals (e.g., Co, Cu, Pb) aside from Ti and Fe were detected in the periostracum of either species. This indicates that if such heavy metals are present, a more sensitive detection method is required. It is positive from this standpoint that no heavy metals aside from Ti and Fe, which were detected only from the periostracum, were detected by EDS, indicating potentially low heavy metal concentrations in Johnson Bayou. However, heavy metals tend to accumulate in soft body tissue (Wolfe and Schelske 1969; Pace and Di Giulio 1987).

Energy dispersive X-ray spectroscopy is a valuable tool for determining the composition and distribution of elements in biomineralized material. The exact mechanism of how clams are able to control calcification remains unknown, but the extrapallial space between the mantle epithelium and accreting shell is the site of calcification. Based on the "matrix" hypothesis, an organic matrix is laid down to control nucleation of crystals (Rosenberg 1980). This is observed in many invertebrates (e.g., corals) (Rosenberg 1980) as well as in calcifying protists (e.g., coccolithophores) (Rickaby et al. 2002; Drescher et al. 2012). Select elements from the water column are incorporated into the growing shell. No matter the mechanism of calcification, elements like heavy metals may end up in shell material, which can be detected by EDS.

Information derived from elemental analyses on shells of *R. cuneata* and *P. caroliniana* could hypothetically be used to gain insight into how Johnson Bayou has changed in water quality. However, research involving isotopic work must take into account that this is an estuarine system with fluctuating salinity levels throughout each year and under tidal influence. As a result, isotopic levels and ratios can change in a short time period. For instance, ^{18}O levels increase with increasing salinity, while ^{16}O and ^{17}O levels decrease (Epstein and Mayeda 1953, Redfield and Friedman 1965). Compared to isotopic levels of these elements in the open ocean, those in estuarine systems could vary several-fold. Researchers may only construct a partial picture of the ecosystem at one time from the results.

This is the first comparative report on shell morphology and ultrastructure between two infaunal clams from different families that coexist in the same estuarine system in MS. It is clear that while *R. cuneata* shells may be useful in future studies on population dynamics from this and surrounding systems (i.e., St. Louis Bay), the shell of *P. caroliniana* may only valuable in terms of analyzing elemental composition. Researchers can exploit methods utilized here and in the extensive literature to examine shell ultrastructure and detect elements in the shell. Fossil shells and extant shells provide a long and a short history of an ecosystem. Results from these shells can be used to elucidate past ecological trends. Future modeling can be constructed with this type of information to determine, for example, resiliency of a population.

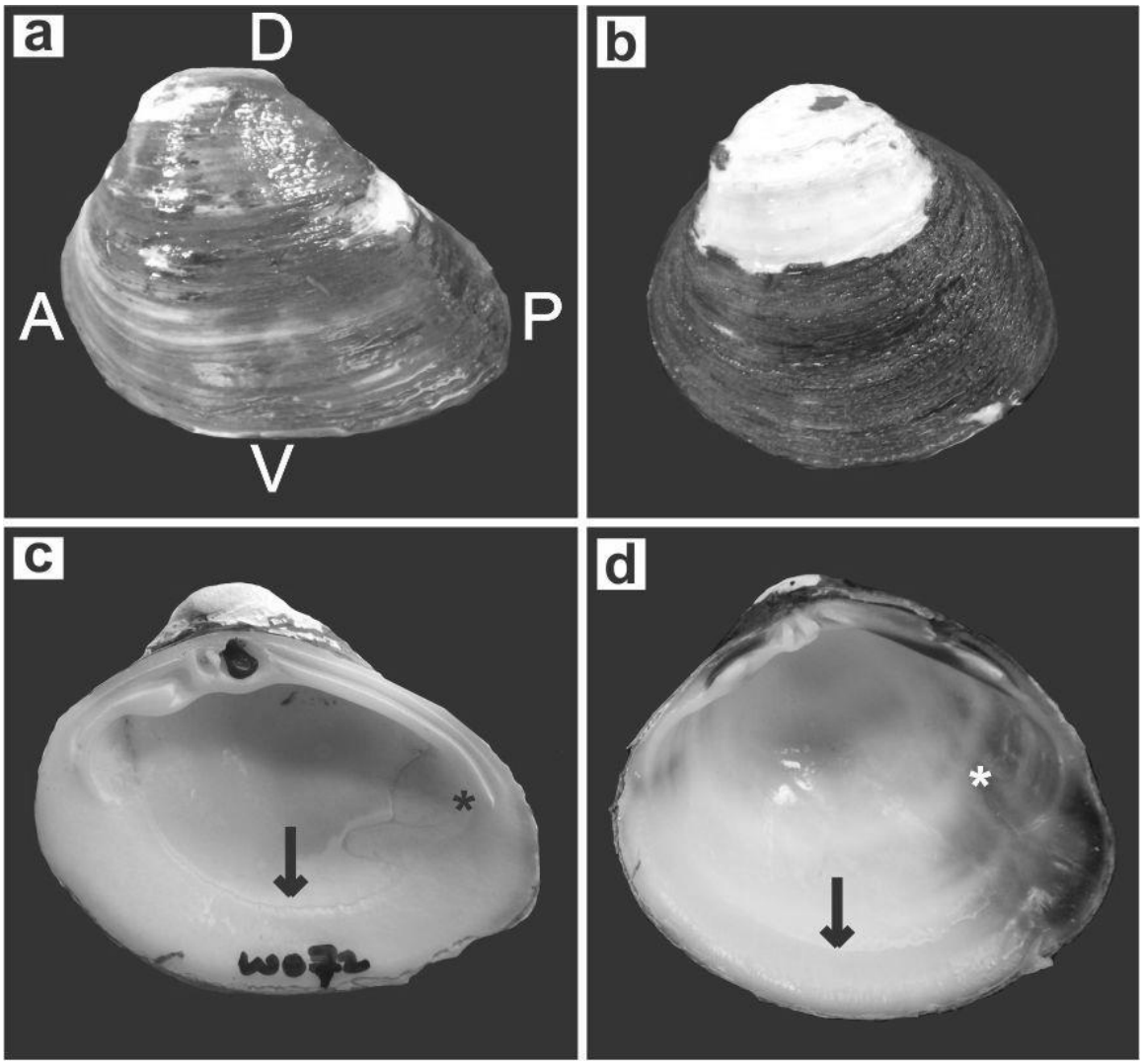

Figure 43. Shell morphology of *Rangia cuneata* and *Polymesoda caroliniana*

The periostracum of *Rangia cuneata* is dark, smooth, and unornamented (a). The periostracum of *Polymesoda caroliniana* is dark brown to black and ruffled (b). The nacre of *R. cuneata* is completely white, but has discernible scars where the adductor and retractor muscle (*) and the mantle tissue (arrow) are attached to the shell (c). The nacre of *P. caroliniana* is a mix of white, pink, and purple with scars that are less discernible, but mirrors those on *R. cuneata* (d). Abbreviations: A = anterior, D = dorsal, P = posterior, V = ventral). All images were oriented with respect to (a).

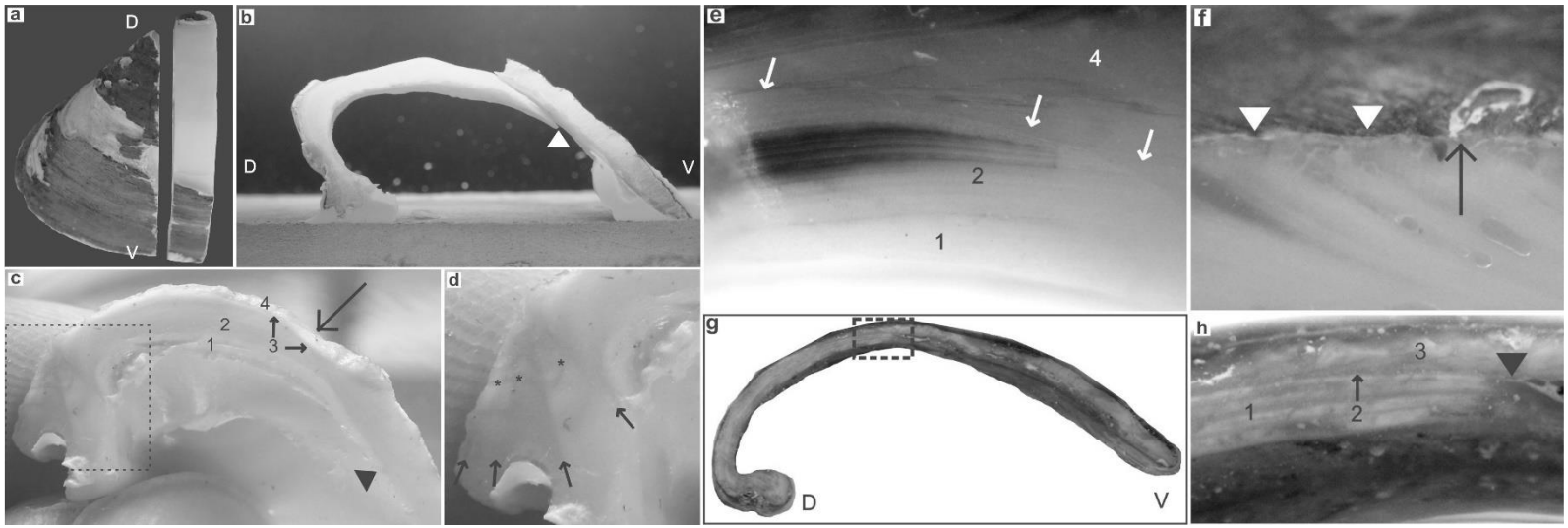

Figure 44. Cut, polished, and stained shells from *Rangia cuneata* and *Polymesoda caroliniana*

A shell of *Rangia cuneata* was cut from the umbo (D = dorsal) to the ventral (V) shell margin along the maximum axis of growth (top to bottom; a). A side-view of (a) revealed a break between the outer layer and the middle and inner layers (arrowhead; b). A polished section shows damage that occurred to the periostracum and outer prismatic layer before preparation (arrow). There are four layers to the shell: (1) inner homogenous layer with the inner nacre, (2) translucent middle layer, (3) pallial myostracum, and (4) outer layer. The pallial myostracum divides the outer layer from the middle and inner layers, but (along with the middle and inner layers) terminates near the ventral margin (arrowhead) (c). A section through the umbo (box from c) shows early life growth with concentric ridges of shell. Narrow, opaque (*) and broad, translucent growth bands indicate seasonal variations. Arrows indicate new growth patterns during ontogeny (d). A closer image of the shell layers reveals the inner layer (1) as a white, compact layer underneath the middle layer (2). The outer layer (4) is sharply separated by the pallial myostracum (arrows; e). Two types of growth breaks were observed in shell of *R. cuneata*. The loss of periostracum in one region is indicative of abrasion, which resulted in a curved, U-shaped growth increment beneath the break (arrow). The ridges indicate possible seasonal change or spawning break (arrowheads in f). There is a greater amount of organic matrix (dark lines) in these locations, indicative of growth cessation (f). A polished and stained section through a shell of *Polymesoda caroliniana* from the D to V (g) revealed three shell layers (h; inset from g): an inner layer (1), pallial myostracum (2), and an outer layer (3). The pallial myostracum terminates approximately halfway towards the ventral margin (arrowhead in h).

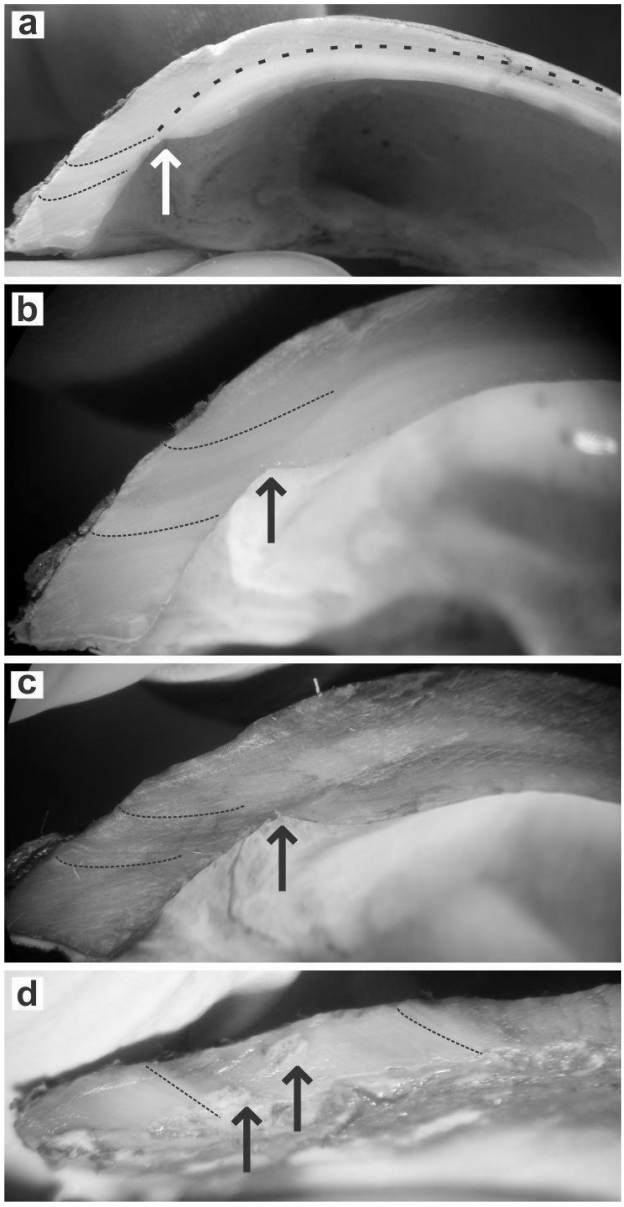

Figure 45. Polished and stained longitudinal sections through a shell of *Rangia cuneata* and *Polymesoda caroliniana*

A longitudinal section through a shell of *Rangia cuneata* near the adductor muscle scar revealed growth bands in the outer layer (thin dotted lines; a-c) and separation of the inner and middle layers from the outer layer (thick dashed line; a) that ceased at the scar (arrows; a-c). Variation in growth band thickness and intensity (light versus dark) was apparent after shells were polished and under transmitted light (b). Alcian blue from the Mutvei solution stained organic matrix and aided in visualization of growth bands (c). Thick dark bands indicate a greater concentration of organic matrix. A longitudinal section through a shell of *Polymesoda caroliniana* near the adductor muscle scar revealed a thinner shell structure and less curvature of growth bands (dashed lines) compared to *R. cuneata*. Arrows indicate possible shift in growth patterns as shell material does not align to the surrounding growth bands (d).

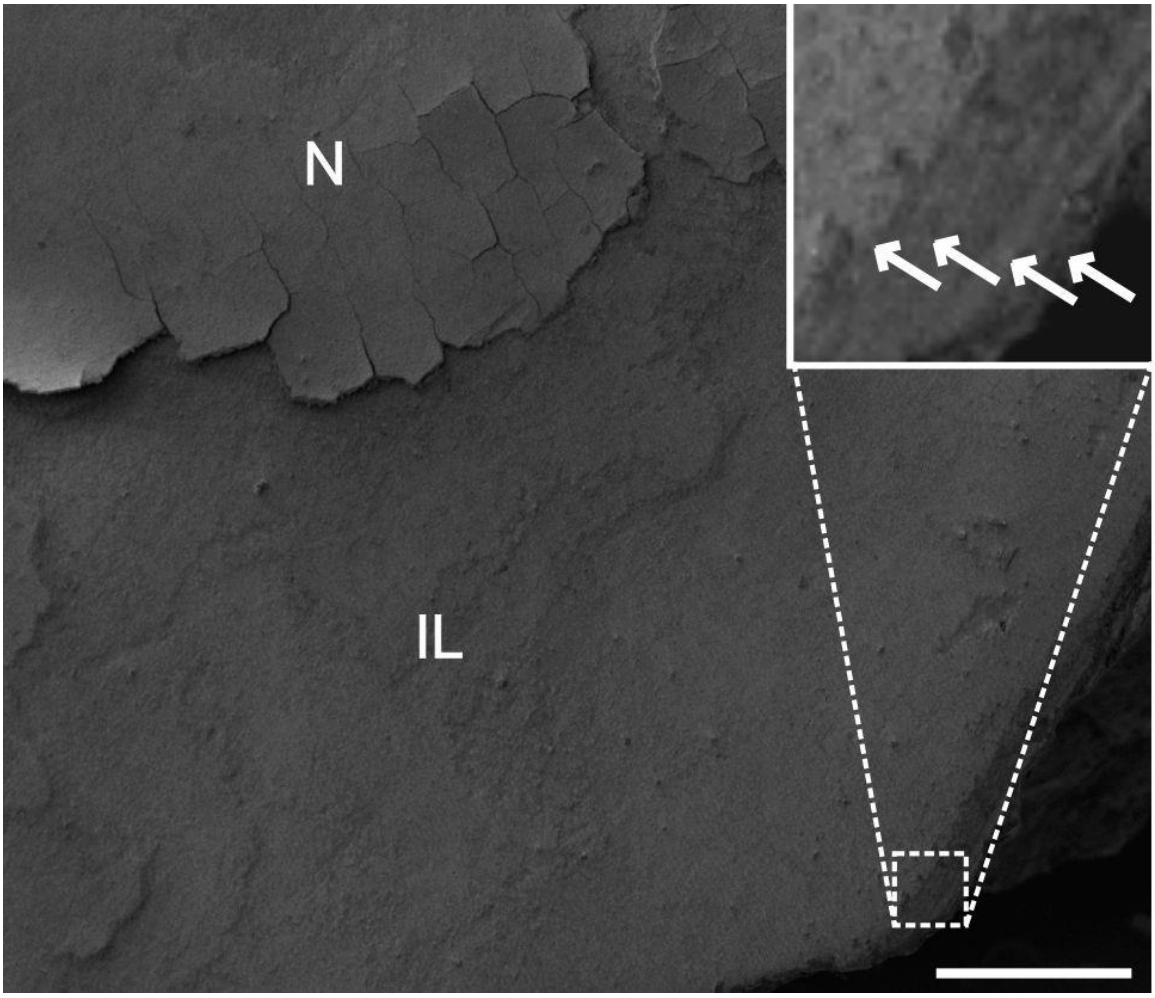

Figure 46. SEM micrograph of the nacre and inner prismatic layer from *Rangia cuneata*

The nacre (N) is thin and will peel off in flakes shell is allowed to dry. The inner prismatic layer (IL) is compact and arranged in foliate-like sheets stacked upon one another (arrows; inset). Scale bar = 500 µm.

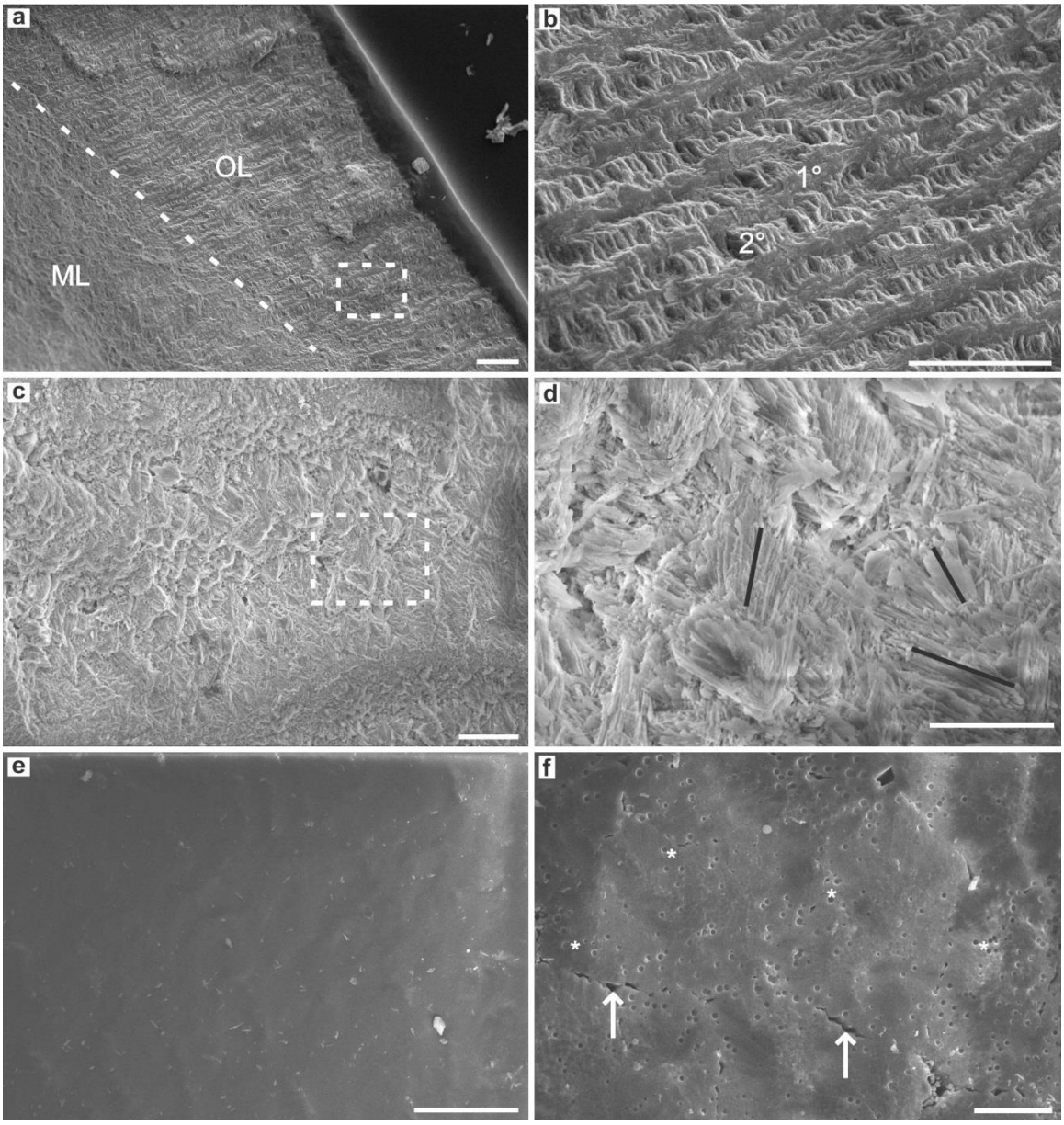

Figure 47. SEM images of shell fragments from *Polymesoda caroliniana*

The ultrastructure of shell fragments from *Polymesoda caroliniana* were examined under SEM. The prismatic outer layer (OL) and middle layer (ML) are separated by the thin pallial myostracum (dashed line; a). (b) is a higher magnification image of the OL showing the first- (1°) and second- (2°) order lamellae. Direction of shell growth is towards the bottom right. The ML is composed of crossed-lamellar crystals (c) that grow in various orientations (dark lines; d). The nacre is extremely thin and uniform. The image shows the nacre on top of the inner prismatic layer (e). The pallial myostracum in *P. caroliniana* is shown above the middle layer. Large, nonuniform bundles of crystals can be seen beneath the myostracum. There were breaks along the pallial myostracum (arrows) and small pore-shaped regions present (*) across this layer (f). Scale bars = 200 µm (a), 50 µm (b, c, e), 25 µm (d, f).

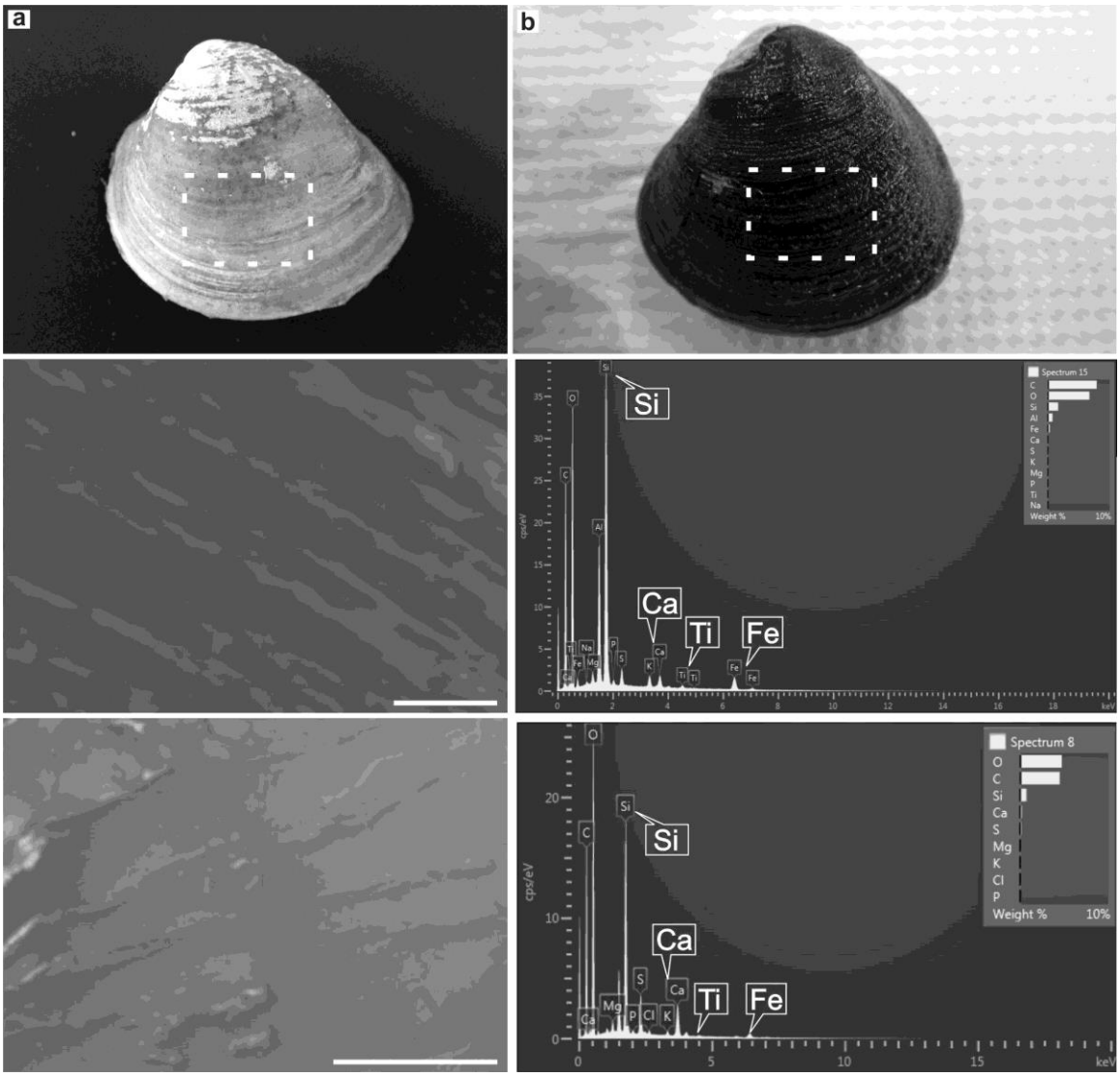

Figure 48. Images, SEM micrographs, and EDS spectra of the periostracum from *Rangia cuneata* and *Polymesoda caroliniana*

The periostracum of a shell from *Rangia cuneata* (a) and *Polymesoda caroliniana* (b) were examined with X-ray microanalysis. A map ROI from each shell was analyzed (c, d; boxes from a and b). Elements detected from the periostracum of *R. cuneata* (e): C, O, Na, Mg, Al (from SEM stub), Si, P, S, K, Ca, Ti, and Fe. Elements detected from the periostracum of *P. caroliniana* (f): C, O, Mg, Si, P, S, Cl, K, Ca, Ti, and Fe. In both species, the counts of Si were far greater than Ca (e and f). Scale bars = 1 mm.

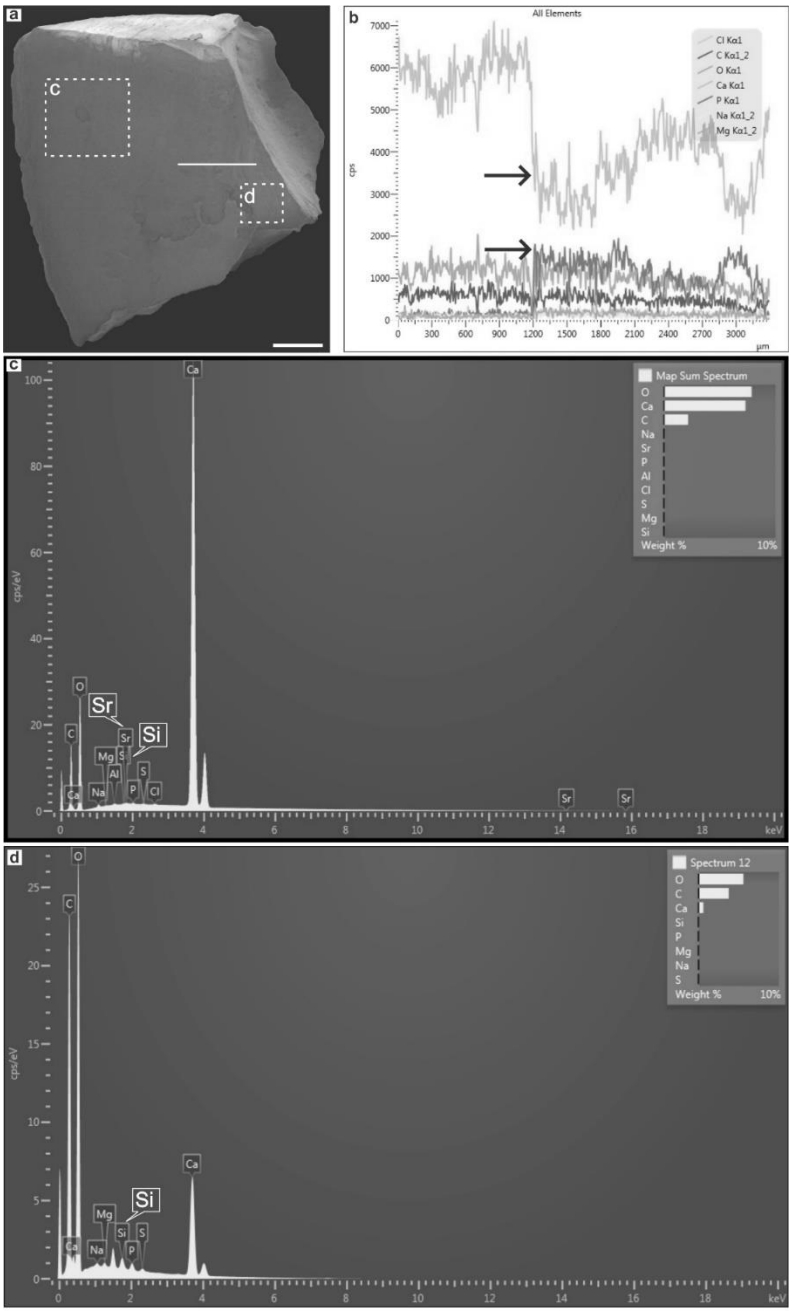

Figure 49. SEM micrograph and EDS spectra across the nacre and adductor muscle scar from *Rangia cuneata*

A shell fragment from the anterior end near the adductor muscle scar was imaged and scanned with EDS. A line spectrum showed a lower amount of Ca towards the muscle scar, while P was detected at a higher concentration. With the exception of C, O, and Ca, all other elements were detected, but with low counts. Elements detected from map (ROI) spectrum over the nacre (large box in (a)) included C, O, Na, Mg, Al (from SEM stub), Sr, Si, P, S, Cl, and Ca (c). Elements detected from map spectrum over the adductor muscle scar (small box in (a)) included C, O, Na, Mg, Si, P, S, and Ca (d). Scale bar = 2 mm.

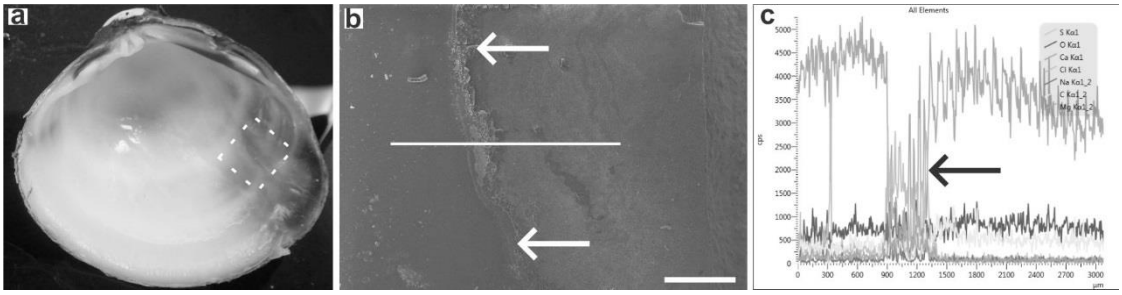

Figure 50. Image, SEM micrograph, and EDS spectrum across the nacre and adductor muscle scar from *Polymesoda caroliniana*

The nacre and adductor muscle scar transition (dashed box in a) is indicated by prismatic microstructures (arrows; b). A line spectrum was performed (solid middle line in b) across this transition (nacre - left side; adductor muscle scar – right side). The spectrum shows the presence of: C, O, Na, Mg, S, Cl, and Ca. Across the boundary between the nacre and scar regions, levels of Ca dropped (arrow; c), while all other elements except O increased (c). Scale bar = 500 µm.

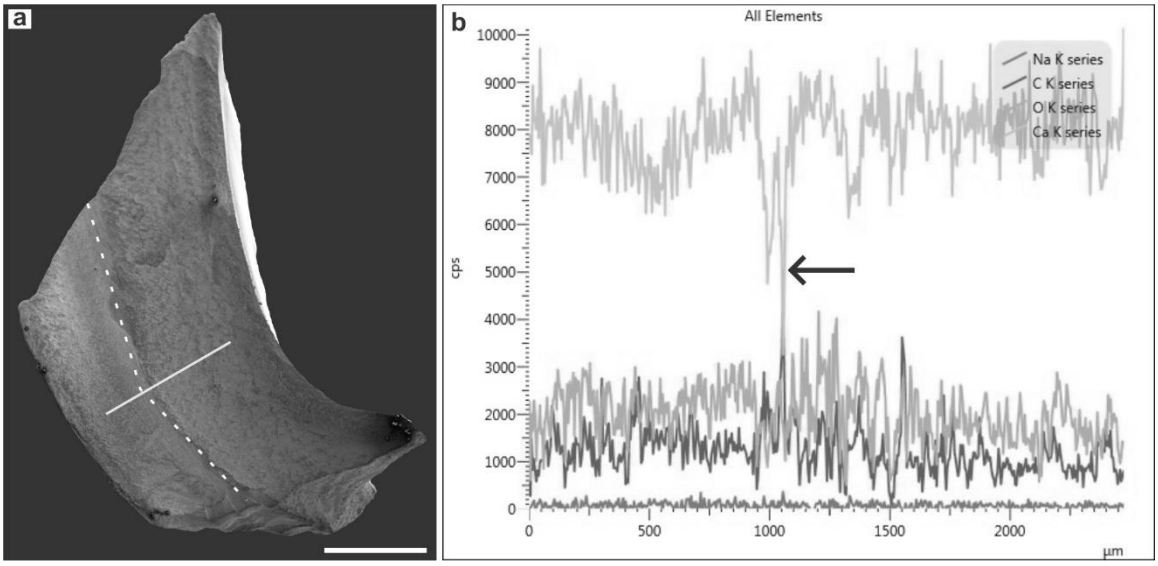

Figure 51. SEM micrograph and EDS line spectrum across the outer and middle prismatic layers from *Rangia cuneata*

A line spectra (solid line; a) across the outer and inner prismatic layers of a fragment of *Rangia cuneata* shell shows that while levels of C, O, and Ca, remained stable throughout both layers, Ca levels dropped across the pallial myostracum (dotted line; a) (arrow; b). Scale bar = 2 mm (c).

References

Ansell AD. 1968. The rate of growth of the hard calm *Mercenaria mercenaria* (L) throughout the geographical range. J Cons Perm Int Explor Mer. 31:364-409.

Cathey AM, Miller NR, Kimmel DG. 2012. Microchemistry of juvenile *Mercenaria mercenaria* shell: Implications for modeling larval dispersal. Mar Ecol Prog Ser 465:155-168.

Clark GR. 1979. Seasonal growth variations in the shells of Recent and prehistoric specimens of *Mercenaria mercenaria* from St. Catherines Islands, Georgia. Anthropol Pap Am Mus Nat Hist. 56:161-179.

Drescher BD, Dillaman RM, Taylor AR. 2012. Coccolithogenesis in *Scyphosphaera apsteinii* (Prymnesiophyceae). J Phycol. 48:1343-1361.

Epstein S, Mayeda T. 1953. Variations in O^{18} content of waters from natural sources. Geochem Cosmochim Acta. 27(4):213-224.

Fritz LW, Haven DS. 1983. Hard clam, *Mercenaria mercenaria*: shell growth patterns in Chesapeake Bay. Fish Bull. 81(4):697-708.

Fritz LW, Ragone LM, Lutz RA. 1990. Microstructure of the outer shell layer of *Rangia cuneata* (Sowerby, 1831) from the Delaware River: applications in studies of population dynamics. J Shellfish Res. 9(1):205-213.

Grovenor CRM, Smart KE, Kilburn MR, Shore B, Dilworth JR, Martin B, Hawes C, Rickaby REM. 2006. Specimen preparation for NanoSIMS analysis of biological materials. Appl Surf Sci. 252:6917-6924.

Lutz RA, Rhoads DC. 1977. Anaerobiosis and a theory of growth line formation. Micro- and ultrastructural growth patterns within the molluscan shell reflect periodic respiratory changes. Science. 198:1222-1227.

Lutz RA, Rhoads DC. 1980. Growth patterns within the molluscan shell: An overview. In: Rhoads DC, Lutz RA, editors. Skeletal growth of aquatic organisms: Biological records of environmental change. New York (NY): Plenum Press. p. 203-254.

Mackinder L, Wheeler G, Schroeder D, Riebesell U, Brownlee C. 2010. Molecular mechanisms underlying calcification in coccolithophores. Geomicrobiol J. 27:585-595.

Matsko NB, Žnidaršič N, Letofsky-Papst I, Dittrich M, Grogger W, Štrus J, Hofer F. 2010. Silicon: The key element in early stages of biomineralization. J Struct Biol. 174:180-186.

Navarro JM. 1988. The effects of salinity on the physiological ecology of *Choromytilus chous* (Molina, 1782) (Bivalvia: Mytilidae). J Exp Mar Biol ecol. 122:19-33.

Pace CB, Di Giulio RT. 1987. Lead concentrations in soil, sediment and clam samples from the Pungo River peatland area of North Carolina, USA. Environ Poll. 43:301-311.

Pannella G, MacClintock C. 1968. Biological and environmental rhythms reflected in molluscan shell growth. J Paleontol. 2, supplemental to 42(5):64-80.

Quintarelli G, Devollo MC. 1966. Age changes in the localization and distribution of glycosaminoglycans in human hyaline cartilage. Histochemie. 7(2):141-167.

Redfield AC, Friedman I. 1965. Factors affecting the distribution of deuterium in the ocean. Symposium on marine geochemistry; University of Rhode Island. Occ Publication. 3:149-168.

Rickaby REM, Shrag DP, Zondervan I, Riebesell U. 2002. Growth rate dependence of Sr incorporation during calcification of *Emiliania huxleyi*. Global Geochem Cy. 16:1-8.

Rosenberg GD. 1980. An ontogenetic approach to the environmental significance of bivalve shell chemistry. In: Rhoads DC, Lutz RA, editors. Skeletal growth of aquatic organisms. New York (NY): Plenum Press. 133-168.

Schoepfer VA, Bernhardt ES, Burgin AJ. 2014. Iron clad wetlands: Soil iron-sulfur buffering determines coastal wetland response to salt water incursion. J Geophys Res: Biogeo. 119:2209-2219.

Schöne BR, Gillikin DP. 2012. Unraveling environmental histories from skeletal diaries – advances in sclerochronology. Palaeogeogr Palaeocl. 373:1-5.

Shumway SE, Parsons GJ. 2006. Scallops biology, ecology, and aquaculture. Boston and Amsterdam: Elsevier.

Stoll HM, Schrag DP. 2000. Coccolith Sr/Ca as a new indicator of coccolithophorid calcification and growth rate. Geochem Geophys Geosy. 1:1-24.

Wolfe Da, Schelske CL. 1969. Accumulation of fallout radioisotopes by bivalve molluscs from the lower Trent and Neuse Rivers. Proc 2nd Nat Symp on Radioecology. USAEC Conf 670502:493-504.

APPENDIX A – PAIRWISE COMPARISON OF OM DATA

Table A1.

Pairwise comparison of OM based on location with presence versus absence of clams

Site Comparison (+/-)	**q values**	**Significant difference (yes or no)**
Lower (+) vs Lower (-)	2.80	No
Lower (+) vs Middle (+)	0.84	No
Lower (+) vs Upper (+)	3.67	Yes
Lower (+) vs Middle (-)	1.43	No
Lower (+) vs Upper (-)	2.89	No
Lower (-) vs Middle (+)	3.64	Yes
Lower (-) vs Middle (-)	1.37	No
Lower (-) vs Upper (+)	6.48	Yes
Lower (-) vs Upper (-)	5.70	Yes
Middle (+) vs Middle (-)	2.27	No
Middle (+) vs Upper (+)	2.83	No
Middle (+) vs Upper (-)	2.06	No
Middle (-) vs Upper (+)	5.11	Yes
Middle (-) vs Upper (-)	4.33	Yes
Upper (+) vs Upper (-)	0.78	No

A pairwise comparison using Dunn's test (q_{crit} = 2.92) was performed between OM collected where clams were present and clams were absent from the three sites (lower, middle, upper). The symbols (+) and (-) indicate presence and absence of clams, respectively.

APPENDIX B – PERMISSION FOR USAGE OF FIGURE 3

Email request for use of Figure 3:

Dear Jennifer,

Please be informed that in accordance with updated Terms and Conditions for reuse of web content (full version available on http://www.fao.org/contact-us/terms/en/), except where otherwise indicated, material may be copied, downloaded and printed for private study, research and teaching purposes, or for use in non-commercial products or services, provided that appropriate acknowledgement of FAO as the source and copyright holder is given and that FAO's endorsement of users' views, products or services is not implied in any way.

All requests for translation and adaptation rights, and for resale and other commercial use rights should be submitted via the online Licence Request Form http://www.fao.org/contact-us/licence-request/en/ when downloading.

Kind regards,

Radhika

Reference from which figure was reproduced:

Carpenter KE. 2002. The living marine resources of the Western Central Atlantic: Introduction, molluscs, crustaceans, hagfishes, sharks, batoid fishes, and chimaeras. FAO species identification guide for fishery purposes and American Society of Ichthyologists and Herpetologists Special Publication No. 5. [Rome] p 1-600.

FAO acknowledgement: http://www.fao.org/contact-us/terms/en/